Studies of the light-induced signal transduction in *Agrobacterium fabrum*

Zur Erlangung des akademischen Grades eines

DOKTORS DER NATURWISSENSCHAFTEN

(Dr. rer. Nat.)

von der KIT - Fakultät für Chemie und Biowissenschaften

des Karlsruher Instituts für Technologie (KIT)

genehmigte

DISSERTATION

von

Afaf El Kurdi

Libanon

Dekan: Prof. Dr. Manfred Wilhelm

Referent: Prof. Dr. Tilman Lamparter

Korreferent: Prof. Dr. Peter Nick

Tag der mündlichen Prüfung: 15.04.2021

Die vorliegende Dissertation wurde sowohl am Botanischen Insitut des Karlsruhe Intituts für Technologie (KIT), Lehrstuhl 1 für allgemeine Botanik, Arbeitsgruppe Prof. Dr. Tilman Lamparter als auch am Institut für Angewandte Physik, Arbeitsgruppe Prof. Dr. Nienhaus, im Zeitraum von Januar 2017 bis Februar 2021 angefertigt.

Ein Teil dieser Arbeit ist in folgender Veröffentlichung enthalten:

Xue P, El Kurdi A, Kohler A, Ma H, Kaeser G, Ali A, Fischer R, Krauß N, Lamparter T (2019) Evidence for weak interaction between phytochromes Agp1 and Agp2 from Agrobacterium fabrum. FEBS letters 593:926–941

Acknowledgments

My sincere gratitude goes to Prof. Dr. Tilman Lamparter, my supervisor. Thank you for giving me this opportunity to be a part of your group and this interesting project. Furthermore, to grant me freedom to work with different challenging topics and giving me constant support since my master thesis till now.

A special thank for my colleague Norbert Krauß for all the scientific knowledge, various perspectives and support you passed on to me specially at the end of my PhD, which was a lot of help and also for the proofreading of my work.

A lot of thanks for Prof. Dr. Ulrich Nienhaus for providing the possibility to perform the time-resolved fluorescence anisotropy in his group and for Dr. Gernot Guigas helping to perform the measurements.

I also thank Prof. Dr. Peter Nick for accepting to be the co-referent.

Furthermore, many thanks for Latifa Hourani, who has helped performing the conjugation and phosphorylation assays as part of her master thesis, for my colleagues Katha Thoulass, for her English-proofreading and for Peng Xue, Gero Kaeser and and Nadja Wunsch for their different contribution in my work.

Finally, yet most importantly, I want to thank my parents and my sisters, especially my sister Riham for believing in me, always pushing me forward and never giving up on me, for being beside me and supporting me all along these years.

Table of Contents

List of Abbreviations

Abbreviation	Meaning
A_A	Absorption of the acceptor fluorophore alone
A_{AD}	Absorption of the acceptor in presence of the donor in the mixture
AB MM	A. tumefaciens minimal medium
Agp1$^-$	Agp1 phytochrome was knocked out
Agp12$^-$	Agp12 phytochrome was knocked out
Agp1A362C	Agp1 mutant, where A at position 362 was replaced with C
Agp1C295	Agp1 mutant, where only the cys at position 279 was replaced with a serine
Agp1K517C	Agp1 mutant, where K at position 517 was replaced with C
Agp1K554C	Agp1 mutant, where K at position 554 was replaced with C
Agp1R535C	Agp1 mutant, where R at position 535 was replaced with C
Agp1R603C	Agp1 mutant, where R at position 603 was replaced with C
Agp1S122C	Agp1 mutant, where S at position 122 was replaced with C
Agp2$^-$	Agp2 phytochrome was knocked out
Amp	Ampicillin
Bp	Base pair
BV	Biliverdin
CF	correction factor
DCO	Double cross over
DOL	Degree of Labelling
E_{FRET}	FRET efficiency
FCS	Fluorescence correlation spectroscopy
FI	Fluorescence intensity
Genta	Gentamycin
HK	Histidine Kinase
I_A	Fluorescence intensity of the acceptor fluorophore alone
I_{AD-M}	Fluorescence intensity of the acceptor in presence of the donor in the mixture
I_{AS}	Fluorescence intensity of the acceptor in the sum spectrum
I_D	Fluorescence intensity of the Donor fluorophore alone

Abbreviation	Meaning
I_{DA-M}	Fluorescence intensity of the donor in presence of the acceptor in the mixture
I_{DS}	Fluorescence intensity of the donor in the sum spectrum
IPTG	Isopropyl-β-D-thiogalacto-pyranosid
Kan	Kanamycin
LB	Luria Broth
MM	Molar mass
OD	Optical density
PCM	Photosensory core module
Prot	Protein
RR	Response regulator
RT	Room temperature
SCO	Single cross over
SDM	Site Direct Mutagenesis
TCSPC	Time correlated single photon counting
Tm	Annealing temperature
TraA-	TraA phytochrome was knocked out
Wt	Wild type

Summary

Organisms regardless of their origin or type, monitor their environment and respond differently to any environmental changes that occur. These changes not only can alter biochemical reactions that are taking part in the signal transmission, but also the properties of the proteins involved. Therefore, biochemical, or biophysical analyses are a useful approach to understand bacterial cellular mechanisms such as the ones in the bacterium *Agrobacterium fabrum* (former *Agrobacterium tumefaciens*) and its phytochrome system.

The biliprotein photoreceptors Agp1 and Agp2, found in *A. fabrum*, exhibit opposite spectral characteristics regarding light-induced and thermal conversion between the red absorbing Pr form and the far-red absorbing Pfr form and could control various cellular mechanisms.

These phytochromes have been shown to be able to act together, regulating various mechanisms or processes, such as bacterial conjugation, plant infection and cell growth, in addition to the phosphorylation, and their photoconversion ability.

Understanding a signal transduction pathway requires the understanding of the function of proteins, which in turn requires a detailed knowledge of their structure, dynamics, and the different conformational states they can adopt.

Therefore, structures studies by X-ray crystallography of the photosensory core modules of various phytochromes were analysed, revealing insights into their conformational changes upon photoconversion. Various hypothesises were already published, on how the structure of phytochromes varies upon photoconversion and in transducing the light signal. Nonetheless, it is still not clear how this signal transduction pathway occurs and how phytochromes are involved in.

For this reason, it is aimed in this research to understand the signal transduction pathways of a bacterial phytochrome. These pathways are protein-driven processes, involving photoisomerization, light induced protein conformational changes and possible protein-protein interactions.

Within this work, *in vitro* studies using Agp1 mutants were performed. These mutants were prepared to introduce a single cysteine residue at defined positions, enabling targeted labelling with a maleimide fluorophore.

First, the influence of mutations in Agp1 on the autophosphorylation was examined, to determine that these single mutations did not significantly affect the protein function, serving thus as a control experiment. The autophosphorylation results of Agp1 mutants revealed a similar behaviour as for Agp1 wild type, exhibiting a higher autophosphorylation activity in the Pr form than in the Pfr form.

Subsequently, these Agp1 mutants were then investigated by time resolved fluorescence anisotropy, to gain insight into the dynamics of the protein. Results have indeed shown that the dynamics of the phytochrome at the corresponding (sub-) domain, changes between the Pr and Pfr form for both the PCM and HK modules, where mainly the dynamics in the Pfr form is lower than in the Pr form. Thus, emphasizing the conformational changes of the phytochrome upon photoconversion that are involved in the transmission of the light signal.

Moreover, interaction studies were also carried out *via* FRET, where Agp1 and Agp2 were labelled with different fluorophores. Results have indeed shown an interaction between both phytochromes, suggesting that the PAS-GAF bidomain of Agp2 interacts with the histidine kinase module of Agp1 and that the FRET efficiency is light-regulated.

A different approach for the study of the signal transduction in *A. fabrum* was realised through *in vivo* analysis of the bacterial conjugal transfer, since it was proved to be affected by the red light sensitive phytochromes and by their histidine kinases.
The conjugation assay in this work revealed the importance of the TraA gene, which is supposed to be the first protein involved in the conjugation cascade of Agp1. Three TraA homologues are presented in *A. fabrum* and are encoded by the Ti plasmid (Atu6127), the linear chromosome and the At plasmid. Results showed that the knockout of the TraA encoded by the pTi, inhibited the conjugal transfer in *A. fabrum* and that phytochromes regulate the expression of the other TraA genes encoded by the linear chromosome and the pAt.

1 Introduction

Cells display a notable ability to respond to the surroundings environmental conditions and make an appropriate adaptive response. The molecular biology studies of regulatory processes in bacteria have brought more insight about the signal transduction pathway involving two types of proteins: a receptor and a response regulator. In response to a stimulus, information form the receptors is then transduced to the appropriate adaptive response elements (Jeffry et al. 1990)

One important element that can affect organisms and plays a significant role for all living organisms, is solar radiation. It does not only provide the necessary energy and heat, but also light, which affects different mechanisms of development, morphology and metabolism (Möglich et al. 2010).

Prokaryotes have developed a range of photosensory receptor proteins, which can detect the visible light of their environment and regulate the cell physiology *via* enzymatic and regulatory protein domains, that are light dependent (Wood et al. 2001)

Light that reaches the earth from 350 – 750 nm is defined as the visible part of the electromagnetic spectrum (Purcell and Crosson 2008).

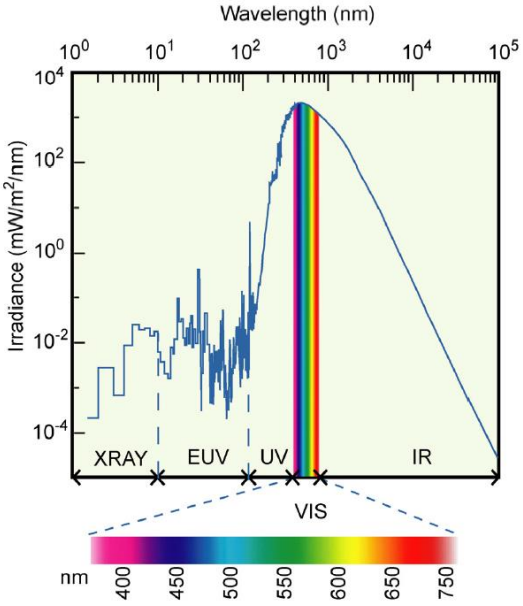

Figure 1: Solar radiation: *Most of the solar radiation that reaches Earth is made up of visible, UV and infrared light. Photoreceptors absorption ranges from the near UV (350 nm) through the blue to the far red (~ 750 nm). Figure adopted from (Purcell and Crosson 2008).*

Every organism uses light in a different way and converts it to a chemical energy storage that is indispensable for its living. For the light intake, organisms use proteins that are considered as their “eyes”, which are called photoreceptors. These photoreceptors are responsible for the perception of light in living organisms and thus gain information about their external world. They react to light *via* photoisomerization or photoreduction upon the binding of small molecule cofactors or chromophores, which triggers structural modifications in the proteins and initiates diverse signal transduction pathways (Purcell and Crosson 2008).

Photoreceptors carry organic chromophores as prosthetic groups and react differently towards diverse wavelength ranges depending on their structure. Furthermore there are different types of photoreceptor proteins such as the rhodopsins and the red light sensitive photoreceptors called phytochromes, the blue-light sensitive cryptochromes and phototropines (van der Horst and Hellingwerf 2004).

One of the red light sensitive organisms is the bacterial species *Agrobacterium tumefaciens* (*Rhizobium radiobacter*) (Young et al. 2001) newly termed *Agrobacterium fabrum*. This ubiquitous soil bacterium has proven to be remarkable in plant genetic engineering and plant molecular genetics, based on its capacity in the horizontal genes transfer namely its capacity of transformation and conjugation. However the bacterium has not only capabilities in the transfer of its DNA into plant cells, but also into algae, fungi and even human cells (Nester 2014).

1.1 Agrobacterium fabrum

1.1.1 Description

Agrobacterium fabrum, a gram-negative bacterium, belongs to the *Rhizobiaceae* family and is considered an α-proteobacterium (Wood et al. 2001). It has no spores and is characterized by its rod shape, in addition to its flagella that allow the bacterium to move on soil to reach the wounded sites of the plants after the recognition of specific components secreted by the wounded plant (Wood et al. 2001).

Normally the bacterium infects the roots in dicotyledonous plants causing the formation of a tumour, called the “Crown Gall tumour”. Since its discovery, *A. fabrum* was involved in a large number of researches, which either had their focus on the mechanisms and the causes of the tumour induction or used its transfection mechanism to introduce new genes into plant genomes, to eventually apply this knowledge to develop drug treatments for cancer disease in animals and humans (La Riva et al. 1998).

Agrobacterium fabrum strain C58 has two types of chromosomes, a linear and a circular chromosome, which contain the necessary genes that are essential for the bacterium’s survival. Additionally, *A. fabrum* has two types of plasmids, which are the *A. tumefaciens* plasmid (pAtC58) and the tumour inducing plasmid (pTiC58) (Wood et al. 2001; Goodner et al. 2001).

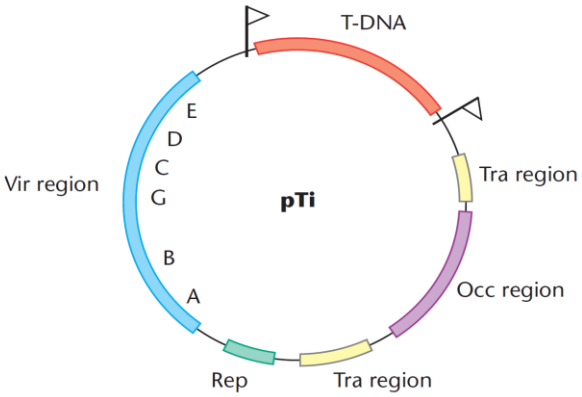

Figure 2: The tumor inducing plasmid (pTi)*: The pTi contains most of the genes that are involved in the infection - Vir genes – to transfer the T-DNA and the Tra genes to ease the conjugal transfer. Figure is based on the pTi figure of Ashraf et al. 2012*

The pTiC58 is responsible for tumour formation, since it contains the necessary genes for its pathogenicity against plants (Goodner et al. 2001). It also contains the Tra and Vir region, which are particularly involved in the horizontal gene transfer mechanism, such as the transformation that uses the Vir genes and T-DNA or the conjugation with the help of the Tra region (Păcurar et al. 2011; Giusti et al. 2012).

1.1.2 Function and horizontal gene transfer

Horizontal gene Transfer (HGT) is a key mechanism of the genome evolution and has profound implications between bacterial strains and species (Bellanger et al. 2014). It allows homologous recombination between strains, thus leading to the integration of new genetic information. This enables the bacterium to adapt to new conditions and environments. Based on its function and its pTi characteristic, *A. fabrum* is used as a vehicle for horizontal gene Transfer (HGT) *via* two essential mechanisms; The transformation that uses Vir genes to transfer a fragment of its pTi (T-DNA) into the plant cells or the whole pTi as a single stranded DNA by means of conjugation, to other bacterial cells (Wood et al. 2001). The pTi is also thought to be very important in research (Cabezón et al. 2015).

1.2 Phytochromes:

Phytochromes are biliprotein photoreceptors that were first discovered in plants (Butler et al. 1959). They regulate various mechanisms, such as plant growth, development, and regulation of metabolic mechanisms in response to light (Rockwell et al. 2006). They are also found in a variety of organisms such as fungi (Fphs) or other bacteria such as cyanobacteria (Cphs), where they regulate different biosynthesis mechanisms (Rockwell et al. 2006; Lamparter et al. 2017).

The structure of phytochromes is generally comparable in plants, bacterial and fungal phytochromes. They consist of two main regions; the N-terminal photosensory region (PCM) includes a tri-domain, PAS (Period/Arnt/Single minded), GAF (cGMP phosphodiesterases/Adenylate cyclase/FhlA) and PHY (phytochrome) domain, which is necessary for the binding of the chromophore. The C-terminal regulatory module typically consists of a histidine kinase to which sometimes a response regulator (RR) is attached to (§ 1.2.3). However, the structure of phytochromes and the corresponding chromophore can differ between species *(Figure 3a).*

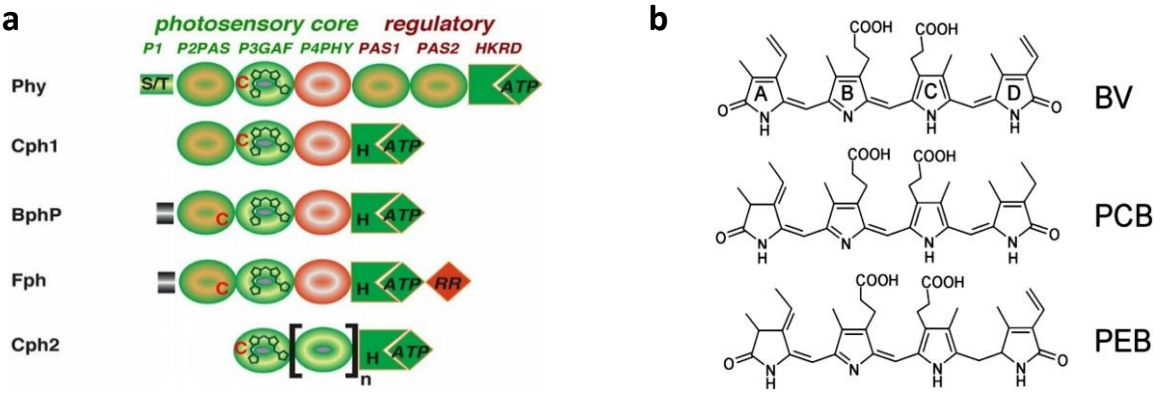

Figure 3: Structure of phytochromes and chromophores: *A) Similarity and differences of the phytochromes structure depending on the type of species, where they are found in. The letter "C" corresponds to the cysteine residue of the appropriate domain, where the chromophore binds. B) Types of bilin chromophores that bind to the phytochromes to the. Figures are adopted from (C. Rockwell et al., 2006 and Lamparter et al., 2002) respectively.*

The basic principle of phytochrome photochemistry is the photoconversion between a red-light absorbing Pr state, and a far-red absorbing Pfr state *(§ 1.2.1, Figure 4)*.

This photoconversion characteristic is reflected through the association with the linear tetrapyrrole bilin chromophore, which binds covalently at the N-terminal side either to the PAS or the GAF domain *via* thio-ether linkage. The nature of these chromophores and their binding sites are different for the various subfamilies of phytochromes at a cysteine residue *(Figure 3a).*

For instance, plant phytochromes Phys bind phytochromobilin (PΦB), while the cyanobacterial phyrochromes Cphs bind phycocyanobilin (PCB), both to a cysteine rest in the GAF domain. The bacterial phytochromes Bphs and Fphs bind the chromophore biliverdin (BV) that attaches to a cysteine residue in the PAS domain (Zienicke et al. 2013). Hence, phytochromes can be divided into three different groups. Group I involves bacterial, fungal, and plant phytochromes', in group II, the photosensory module consists solely of a GAF-PHY bidomain , whereas in group III, the PCM is only made up of the GAF domain, which suffices for bilin binding (Assafa et al. 2018; Rockwell et al. 2006).

1.2.1 Phytochromes of *A. fabrum*

The genome sequence C58 of *A. tumefaciens* was first published in 2001 by two independent groups (Wood et al. 2001; Goodner et al. 2001), revealing the presence of genes, which code for two types of phytochromes Agp1 (AtBphP1) and Agp2 (AtBphP2) (Zienicke et al. 2013; Lamparter et al. 2002).

Agp1 and Agp2 Phytochromes have a similar N-terminal structure, consisting of the PAS-GAF-PHY-domains, called photosensory core module (PCM). They bind the chromophore biliverdin at a conserved cysteine either at C20 or C13 in the N-Terminal of the PAS domain of Agp1 or Agp2 respectively (Lamparter et al. 2004; Lamparter et al. 2002). However, they differ with their C-terminal component, where Agp1 has a type I like Histidine Kinase (Rottwinkel et al. 2010), while Agp2 has a HWE-type like histidine kinase, in addition to the response regulator domain *(Figure 4)* (Zienicke 2011).

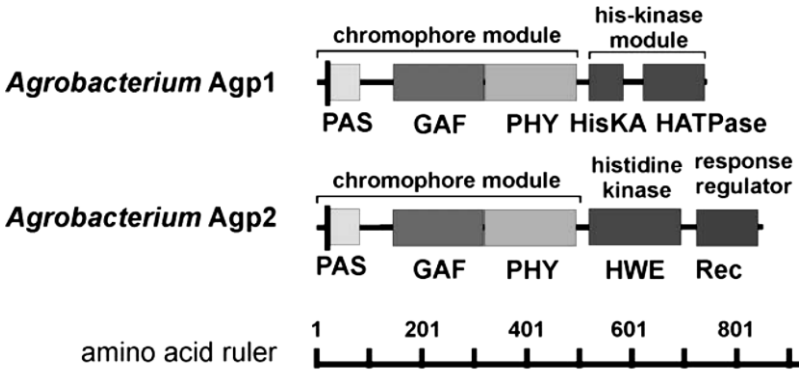

Figure 4: Agp1 and Agp2 domain structure: *Agp2 has a response regulator domain in addition to Agp1 structure. Figure adopted from (P. Scheerer et. al 2010)*

Furthermore, they exhibit opposite spectral characteristics, where Agp1 acquires the Pr-Form as a ground state and converts to the Pfr-form after red light absorption at ~ 660 nm, and slowly returns to the ground state when placed in the dark or after irradiation with far red light at ~ 730 nm (Noack and Lamparter 2007).

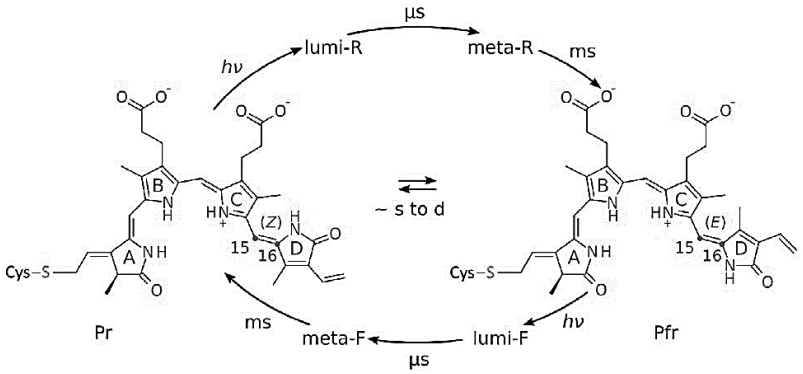

Figure 5: Photochemistry of bacterial phytochromes: *Photoconversion mechanism from Pr, the red-light absorbing form to Pfr state, the far-red light absorbing form, involving the isomerization of the BV chromophore from a Z configuration around C15=C16 to an E configuration. Figure adopted from (Möglich 2019)*

On the other hand, the bathy phytochrome Agp2 has the Pfr-form as ground state, which converts to the Pr-state after far red light irradiation and switches back to the Pfr-form during the dark photoconversion or irradiation with red light (Rottwinkel 2011; Zienicke et al. 2013; Zienicke 2011; Păcurar et al. 2011; Li et al. 2011).

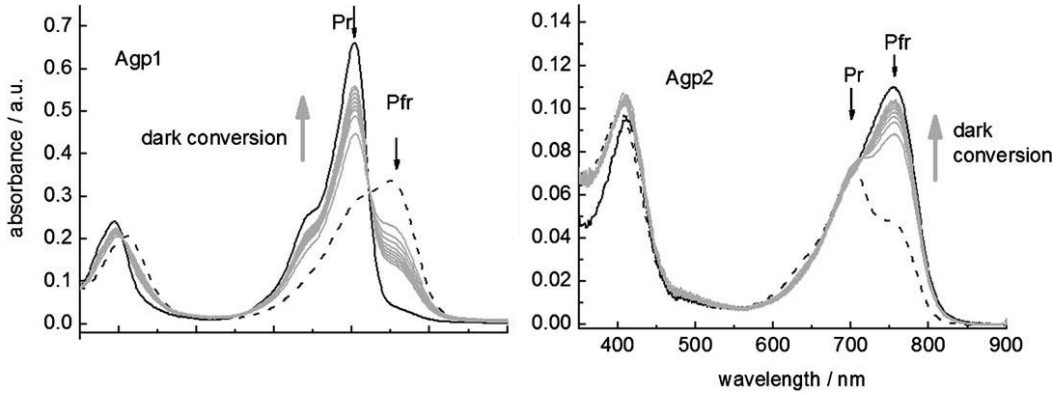

Figure 6: Dark reversion of Agp1 and Agp2: *A) shows the absorption spectra of Agp1 in Pfr (black dashed lines) and its dark conversion process (grey lines) into Pr form (black dashed lines). B) represents the absorption spectra of Agp2 in the Pr ground state (grey lines) and its dark conversion into Pfr. Figure adopted from (P. Scheerer et al. 2010)*

1.2.2 Agp1 and Agp2 phytochrome structures

The crystal structure of the PCM domain of both types of phytochromes in their Pr and Pfr form respectively has enabled the determination of the conformational changes that occur in the phytochromes upon photoconversion (Lamparter et al. 2017).

However, there is still no clear structure for the Histidine kinase (HK), but it is still obtained from several models, such as the homolog *Thermotoga maritima* (PDB code 2C2A) (Bhate et al. 2015; Kacprzak et al. 2017).

According to these structures, the chromophore pocket is formed by the GAF domain, which is connected to the PAS domains forming a figure of eight knot (Wagner et al. 2005). The PHY domain, which can be responsible for the mediation of signal transduction is linked *via* its C-terminal to the HK and *via* its N-terminal to the chromophore-binding GAF domain, where the tongue of the PHY domain folds back onto the pocket of the chromophore resulting in an interaction with the GAF domain. Moreover, the long helices that connect the GAF and PHY domain or the PHY with the HK domain, could structurally stabilize the domain connections, restricting hence the movements of the domains (Lamparter et al. 2017). Comparing both crystal structures of the PCM in the Pr (PDB code 5I5L) and in the Pfr form of *DrBphP*-PCM (PDB code 5C5K), a bending of the helix could be observed that connects the GAF and PHY domains in the Pr state, which shows on the contrary only a stretched conformation in the Pfr form (Nagano et al. 2016).

Furthermore the tip of the tongue interacts with the ring A of the chromophore in the Pr form but with the ring D in the Pfr form and the base of the tongue consists of two -stranded antiparallel *β-sheets in the Pr,* whereas in the Pfr form it is a one α-helix and a loop *(figure 7)* (Lamparter et al. 2017; Essen et al. 2008; Yang et al. 2008).

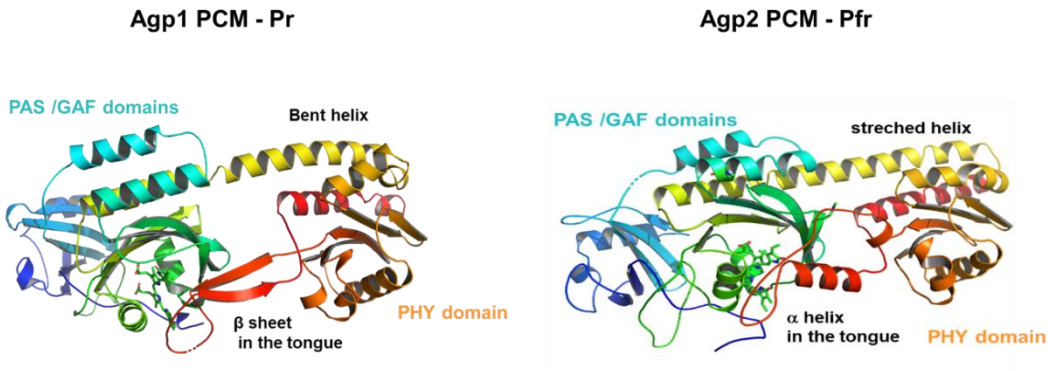

Figure 7: Crystal structure of Agp1 and Agp2 PCM: *A) PCM structure of Agp1 showing the long-bent helix and the β-sheets of the tongue. Whereas B) shows the stretched helix and secondary structure changes of the tongue into an α helix (T. Lamparter unpublished work). These structures are based on the published structures by (Nagano et al. 2016; Schmidt et al. 2018), PDB entries 5I5L and 6G1Y for Agp1 and Agp2 respectively.*

Further studies involving the structure of the long scaffolding α helix, connecting the PHY domain with the DHp domain of the HK and the GAF domain have shown additional conformational heterogeneity ((Nagano 2016; Assafa et al. 2018), where the helix seems to be more flexible in the Pr form, having different orientations (PDB codes 6R26 and 6R27), but still stretched in the Pfr form *(Figure 82)*.

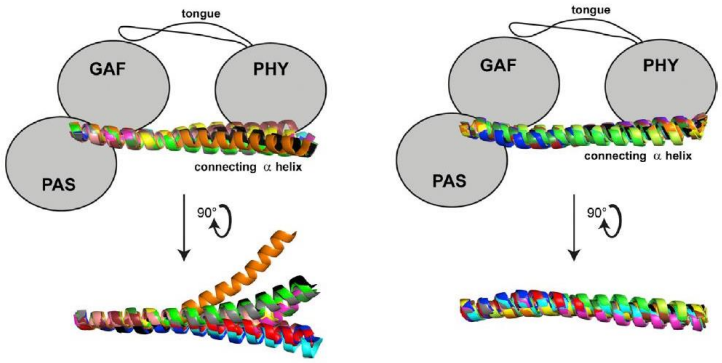

Figure 8: *Possible conformations of the long helix adapted in the Pr form of the PCM module of group I and II phytochromes, showing its flexibility. Whereas it loses its flexibility in the Pfr form. Figure adopted from (Assafa et al. 2018)*

1.2.3 Histidine kinase

The translation of environmental signals into cellular behaviour is an essential process in all forms of life, especially for single-celled organisms. In bacteria this process requires two-component systems that consist of a sensor histidine Kinase (HK) and a cognate response regulator (West and Stock 2001; Casino et al. 2007).

Many of the bacterial phytochromes identified so far, belong to the large group of sensory histidine kinases. These Histidine Kinases act as a molecular “switch button”, that triggers a cascade of signals, to control diverse cell effector activities, through its response regulator and its phosphorylation.

The C-terminal effector module consists of a dimerization and a histidine phosphorylation domain (DHp), that exhibit an autophosphorylation activity in response to a definite stimulus and a catalytic ATP-binding (CA) domain. The activated HK will then transfer the phosphoryl group either to its cognate response regulator or to another domain, which will oligomerize to activate or down regulate a variety of cellular functions (Dikiy et al. 2019; Cai et al. 2017; Njimona et al. 2014).

This phosphotransfer-mediated signalling allows cells to sense and respond to environmental stimuli and therefore, control diverse effector activities. It is presented in eukaryotes, where they phosphorylate both themselves and other protein substrates, thereby regulating protein activities (West and Stock 2001). This signalling can influence different cellular mechanisms, such as chemotaxis, metabolism, transport, cell growth, in addition to other processes that differ in bacteria, fungi or plants (West and Stock 2001; Elich and Chory 1997).

Based on their DHp sequence, the HK proteins can be divided into four subtypes, called HisKA, HisKA_2, HWE_HK and HisKA 3, 4,5 (Multamäki et al. 2020).
Bacteria, such as *A. fabrum* also have HKs that are part of two-component systems (Lamparter et al. 2004) with an N-terminal sensor signal input domain, C-terminal transmitter histidine kinase domain and a response regulator region (RR). The latter consists of a N-terminal receiver domain and a C-terminal output domain (effector domain) *(Figure 9).*

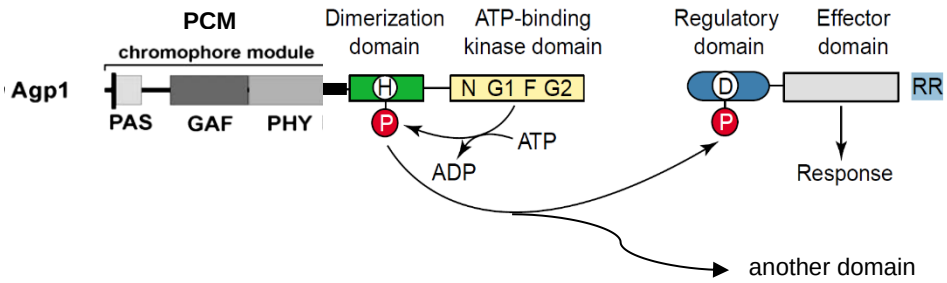

Figure 9: *Schematic illustration of a histidine kinase domain and its function in transmitting the signal, which will be captured by the PCM. Figure is based on the one adopted from (A. Westand et al., 2001)*

Phytochromes of *A. fabrum* are shown to be light and temperature regulated histidine kinases (Noack and Lamparter 2007; Njimona et al. 2014; Njimona and Lamparter 2011; Zienicke et al. 2013), where Agp1 has a classical HK, and Agp2 belongs to the HWE HK type (Karniol and Vierstra 2004). In addition to its capacity of autophosphorylation, a HK shows dimerization properties that are light dependent, which eventually alters the HK activity and influences the phytochromes action (Noack and Lamparter 2007; Krall and Reed 2000; Fankhauser 2000). After light absorption, conformational changes occur in the chromophore module at its N-terminal part, which

are then transmitted to the C-terminal of the HK. These conformational changes, lead to an alteration of the autophosphorylation activity, thus the phosphorylation activity of the RR, which will ultimately modify the entire signal transduction cascade (Takala et al. 2018).

Agp1 was shown to be more active in the Pr form, by exhibiting a higher autophosphorylation yield than the Pfr form, where it decreases after irradiation with red light (Lamparter et al. 2002; Njimona et al. 2014). On the contrary the kinase activity of Agp2 is more active in the Pfr than in the Pr form and therefore shows a higher phosphorylation activity in Pfr state (Karniol and Vierstra 2004). Nonetheless, recent autophosphorylation studies of Agp2, revealed no phosphorylation activity for Agp2, which contradict the previous findings (Xue et al. 2019).
Furthermore, temperature can affect the phytochrome function too, particularly the activity of its histidine kinase domain, where it had been demonstrated that Agp1 expresses a higher rate of autophosphorylation at 25°C and by increasing the temperature, the autophosphorylation activity decreased to be almost undetectable (Njimona et al. 2014; Njimona and Lamparter 2011).

1.3 Horizontal gene transfer: Conjugal transfer

A. fabrum has evolved a mechanism in order to transfer genes into wounded plant tissues, which causes the formation of the crown gall tumour followed by a release of amino acids derivatives into the soil – called opines. In addition to the transformation, the conjugation is well characterized in *A. fabrum (La Riva et al. 1998; Lacroix and Citovsky 2019).*

The conjugation mechanism is similar to the plant transformation mechanism; however, some differences can be observed. When plant tissue is wounded the cells release sugars and phenolic compounds, such as acetosyringones. As response to these released substances *A. fabrum* cells detect the wounded plant tissue and move towards it *via* chemotaxis. (Păcurar et al. 2011). Once they enter their plant host, they inject a part of the tumour inducing plasmid pTi termed the T-DNA.

The Vir genes that are involved in this transformation/ infection mechanism, integrate the DNA in its single stranded form and help with its transcription. Furthermore, auxins

and cytokinins will be synthetised, which induce the cells to become irregularly shaped and to form a visible tumour designated “crown gall” (La Riva et al. 1998; McCullen and Binns 2006).

On the other hand, during the conjugation mechanism, the whole pTi will be transferred as single stranded DNA from a donor into another recipient bacterial cell. This mechanism needs a cell-cell contact, for the transfer to be performed.

As for the transformation, several genes and proteins are involved in the conjugation process and only specific types of plasmids are involved. For this process to be performed, plasmids should either be conjugative or mobilizable.

Conjugative plasmids are self-transmissible and code for components with two essential functions; one for plasmid survival and one for the conjugative apparatus, which includes the DNA replication and horizontal spread *(Figure 10)* (Smillie et al. 2010; Llosa et al. 2002).

The horizontal spread occurs during conjugation, if the plasmid carries the mobility genes – MOB genes also called Dtr genes (DNA-transfer replication). MOB genes include three components; OriT, a relaxase and the type IV coupling protein (T4CP).

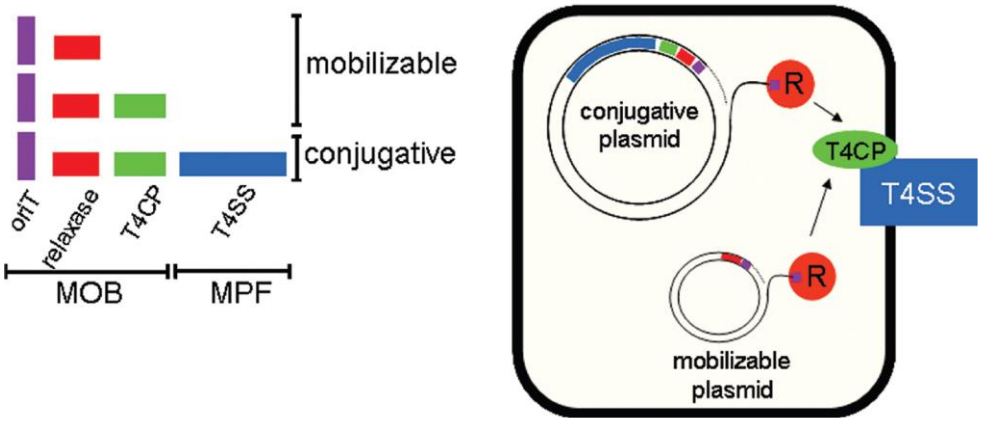

Figure 10: Illustration of the constitution of transmissible plasmids. *Self-transmissible or conjugative plasmids code for the four components of a conjugative apparatus: an origin of transfer (oriT) (violet), a relaxase (R) (red), a type IV coupling protein (T4CP) (green), and a type IV secretion system (T4SS) (blue). Figure is adopted from (Chris Smillie et al., 2010)*

Furthermore, a membrane-associated mating pair formation – MPF complex – a form of Type 4 secretion system (T4SS) is also needed, in order to provide the formation of the mating channel between the donor and the recipient cell *via* the T- pilus (Cabezón et al. 2015; Smillie et al. 2010).

Mobilizable plasmids only contain a MOB module (with or without the T4CP) and need the MPF of a co-resident conjugative plasmid to become transmissible by conjugation (Smillie et al. 2010).

1.3.1 Conjugation mechanism

The conjugation is a DNA rolling circle replication (RCR) system that uses the type IV secretion system (T4SS) (Llosa et al. 2002), enabling a cell-cell contact to deliver the transfered DNA (Christie 2004).

Conjugative plasmids such as pTi in *A. fabrum* carry the machinery needed for the self-transfer. This includes the relaxosome components with a relaxase that recognizes the OriT of the plasmid in the donor cell. The role of the relaxase is to catalyse the DNA cleavage by inducing a nick in the OriT. This nick unwinds the plasmid, to transfer a single stranded DNA into the recipient bacterial cell. Furthermore, the relaxase catalyses the final ligation of the transported DNA and its replication in the recipient cells, to rebuild the conjugated plasmid, in addition to the replication of the remaining strand in the donor cell from its free 3'OH *(Figure 11)* (Llosa et al. 2002).

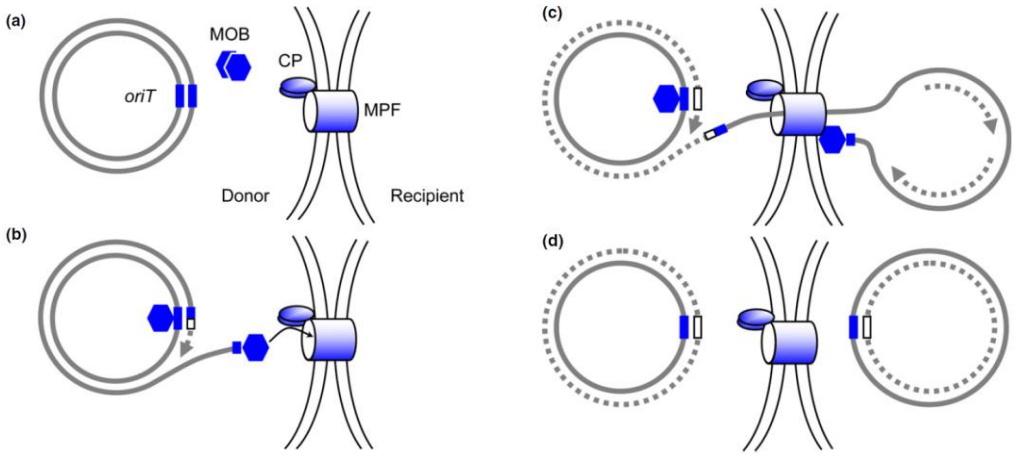

Figure 11:Steps of the conjugal transfer: *It comprises the recognition of the OriT by the MOB genes, which will induce a nick and transfer the single stranded DNA to the recipient cell, where it will be replicated. Figure is adopted from (Bellanger et al. 2014).*

Besides the components of the relaxosome, the T4CP encoded by the genes of the pTi acts with the relaxosome and the MPF proteins to guide the complex DNA-protein toward the T4SS, in order to deliver the DNA across the cell envelope (Llosa et al. 2002). Once it enters the recipient cell, a complementary strand is then synthesized *(Figure 11).*

1.3.2 Tra genes - TraA

For the DNA transfer in both the infection and the conjugation mechanism, pTi harbours the necessary genes. Vir genes are responsible for the transformation mechanism, whereas the Tra genes are supposed to be the genes involved in the conjugation, such as traA-traD and traF-traH. These genes are important for plant transformation, but are also involved in the conjugation, since conjugation shows resemblance with the plant transformation process, where both Vir genes and TraA are involved in the formation of the T4SS (Wood et al. 2001; Jiang et al. 2016; Bai et al. 2016; Lang and Faure 2014).

It was found that Tra genes are not only present in the pTi but some of them are also present in the pAt and in the linear chromosome, mainly the TraA genes (Goodner et al. 2001; Wood et al. 2001; Bai et al. 2016).

Furthermore, based on domain homology with relaxases from other organisms, it is assumed that TraA acts as a relaxase during conjugation (Cho and Winans 2007; Kopec et al. 2005). It was also discovered that TraA and TraG in Agrobacterium are the main proteins that cause the nick in the OriT and guide the substrate to the T4SS. It is assumed that the TraG gene codes for the T4CP and that the TraA protein plays the essential role of a relaxase (Llosa et al. 2002; McCullen and Binns 2006).

The role of the relaxase ensures that the double-stranded Ti plasmid on one strand is broken by its nucleophilic interaction with the phosphate backbone of the DNA, which sets the conjugation in motion. This means, without this break, no conjugation would take place. It is also assumed that TraA has a helicase function, but it is still unclear whether this plays a role in the conjugal process (Kurenbach et al. 2002; Llosa et al. 2002).

1.4 Fluorescence

In order to track biomolecules such as proteins, or amino acids, they should be labelled with a specific marker. These markers could be e.g. colorimetric, electrochemical or even fluorescent labels (Sahoo 2012).
For the following work fluorescence-based methods were used. These methods enable studies of protein – protein interactions, conformational changes, localization of proteins or also the motility and flexibility of proteins (Toseland 2013).

These fluorescence-based experiments require the selection of an optimal fluorescence marker, designated as fluorophore, to monitor definite protein activity.

For intrinsic fluorescence emission, tryptophan is useful to study the folding, conformational dynamics and interactions of a protein (Modesti 2011). Nevertheless, the attachment of an extrinsic fluorophore moiety to the protein of interest is found to be the most adaptable way to label proteins and studies in vitro or in vivo (Modesti 2011). Different types of fluorophores are applied for these purposes including Atto dyes, which showed to be photostable and less sensitive to variable buffer conditions.

1.4.1 Fluorophore properties

When choosing a fluorophore, it is important to consider its excitation and emission cycle. When a fluorophore absorbs a photon, it will be excited to a high-energy singlet state, either the S1 or the S2 state. Nonetheless, the fluorophore can emit light as fluorescence only from the lowest energy level of S1.

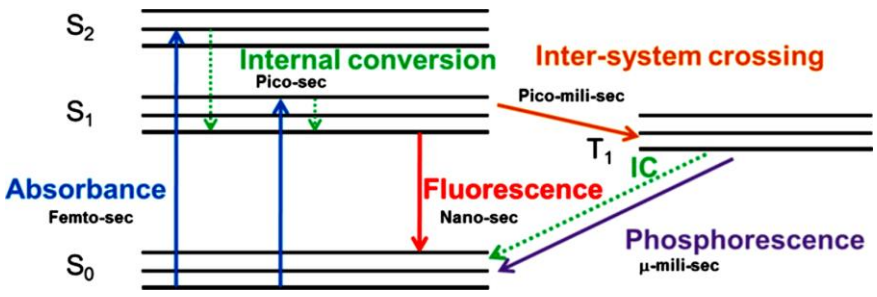

Figure 12: Excitation and emission of a fluorophore. *A modified Jablonski diagram representing the excitation and emission cycle of a fluorophore. Figure adopted from (Toseland 2013).*

Therefore, the molecule must relax to reach the lowest level S1, this process is called nonradiative loss of energy (Toseland 2013).
Another important parameter while choosing a fluorophore is its brightness, which is defined by the quantum yield of its fluorescence emission and its extinction coefficient.

The extinction coefficient (ε) is a measure of the ease, in which a substance absorbs light at a particular wavelength, to enter the excited state. Therefore, a higher extinction coefficient means that a larger amount of light is absorbed (Lambert-Beer law).

On the other hand, the quantum yield is related to the capacity of the substance to emit photons through its fluorescence once they are absorbed and refers to the ratio of the number of photons emitted compared to the ones absorbed.

In addition to the extinction coefficient and fluorescence quantum yield, the fluorescence life time of the fluorophore describes how long the molecule stays in its excited state (Toseland 2013).

1.4.2 Fluorescence labelling

There are different types of fluorescent labels, such as genetically encoded labels (GFP), peptides and protein tags, nanoparticle labels and organic fluorophores. Despite the use of several fluorescent-label methods and techniques, the chemical labelling is of a great interest and allows new types of experiments. They target the thiol groups of cysteine or amine groups, can covalently bind to the molecule of interest and are therefore very suitable for in vivo or in vitro studies (Toseland 2013; Sahoo 2012).

Nevertheless, cysteine labels provide flexibility for choosing the location of the labelling, since they are rare to find in the protein sequences and they should be thus introduced at the region of interest. Among the fluorescent dyes which are highly specific for the thiol groups of cysteines are the so-called maleimide fluorophores, such as the used Atto dyes Atto495, Atto565 and Atto488 used in this work and are highly specific for the thiol groups of cysteines (Toseland 2013).

These maleimide-based dyes are widely used to label proteins for the study of conformational changes, assembly and ligand binding processes (Kim et al. 2008). In addition to studying protein-protein interactions *via* Förster resonance energy transfer, these dyes are used to monitor protein mobility or dynamics by means of time resolved fluorescence anisotropy, also called time-resolved fluorescence depolarization. Nonetheless, the only challenge is the maintenance of the reactive thiol groups in their reduced form and the prevention of their oxidation before the labelling reaction take place, in addition to the removal of unreacted molecules prior to the fluorescence studies (Atto-tec GmbH, Atto catalogue 2016-2018).

1.5 Fluorescence based methods

Different cellular processes and functions in living cells are often manipulated by the action of single proteins or as an ensemble of proteins that could be associated.

To understand the function and the importance of macromolecular assemblies, it is required to gain information about their structures and dynamics (Pengguang and Ludwig 1994).

Several methodologies have been developed for that purpose and are used to investigate either protein dynamics and mobility such as time-resolved fluorescence anisotropy or protein-protein interactions such as Förster (fluorescence) Resonance Energy Transfer (FRET) or Bimolecular fluorescence complementation (BIFC) and have been adapted in a large scale.

1.5.1 Förster resonance Energy transfer

For the operation and identification of biological activities in living cells, proteins can associate with others and possibly assemble in large complexes. Therefore it is important to know if any interaction between proteins occur, to understand its cellular functions (Dilucca et al. 2019).

The basic principle of resonance energy transfer (RET) was first described by Theodor Förster in the late 1940s (Förster 1948). Förster resonance energy transfer is one of the most popular approaches to study protein–protein interactions. It is highly

dependent on the distance between the donor chromophore and the complementary neighbouring acceptor (Söveges et al. 2018).

It is based on a nonradiative transfer of energy *via* Coulombic interactions from a donor chromophore to an acceptor. After electronic excitation, the donor will transfer its excitation energy non-radiatively to a neighbouring acceptor, provided that the chromophores are in close distance and adopt favorable relative orientations (Söveges et al. 2018; Ciruela 2008). The excited acceptor will in turn emit its fluorescence characteristics (a photon), when returning to its electronic ground state.This transfer occurs, only if the distance between the donor and the acceptor ranges between 1-10 nm, depending on the fluorophore, in particular their spectral properties, and their relative orientations (Bajar et al. 2016).

Two types of FRET can be distinguished between differently coloured fluorescent proteins; The intramolecular type, when the donor and acceptor fluorophores are located on the same molecule, and the intermolecular type , is when the fluorophores are located on different molecules, whose interaction is to be analysed (Piston and Kremers 2007). Therefore, for the detection of interactions between proteins of interest using RET approaches, the proteins to be investigated, are fused either to a donor or to an acceptor fluorophore, respectively.

In the case of FRET methodology, a fluorophore will be attached to the Donor, which will be excited with a monochromatic light and if an acceptor fluorophore is in its proximity an energy transfer will occur. As a result of an interaction, the energy transfer will occur, and there will be a reduction in the donor emission and a consequent increase in the acceptor emission.

The FRET efficiency (E_{FRET}) (§ 4.5) is inversely proportional to the sixth power of the Förster distance (r) between the donor and the acceptor chromophore (Piston and Kremers 2007; Ciruela 2008; Lakowicz 2006a, 2006b). Therefore, RET-based techniques can serve as a ‘molecular ruler’ for distance calculations in this range.

1.5.2 Time-resolved fluorescence anisotropy

Fluorescence-anisotropy analysis is a powerful tool and is of importance in biochemical and medical research. For instance, it can be used not only to measure the dynamics of proteins, but also to quantify protein denaturation, which results in an increase of the flexibility of the peptide backbone or protein interactions with macromolecules, which changes the overall rate of rotation (Lakowicz 2006b)

The term anisotropy (r) measures the depolarization of the fluorescence emission, when a sample is excited by linearly polarized light. This depolarisation is usually due to different orientations of the molecule or the molecular rotation that is caused by Brownian motion. Brownian motion is considered as a random, uncontrolled movement of particles in a fluid as they constantly collide with other molecules or as a result of their tumbling (Lakowicz 2006b; Mitchell and Kogure 2006)

For time-resolved fluorescence Anisotropy measurements, it is always in need of a fluorophore that is bound to the molecule or protein of interest. Fluorophores have transition moments for absorption along a definite direction in the molecular axis and are randomly oriented in a solution. Preferably they absorb light in a parallel direction to their absorption transition dipole. For this reason, when a sample is excited, only molecules with absorption dipoles parallel to the electric vector of the incident light, will be excited, corresponding to the phenomenon called photoselection.

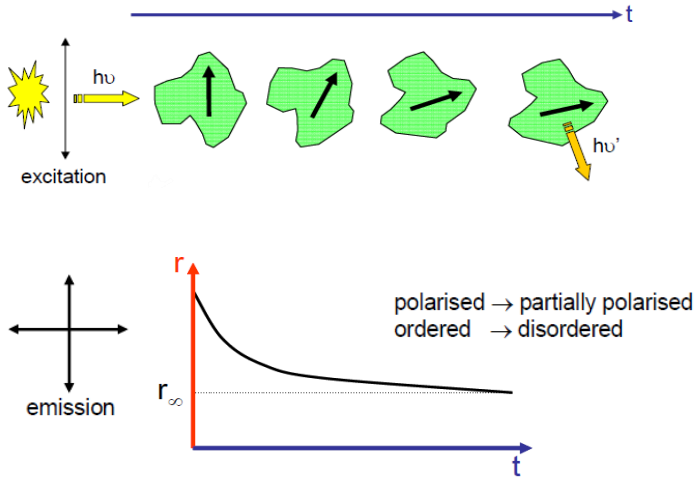

Figure 13: Illustration of the molecular rotation and the resulting anisotropy decay: *After the excitation of the molecule with the parallel vertically polarised light, the Brownian motion causes the rotation of the molecule, which in turn causes the anisotropy to decay with the time, from a r_0 value to a r_∞ corresponding to the shift towards the depolarisation of the light and the disorder (HORIBA Scientific 2020b- Technical note TFRT-2)*

Hence, in case of a rotation, these transition moments of the fluorophore can change their direction, causing a depolarization of the emission after excitation (Lakowicz 2006b).
Time-resolved fluorescence anisotropy measurements are based on the excitation of the fluorescence dye by means of a pulsed polarized light and the detection of the emission of the fluorescence at different polarization angles, thus reporting the average of the angular displacement of the fluorophore that happens between the absorption and the subsequent emission of a photon, after excitation of the fluorophore (Lakowicz 2006b; Jiang et al. 2016).

This angular displacement depends on the rate of the rotation during the lifetime of the exited state of the fluorophore. This molecular motion depends on various environmental factors, such as the viscosity of the solvent used, as well as the shape and the size of the rotating molecule. Hence the fluorescence anisotropy can provide either information concerning the molecular size or the mobility of the molecule (HORIBA Scientific 2020a, 2020b). Therefore, the anisotropy is related to the degree of this displacement or randomization and the kinetics of the process is defined as $r_{(t)}$;

$$r_{(t)} = r_{(\infty)} + r_0 \exp(t/\tau)$$

It thus shows the highest value at the moment of excitation and corresponds to r_0 at t_0. Depending on the polarization degree, it decreases in time to reach either zero or r_∞. The later refers to the residual anisotropy and describes the level of the lost anisotropy characteristics due to dipole reorientation. The depolarization time τ describes the decay time of the depolarization (rotational correlation time) and *t* corresponds to the time of the respective measurement (Jiang et al. 2016; Smith et al. 2017; Smith and Ghiggino 2015) (see also § 4.6.1).

Nevertheless, these anisotropy kinetics cannot be recorded directly, but they derive from the fluorescence decays of the parallel and perpendicular polarized emissions (Kapusta et al. 2003; Jiang et al. 2016).

Hence, fluorescence anisotropy measures the polarisation degree of the fluorescence emission. Using a Time-Correlated Single Photon counting spectroscopy (TCSPC) technique, it is possible to measure the time-resolved anisotropy, by monitoring the

parallel and perpendicular planes of polarised emission, allowing the path from the order to disorder (Peter Kapusta 2002; HORIBA Scientific 2020a).
This technique can be used to describe various time-dependent processes. It allows the determination of the dynamics of the dipole moment of the fluorophore bound to the molecule (protein) of interest, by measuring the time-dependent polarisation degree of the fluorescence emission. This enables the investigation of the intramolecular dynamics of the molecule of interest, thus allowing to study the movement of individual segments or domains within the entire molecule.

Another technique used for the time-resolved fluorescence anisotropy is the Fluorescence Correlation Spectroscopy (FCS), which is a correlation analysis of temporal fluctuations of the fluorescence intensity (Schwille and Haustein), and allows to study dynamic and hydrodynamic properties of biomolecules. Thus, it enables the determination of the size of proteins or molecules used, through the measurements of diffusion coefficients and hence the hydrodynamic radius R_h of the probed molecule (Schwille and Haustein).

Both techniques are very prominent to detect the fluorescence fluctuation in the observation volume, since they record temporal changes in the fluorescence intensity of the emission that is caused by the fluorophore. These changes are then quantified depending on their strength and duration by autocorrelating the recorded signals. This leads to the average number of the fluorescence particles and their average diffusion time through the detection volume. Hence, it is possible not only to study the dynamics (see also § 4.6) and conformational changes but also to determine the size, aggregation, and the concentration of the probed molecule (Schwille and Haustein).

2 Aim of the project

The translation of environmental signals into cellular responses is a crucial process in all forms of life. The light signal transduction in bacterial phytochromes has gained interest in research nowadays, to reveal information about the function of phytochromes in terms of regulating physiological processes. Various hypotheses were discussed recently involving the mechanism of the light-stimulated signal transduction. However, the underlying molecular mechanism is yet not fully understood.

To address this challenge and to comprehend the signal transduction of a bacterial phytochrome system, biophysical and biochemical approaches were combined to examine the function of phytochromes of *A. fabrum* in this process on a molecular level.

First knowledge about conformational changes of bacterial phytochromes upon light induction has already been obtained. Furthermore, it has also been demonstrated that phytochromes down regulate the tumour induction in Arabidopsis roots (Rottwinkel 2011; Lamparter et al. 2017), in addition to their regulation of the conjugation mechanism in a light dependent manner (Lamparter et al. 2017; Bai et al. 2016) and that the histidine kinase domain shows an effect on this mechanism (El Kurdi 2016).
For a better understanding of the signal transduction pathway in *A. fabrum* and its phytochrome system, this project has combined *in vitro* and *in vivo* studies.

The *in vitro* studies *via* fluorescence-based methods were performed, using several mutants of Agp1 phytochrome, where specific amino acids at different positions were mutated, enabling the fluorescence labelling.
In the first step, the signal transmission *via* the kinase activity of these Agp1 mutants was investigated. This was mainly to detect, if the phosphorylation yield at specific positions is light regulated and if it is influenced by these mutations. This trial has served then as control for further investigation by means of biophysical approaches.

Secondly, it is well known how the motion of proteins and their conformational dynamics are crucial to gain insights into their function that regulates various cellular

mechanism. In addition to the fact that the transmission of the signal in *A. fabrum* is mediated *via* its phytochromes, which may involve changes in the arrangement of their subunits, it was relevant to gain insights into the dynamics of these phytochromes upon photoconversion. For this purpose, the dynamics of Agp1 phytochrome was investigated *via* time-resolved fluorescence anisotropy, hence investigating if any changes in the dynamic could occur upon photoconversion at definite positions in the protein domains.

Furthermore, knowing that phytochromes may act together influencing several processes and cellular mechanisms such as conjugation (Bai et al. 2016), in addition to the infection mechanism in plant cell or biochemical processes such as autophosphorylation (Xue et al. 2019), interaction studies using Förster Resonance Energy Transfer (FRET) technique, were performed between both Agp1 and Agp2 phytochromes in order to investigate their interaction possibility.

Finally, a further method in order to understand the signal transduction pathway in *A. fabrum* was to test the conjugation process *in vivo*. Computational studies suggest that the relaxase (Kopec et al. 2005; Kurenbach et al. 2002), named TraA, is involved in this process and plays an essential role in initiating the conjugal transfer. Since *A. fabrum* contains three TraA protein encoded on the linear chromosome, pAt and pTi, in addition to the published conjugation results without pTi (Bai et al. 2016), knockout studies of the TraA gene encoded on the pTi were performed, to characterize its role in the light regulated conjugation.

3 Materials

If not mentioned the used chemicals are obtained from Sigma-Aldrich, or Carl Roth (Karlsruhe, Germany) and the molecular biology reagents and enzymes from New England Biolabs (NEB, Frankfurt, Germany).

3.1 Plasmids and constructs

Several plasmids were used as cloning vectors such as pJQ200SK and pGEM-T easy vectors. Others were used to introduce mutations by means of site directed mutagenesis – pQE-Agp1 or pQE-Agp2 or just to amplify sequences for knockout experiments. Furthermore, the mobilizable plasmid pBin-Gus was used in order to perform and observe the conjugation analysis, and it was already incorporated in the *A. fabrum* cells in previous research.

Table 1: *List of the used vectors and constructs*

Plasmid	Resistance	Reference
pET21b - TraA	Amp	Peng Xue
pGEM-T easy vector	Amp	Promega
pJQ200SK	Gen	Lab stock
pBin-Gus	Kan	Y. Bai
pQE12-Agp1 (pAgp1)	Amp	Lamparter et. al 2012
pET21b -Agp2 (pAgp2-M1)	Amp	Inomata et al. 2005

Furthermore, different constructs were used for the protein expression and purification of Agp1 and Agp2 either wt or mutants.

Table 2:*List of the used constructs for protein expression and purification*

Plasmids	Features	Reference
pAgp1	**Agp1-wt**	**Lab stock**
pAgp2 – M1	**Agp2-wt**	**Lab stock**
pAgp2-M2	**Agp2-PCM**	**Lab stock**
pAgp1-M15	**Agp1-PCM**	**Lab stock**

Plasmids	Features	Reference
pAgp1-M505	SDM A362C	I.Njimona
pAgp1-S122C	SDM S122C	I.Njimona
pAgp1-M505-kurz	SDM A362C-PCM	N. Wunsch
pAgp1- M406	SDM K517C	I.Njimona
pAgp1- M429	SDM H528C	I.Njimona
pAgp1- M430	SDM R535C	I.Njimona
pAgp1- M504	SDM K554C	I.Njimona
pAgp1- R603C	SDM R603C	I.Njimona

3.2 Bacterial strains

In this work, two types of strains were used, either for the transformation purposes such as *E. coli* or *A. fabrum* C58 for conjugation assay in addition to its phytochromes knockout mutants. These strains were used as donor strains, where the gene TraA of the pTi was knocked out *via* homologous recombination (see § 4.7).

3.2.1 Agrobacterium *fabrum*

Table 3: *List of used A. fabrum strains for transformation and conjugation experiments*

Strain	Genotype	Reference
Wt-Ti	C58 Wt	Y. Bai
Agp1$^-$-Ti	C58 ΔAgp1 - Transformation	Y. Bai
Agp2$^-$-Ti	C58 ΔAgp2	Y. Bai
Agp12$^-$-Ti	C58 ΔAgp1/Agp2	Y. Bai
TraA$^-$	C58 ΔTraA – Donor strain	This work
Agp1$^-$/TraA$^-$	C58 ΔAgp1 ΔTraA – Donor strain	This work
Agp2$^-$/TraA$^-$	C58 ΔAgp2 ΔTraA – Donor strain	This work
Agp12$^-$/TraA$^-$	C58 ΔAgp1/Agp2 ΔTraA – Donor strain	This work
Wild type (wt)	C58 Wild type – Recipient strain	Lab stock

3.2.2 Escherichia Coli

Table 4: *List of used E. coli strains for transformation experiments*

Strain	Genotype/ Condition	Reference
DH5 α	Heat competent LB, 37°C	NEB
XL1-Blue	Heat competent LB, 37°C	NEB
BL21	Heat competent LB, 37°C	NEB

3.3 Bacterial growth media and buffers

All necessary media were prepared using distilled pure water autoclaved for 20 min at 121°C. The used liquid LB media were prepared using LB-medium powder from Roth with a final concentration 20 g/l. For the solid LB-Media 15 g/l agar was added to the medium before autoclaving. The media were used with appropriate antibiotic or selection constituents according to the experiments that were conducted.

Table 5: *List of used media and buffers and their composition*

Agrobacterium tumefaciens **minimal medium (ABMM)**	
K_2HPO_4 * 3 H_2O	3 g/l
NH_4Cl	1 g/l
KCl	0.15 g/l
$FeSO_4$ * $7H_2O$	2.5 mg/l
NaH_2PO_4 * 2 H_2O	1 g/l
$MgSO_4$ * $7H_2O$	0.3 g/l
$CaCl_2$ * H2O	0.01 g/l
Glucose, H_2O free	5g/l

Buffers	
SYBR Safe® - Stock solution – Invitrogen	10000 x
Agarose gel electrophoresis 1%	
Electrophoresis running buffer (0.5 x TAE)	
Tris-Acetate	20 mM
EDTA	0.5 mM
pH	8.3
Loading buffer (5x)	
Glycerine	50 %
Bromophenol blue	0.05 %
Xylene cyanole	0.05 %
SDS gel electrophoresis	
Separation gel (10%)	
30 % Acrylamide	8.2 ml
Separation Buffer (1,5 M Tris/HCl, 0,6 % SDS, pH 6,8)	6.2 ml
ddH_2O	10.3 ml
TMED	108 µl
APS	215.9 µl
Stacking gel (4%)	
30 % Acrylamide	1.3 ml
Stacking buffer (0,5 M Tris/HCl, 0,6 % SDS, pH 6,8)	2.3 ml
ddH_2O	6.2 ml
TEMED	52.8 µl
APS	105.7 µl

Running buffer	
Glycine	200 mM
Tris	25 mM
SDS	0.15%
Comassie brilliant blue	
Acetic acid	10 %
Methanol	50 %
Brilliant Blue	0.04%
Destainer	
Acetic acid	10 %
Ethanol	30 %
Buffers for protein expression and purification	
Basis buffer – pH 7.8	
Tris	50 mM
EDTA	5 mM
NaCl	300 mM
AS Buffer without EDTA – pH 7.8	
Ammonium sulfate	3,3 M
Tris	50 mM
AS Buffer with EDTA – pH 7.8	
Ammonium sulfate	3,3 M
EDTA	5 mM
Tris	50 mM

Low-Imi Washing buffer – pH 7.8	
Tris	50 mM
Imidazole	10 mM
NaCl	300 mM
Cholic acid	100 mg/l
Washing buffer without Imidazole – pH 7.8	
Tris	50 mM
NaCl	300 mM
Cholic acid	100 mg/ml
Low-Imi, high NaCl Washing buffer – pH 7.8	
Tris	50 mM
Imidazole	200 mM
NaCl	300 mM
Cholic acid	100 mg/l
High-Imi Elution buffer – pH 7.8	
Tris	50 mM
Imidazole	200 mM
NaCl	300 mM
Cholic acid	100 mg/l

3.4 Antibiotics

For the selection and maintenance of bacterial strains, several antibiotics with the following final concentrations were used either separately or combined.

Table 6: *List of used antibiotics and their concentrations*

Antibiotic	Use	Concentration
Ampicillin	*A. fabrum* recipient strain, pGEM T vector, pAgp1 and pAgp2 strains	100 µg/ml
Gentamycin	PJQ200SK	50 µg/ml
Kanamycin	*A. fabrum* donor strains	50 µg/ml

3.5 Enzymes

For the different purposes in this work, several enzymes were used, such as restriction enzymes, ligases, or various polymerases. These were used either for the preparation of constructs or to perform PCR-based methods.

Table 7: *List of used enzymes*

Enzyme	Use
XbaI/ XhoI	To introduce restriction sites for the preparation of the TraA$^-$ construct
DpnI	Restriction enzyme used to digest the methylated DNA fragments after SDM and ligation
T4-DNA-Ligase I	Ligase
PfuTurbo® Polymerase	For SDM
Q5 /Taq Polymerase	DNA-Polymerase used for amplification of desired sequences

3.6 Primers

Different primers were used for different purposes, either for the cloning processes, the introduction of the point mutation by means of SDM, for the amplification and for sequencing. The sequencing took place through GATC (Konstanz, Germany) using the prepared primers.

Primer codes with an impair number correspond to forward primers, whereas the primers with a pair number are reverse primers, unless mentioned otherwise.

Table 8: *List of used Primers for amplification, sequencing and SDM*

Code	Sequence	Goal
Bai01 **Bai02**	TCACGGTACAGATTTTCC TTAGCCCTGAGCCTGATT	Amplification of pTi
Bai03 **Bai04**	TCAGCGCGAAGTCTTT GTCGCGAGTGAAGATC	Amplification of pBin-Gus
A/L 1 **A/L 2‘**	TCGCAGAGGTCAATGTTCCC CGAACCAGCTGGCCGTC	Amplification of pET21b, without TraA
A/L 3 **A/L 4**	TTAGGTGGCGGTACTTGGGT ATGTTACGCAGCAGCAACGA	Amplification of Gen
A/L 5 **A/L 6**	CTCGAGATGGCCATCGCCCACTTCTC TTGTTTCAGCACCGGTGCCTTCTAG	Amplification Genta-Insert
A/L 7 **A/L 8**	TATCTAGAATGGCCATCGCCCACTT ATCTCGAGTTGTTTCAGCACCGGTG	Amplification of $TraA^-$ construct
Seq 4 **Seq 5**	CATGGATTTGACTTGGTCAGGG CATTGCCACCGCGCTCATC	Sequencing of construct

Table 9: *Primers used for the introduction of a serine residue instead of the cysteine in Agp2 at the indicated positions*

Code	Sequence	Goal
T01 **T02**	AACCGCATGGCTCCCTCATCGCCTCCGATAACGC GCGTTATCGGAGGCGATGAGGGAGCCATGCGGTT	C29S/ C33S
T03 **T04**	GCATTCCGAAAACTCCGGCGAACTGCTGGGACTT AGTCCCAGCAGTTCGCCGGAGTTTTCGGAATGC	C42S
T05 **T06**	GTCTCGCCCATCCATTCCGAATATCTCCGCAATAT ATATTGCGGAGATATTCGGAATGGATGGGCGAGA	C249S
T07 **T08**	CCGATCTGATGCCCTCCGACGGTGTC GACACCGTCGGAGGGCATCAGATCGG	C277S
T09 **T10**	CCGATCTGATGCCCTCCGACGGTGTC GACACCGTCGGAGGGCATCAGATCGG	C353S

4 Methods

4.1 Microbiological methods

4.1.1 Cultures and Storage

For the protein purification, bacterial strains were first plated on agar plates with Amp and incubated at 37 °C and single colonies were used for further preparations or preparation of overnight cultures.

*A. fabrum b*acterial strains used for conjugation, were also first plated on agar plates with the correspondent antibiotics for donor or recipient strains and incubated at 28°C for 1 or 2 days or until colonies appeared, depending on the type of the strain used.

New cultures using 500 µl of the overnight culture were mixed with 500 µl of 50% glycerine, and deep frozen using liquid nitrogen then stored at -80°C for next use.

4.1.2 Preparation of competent cells

For this work both *E. coli* and *A. fabrum cells* were used, which were made competent either by means of electroporation or heat chock.

For the transformation of the TraA construct and the Agp2 SDM mutant strains, the heat competent cells DH5α and BL21 strains were used and were purchased directly from NEB.

For the conjugation assay, electrocompetent cells of *XL1-blue* and *A. fabrum* (wt, *Agp1*$^{-}$, A*gp2*$^{-}$ and *Agp12*$^{-}$) strains were prepared. First cells were cultivated in 5 ml LB medium containing the appropriate antibiotic and incubated overnight at 37°C or 28°C, respectively. Two ml of the overnight culture were incubated again in 100 ml LB medium including the respective antibiotic till the cells reached an optical density OD_{600} of 0.3 – 0.4. The culture was set on ice and centrifuged to recuperate the pellet. Several washing steps were then performed, two times with 10 ml ddH_2O and then one time with 10 ml 10% glycerine. Finally, the pellet was re-suspended in 1 ml 10% glycerine

and divided in 100 µl aliquots. Cells were then frozen using liquid nitrogen and stored at -80°C for further electro-transformation procedures.

4.2 Molecular biology methods

4.2.1 Bacterial transformation

For the bacterial transformation, either a heat shock or an electroporation method was used. The heat shock transformation was used for the transformation of the construct in pGEM T easy vector and for the Agp2 SDM mutants in *E. coli* strains. Whereas the electroporation was used for the transformation of pET21b-TraA$^-$ construct into *E. coli* and pJQ200SK-TraA$^-$ construct into various *A. fabrum* donor strains.

- **Heat shock transformation**

100 µl of the frozen *E. coli* bacterial cells were incubated on ice for 10 min, then were gently mixed with 5-10 µl desired Plasmid or ligation construct and incubated for 25 min on ice. Heat shock at 42°C for 45 sec then directly placed on ice for 2 min. 950 µl LB or SOC medium was then added and incubated 1-2h h at 37°C. The culture was then centrifuged for 3 min at 5000 g and 950 µl of the supernatant was subsequently discarded. Finally, the pellet was dissolved and plated on the correspondent agar plate containing the corresponding antibiotic and incubated at the appropriate temperature overnight.

- **Electroporation**

Bacterial cells were mixed with 2-5 µl of the plasmid solution and incubated for 10 min on ice together with the electroporation cuvette (1 mm electrodes spacing; Peqlab Biotechnology GmbH, Erlangen, Germany). The pre-protocols for *E. coli* and for *A. fabrum* were used, respectively.

Right after the pulse (1,8/ 2,4 kV; 5 ms), 950 µL LB Medium were slowly added to the cells. After incubation for 1-2 h at the respective temperature, the culture was centrifuged for 3 min at 5000 g and 950 µl of the supernatant was discarded. Finally,

the pellet was dissolved and dropped on the correspondent plate with the appropriate antibiotic and incubated over night at the respective temperature.

Table 10: *Pre-protocols used for the electroporation in both E. coli and A. fabrum*

Pre-protocol	***E. coli***	***A. fabrum***
Voltage (V)	1800	2400
Capacitance (µF)	25	25
Resistance (Ω)	200	200
Cuvette (mm)	1	1

4.2.2 Polymerase chain reaction (PCR)

The polymerase chain reactions were either used for amplification purposes or for site directed mutagenesis (SDM).

On one hand the PCR reaction was used in the intent to introduce single mutations in the Agp2 phytochrome *via* SDM and on the other hand for the amplification of specific segments for the preparation of the TraA$^-$ construct, which was used for the conjugation assay. Therefore, a Gentamycin resistance cassette was amplified from pJQ200SK and a fragment containing 500 bp of TraA at both ends was amplified from pET21B-TraA. In addition, the PCR reactions were used as a control to verify the presence or absence of the desired DNA sequence.

4.2.2.1 PCR based site directed mutagenesis

In vitro site- directed mutagenesis is used to create a specific mutation in a gene using a PCR-based method *via* amplification followed by a transformation.

SDM was used to introduce a point mutation in the Agp2 protein, replacing a cysteine residue with a serine.

For this purpose, the forward and reverse primers were designed to include the point mutation. After the PCR reaction, the restriction endonuclease *DpnI,* which targets the methylated DNA sequences, was used for the cleavage of the template DNA. Ultimately the PCR product was transformed in DH5α or BL21, where the plasmid will completely circularize (*Figure 14*).

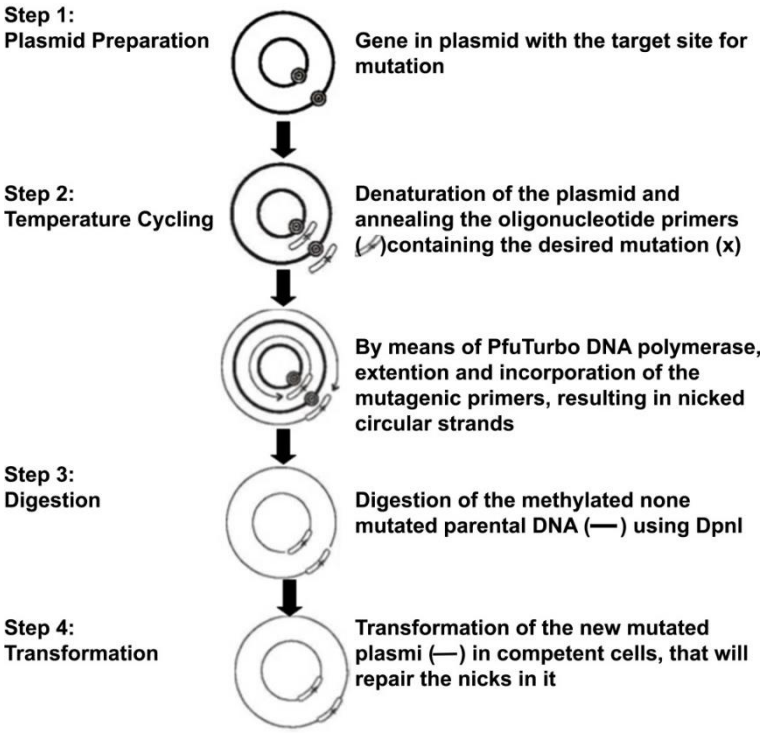

Figure 14: *Schematic illustration of the site directed mutagenesis mechanism. Quick change® site-directed mutagenesis kit.*

- **SDM PCR Program**

Table 11: *PCR based SDM programme*

Step	Temperature	Time
Pre-denaturation	95°C	30 sec
Denaturation	95°C	30 sec
Annealing	55°C	60 sec
Elongation	68°C	8 min
After-Elongation	68°C	10 min
Hold	14°C	10 min

- **SDM PCR reaction**

The Pfu DNA polymerase buffer and PfuTurbo® polymerase were used for this purpose and were purchased from Agilent Technologies, USA.

Table 12: *PCR based SDM reaction protocol used with pAgp2 vector*

Components	**Volume**
Template (10–50 ng/µl Plasmid)	1 µl
10x *Cloned* Pfu DNA *polymerase buffer*	5 µl
5 mM each dNTP Mix	1 µl
Forward primer	1.25 µl
Reverse primer	1.25 µl
2.5 U/µl PfuTurbo® Polymerase	1 µl
DMSO	0.75 µl
ddH2O	13.75 µl

4.2.2.2 Standard PCR reaction

Standard PCR reactions were used for the generation of the desired segments for the TraA knockout approach or as a control for the prepared plasmid fragments. For this approach, Gen cassette was amplified from the pJQ299SK using phosphorylated primers and a segment from pET21b-TraA, that contains only 500 bp of the TraA gene from each side.

The phosphorylation reaction of the primer was incubated at 37°C for 30 min and used for the amplification of the Gen resistance cassette.

***Table 13**: Phosphorylation reaction of the primers used for the amplification of Gen cassette.*

Components	Volume
T4 – DNA – ligase buffer	5 µl
Primers (10 µM)	5 µl
ddH_2O	14 µl
T4 - kinase	1 µl

***Table 14:** PCR reaction used for the Gen and TraA knockout fragment amplification*

Components	Volume
***Template* (10–50 ng/µl Plasmid)**	1 µl
10x Q5 buffer	2.5 µl
5 mM *each* dNTP Mix	0.5 µl
Forward Primer (10 µM)	1 µl
Reverse Primer (10 µM)	1 µl
5 U/µl Q5 polymerase	0.125 µl
ddH2O	To 25 µl

- **PCR Program**

The following table indicates the program used to perform the PCR reaction. However, different annealing temperatures and elongation times were used, depending on the annealing temperature of forward and reverse primers used and the length of the sequences to be studied. The exact annealing temperature and elongation time are presented in table 15.

Table 15: *General PCR program used in the various approaches*

Step	Temperature	Time
Pre-denaturation	95°C	5 min
Denaturation	95°C	30 sec
Annealing	variable	30 sec
Elongation	68°C	variable
After-Elongation	68°C	5 min
Hold	14°C	10 min

Table 16: *Annealing temperature and elongation time*

Primers	Tm	Sequence / length	Time
A/L 1/2	68°C	6000 bp	2 min 30 sec
A/L 3/4	69°C	500 bp	20 sec
A/L 7/8	72°C	1500 bp	1 min 30 sec
A/L 9/10	72°C	1500 bp	1 min 30 sec

4.2.3 DNA restriction double digestion

The double digestion was used in the course of the conjugation project, for which the restriction enzymes *XbaI* and *XhoI* were used, to allow a subsequent ligation of the TraA construct with the pJQ200SK.

Table 17: *pJQ200SK and pGEM-T-TraAKO double digestion protocol*

Components	Volume
ddH2O	To 50 µl
CutSmart buffer	5 µl
Plasmid 0,25-1 µg DNA	1 ng
XbaI	1 µl
XhoI	1 µl

The mixtures were incubated for 3 h at 37°C, inactivated at 80°C for 10 min and subsequently analysed using gel electrophoresis, where the adequate DNA bands – pJQ200SK and TraA$^-$ construct – were then extracted from the gel and ligated.

4.2.4 DNA-Ligation into pGEM-T easy vector and pJQ200SK

Ligation was used in the conjugation assay, where first the construct was prepared in pET21b containing the knocked out TraA that was ligated with the Gen resistance, to gain the construct TraA-Gen-TraA. This construct was then ligated with the pGEM-T easy vector and afterwards with the pJQ200SK, after its digestion from the pGEM-T vector using the same restriction enzymes used to cleave the pJQ200SK vector.

The the appropriate amount of insert in order to obtain (insert : vector) ratio of 3:1 using 50 ng of the vector was calculated according to following formula:

$$m\ (insert)[ng] = \frac{m\ (vector)\ [ng] * \ length\ of\ Insert\ [kb]}{length\ of\ vector\ [kb]} * \frac{3}{1}$$

Table 18: *Ligation protocol of Agp1H528R with pJQ200SK suicide vector*

Components	**Volume**
ddH2O	to 20 µl
10x ligation Buffer	2 µl
pJQ200SK	50 ng
TraA$^-$	37,5 ng
T4 DNA ligase	1 µl

The ligation sample was then incubated at 16°C overnight and before the following transformation it was deactivated by 65°C.

4.2.5 Agarose gel electrophoresis

PCR products were analysed using a 1% (w/v) agarose gel that was prepared with 0.5% TAE. In Order to make the bands visible, samples were mixed with (1:2) of 5x loading buffer and SYBR Safe was added with a final concentration of 1:2000 (v/v) to the liquid gel. For the identification of the bands, 1 kb DNA ladder was used. The fractioning of the nucleic acids was carried out at a 100V voltage for 30 min. The gel was finally analysed by means of a Safe Imager blue light Transilluminator.

4.2.6 DNA-plasmid preparation

- **Extraction of plasmids from *E. coli***

After transformation in *E. coli*, the prepared plasmids were extracted for further use. Hence, one clone had to be picked and cultivated in 5 ml LB at 37°C overnight.

4 ml of the overnight culture were used for the extraction process. This was done by means of the Roti®-Prep Plasmid MINI Kit (Carl ROTH GmbH & CO, Karlsruhe, Germany), according to the indications given by the manufacturer. Plasmids were then stored at -20°C for next use.

- **Gel extraction of PCR-products**

For the preparation of the TraA$^-$ construct, the amplified DNA sequences *via* PCR and used for further ligation and molecular cloning procedures, were extracted, and purified from the agarose gel with the aid of NucleoSpin Extract II Kit (Macherey-Nagel, Düren, Germany) according to the indications provided by the manufacturer.

- **Concentration and quality determination of nucleic acids**

Nucleic acid concentration was measured using a NanoDrop ND-1000 spectrophotometer. For that, 1 µl of the sample was used and the purity of the nucleic acids was determined through the quotient E_{260nm}/E_{280nm}.

4.3 Biochemical methods

4.3.1 Sodium Dodecyl Sulfate gel electrophoresis (SDS-PAGE)

SDS PAGE was used in combination with different experiments in the course of this project. For instance, during protein purification, for the detection of free Atto after labelling of Agp1 used in the time-resolved fluorescence anisotropy and throughout the autophosphorylation assay.

Samples were first denatured by adding 3x of loading buffer and incubated at 95 °C for 10 min. The samples were then centrifuged at 9000 x g prior to loading on the gel. Colorplus Prestained protein marker was used to estimate the molecular weight of the used protein. The electrophoresis gel was run in a mini-PAGE chamber at 25 mA per gel for 1-2 h filled with running buffer. For the visualization of the band, the gel was stained with coomassie brillant blue solution for 1h and subsequently de-stained with a destainer. In case of the fluorescence detection of the protein bound to the Atto dye, the gel was examined using Safe Imager Transilluminator (Safe Imager blue light transilluminator, Invitrogen, Karlsruhe, Germany) prior to the colouring with the Coomassie.

4.3.2 Western blot

For the detection of the phosphorylation, proteins were transferred onto a PVDF membrane as described by Towbin (Towbin et al., 1979).

Prior to the electroblotting, the membrane was activated with 100% MeOH for 2 min and then equilibrated with transfer buffer (14, 4 g/l Glycine, 12.07 g/l Tris-HCl, 20% MeOH) for 15 min. The blotting filter papers were also soaked in the transfer buffer for 15 min.

The gel was then placed on the activated PVDF membrane that was placed between 8 pieces of blotting paper. First, two layers of the filter paper were placed on a blotting system (Biorad, München, Germany). The prepared membrane was then placed on top, and the SDS separating gel on which the proteins were located, was carefully placed on the membrane. Finally, two layers of the filter paper were additionally placed on the gel. The blot was executed for 30 minutes at 10V.

4.3.3 Protein expression and purification

For the fluorescence-based assay, Agp1 and Agp2 wt proteins, either in their full length, or just using the PCM part, as well as several mutants, were first expressed and then purified as apoproteins. The corresponding vectors of these proteins encode for proteins with a His-tag at their C-terminus and were all expressed in the *E. coli* expression strain XL1-Blue in the case of Agp1 or in BL21 in case of Agp2.

Bacterial strains with the desired expression vector were cultivated in 3 l LB medium with 0.3 mM Amp at 37 °C until the cell density reached an $OD_{600\ nm}$ of 0.6 – 0.8.

Protein expression was induced by IPTG (isopropyl-1-thiol-β-D-galactopyranoside) with a final concentration of 300 µM and incubated at 18°C till the cell culture reached an $OD_{600\ nm}$ of ~2; subsequently the cells were harvested. The cells were centrifuged at 9000 x g for 10 min at 4°C and the pellet was washed in 200 ml basis buffer and centrifuged again at 9000 x g for 10 min. The resulting pellet was suspended in 20 ml extraction buffer.

Cells were afterwards lysed using a French Pressure Cell Press, applying a max pressure of 1000 psi. The lysed cells were centrifuged at 12000 x g for 30 min in order to recuperate the soluble protein in the supernatant. The latter was precipitated using 50% of ammonium sulphate without EDTA for full length proteins and 66% of Ammonium sulphate for the shorter protein mutants Agp1-PCM, Agp1A362C-PCM and Agp2-PCM.

The pellet was then dissolved in washing buffer and the sample was centrifuged again. The resulting supernatant was loaded to a nickel affinity chromatography column (Qiagen, Hilden Germany), which is able to bind the His-tagged proteins to finalize the purification process. The Nickel column was first equilibrated with 200 ml water, followed by 200 ml washing buffer. The loaded column was then washed with 1 l washing buffer, then with 300 ml low-Imi high NaCl buffer and finally with 2 l washing buffer until all the unspecific and non-bound proteins were washed out of the column. The apoprotein was eluted with the elution buffer. The elution steps were followed by measuring the absorption at 280 nm of various aliquots using an Eppendorf biophotometer. The elution pool was precipitated by mixing it with an equal volume of ammonium sulfate buffer with and centrifuged at 12000 x g for 20 min. The resulting

pellet was dissolved with 1 – 2 ml basic buffer, centrifuged again. Finally, the supernatant was divided into 100 µl aliquots, frozen in liquid nitrogen and stored at -80 °C for further use.

Both Agp1 and Agp2 proteins were essentially pure after purification, which was confirmed through evaluation of the SDS-PAGE results. Their concentrations varied between 0,1 – 0,4 mM. The purified proteins were then used for the assembly and the labelling process as described later.

4.3.4 Preparation of Biliverdin for the assembly

For the assembly of the apoproteins Agp1 and Agp2, biliverdin BV (Sigma-Aldrich, Munich, Germany) was pre-purified by loading BV in aqueous solution to 1 mL Sep-Pak C18 cartridges (Waters, Milford, MA, United States). The column was washed several times with water and the BV was eluted with methanol. The eluate was incubated overnight at 60°C in a spin Vacuum. BV was then finally dissolved in DMSO and stored at -80°C for further experiments. In the resulting solution, the concentration of BV was obtained by measuring the absorption at 696 nm in methanol/HCl using the extinction coefficient of 30.8 mM^{-1} cm^{-1}. The concentration of the BV stocks varied between 10 - 24 mM.

4.3.5 Preparation of the holoproteins and their labelling

The assembly and labelling assays were performed under green safety light, where the phytochromes Agp1 and Agp2 have their dark-adapted Pr and Pfr form respectively.

- **BV assembly**

All the apoproteins used, had a starting absorption A_{280nm} of ~1 that corresponds to ~ 10 µM for Agp1 and 12 µM for Agp2 using the corresponding extinction coefficient *(§ 4.4.2, Table 19).*

The holoproteins Agp1 or Agp2 were first reduced using 10 mM of TCEP (tris(2-carboxyethiyl) phosphine) for 30 min at RT. BV was added three times successively in

equimolar amounts corresponding to ~ 10 µM and the solution was incubated each time for 5 min at RT followed by 15 min on ice. In total BV was added in an approximately 3-fold molar excess (30 µM) to the apoprotein and the mixture was in total incubated for one hour for Agp1. Agp2 was additionally incubated for another hour on ice.

Absorbance spectra were measured in order to follow the assembly process in addition to the labelling process.

The holoprotein was then purified to remove the excess of free BV and TCEP by using NAP-5 columns (GE healthcare, Munich, Germany). The column was first washed three times with water then with basic buffer. Proteins were eluted using 1 – 1.5 ml basic buffer. Subsequently absorption spectra were recorded to assess the appropriate amount of the required fluorescence Atto dye.

- **Fluorescence labelling**

For FRET measurements Agp1 and Agp2 proteins were labelled with Atto565 and Atto495 fluorescent dyes (Atto-Tec, Siegen, Germany), respectively, whereas for time-resolved fluorescence anisotropy and phosphorylation measurements, the used Agp1 proteins were labelled with Atto488.

These Atto dyes have a maleimide reactive group and can therefore bind covalently to thiol groups of cysteines. Atto stock solutions were prepared in DMSO with a concentration of 10 mM and stored at -80°C in 6 µl aliquots until further use.

The labelling and spectral measurements of the phytochromes were also performed under green safelight in order to maintain the dark ground state of the phytochrome proteins.

Different mutants of Agp1 and Agp2, in addition to the wt full length or PCM variant, were used for the different fluorescence-based methods performed and were therefore labelled and assembled similarly as described.

After the purification of the assembled proteins, absorption spectra were measured to identify the concentration of the holoproteins and the required amount of the Atto dye

to be added. The fluorophore Atto should be added directly to the purified protein, to ensure that as much cysteines as possible are still in their reduced state, therefore enabling the binding of the fluorophore. Any delay will result in a reduced degree of labelling. The concentration of the holoproteins varied between 4 and 8 µM and 1,5 – 2-fold molar excess of Atto dyes was then added to the holoprotein solution. The samples were then incubated either for 2 h at RT, or overnight at 4°C in darkness under constant shaking, if not used directly for further measurements. Subsequently free Atto was removed by running the mixture through a NAP-5 size exclusion column and afterwards by ultrafiltration using centrifugal filter Units (Amicon® Ultra -15, Ultracel – 30K, Merck Millipore Ltd.) to remove any traces of free and unbound BV or Atto. The samples were finally characterized by UV/vis spectroscopy.

The assembly of both phytochrome proteins Agp1 and Agp2 was carried out simultaneously, to ensure to ensure an identical assembling and labelling process. BV and the Atto fluorophore were added to the protein once at a time to ensure that no aggregates would form which could have likely complicated the binding of the chromophores and therefore would have reduced the labelling and assembly efficiency. This was also carried out to ensure a maximal amount of labeled protein as well as to guarantee that the majority of apoprotein would bind to BV. This reasoning was figured out during the frequent protein preparations for BV assembly and Atto dye labelling.

Furthermore, after each assembly of BV and of Atto, a gel filtration was performed with a NAP-5 column respectively, which was necessary to eliminate all free excess of BV or Atto molecules that could not bind to the phytochromes, since they could influence the fluorescence measurements either *via* FRET or time resolved fluorescence anisotropy.

To also minimize the fluorescence fluctuations an ultrafiltration method using another centrifugal filter was applied, to eliminate final traces of the free dyes and unbound BV molecules. Even if the same protocol was used and under the same conditions, there always were small differences in the degree of labelling and the BV assembling yield.

4.3.6 Absorption measurements

For FRET and time-resolved fluorescence anisotropy and phosphorylation measurements, it was necessary to measure the absorption spectra in order determine the final concentration of the labelled protein and perform an adequate dilution. Absorption spectra were measured with a Jasco V-750 photometer, with a scan speed of 1000 nm.min^{-1}.

For measurements including photoconversion assays, samples were irradiated either with red light (R) or with far red light (FR). For the photoconversion from Pr to Pfr in case of Agp1, the samples were irradiated for 2 min using a 655 nm red light-emitting diode with a light intensity of 32 µmol m^{-2} s^{-1} (R). Whereas, for the Pfr to Pr photoconversion in case of Agp2, samples were irradiated with a 780 nm far-red light emitting diode with an intensity of 80 µmol m^{-2} s^{-1} (FR) (Ibrahim Njimona 2011).

To minimize the spectral artifacts deriving from self-absorption, the absorption of BV at 703 nm for Agp1 or 750 nm for Agp2 was set to ~ 0.1. Therefore, samples were first prepared with an A_{703nm} or A_{755nm} of 0.2 as a start solution, in order to have a final A_{703nm} or A_{755nm} of 0.1 after the dilution or mixing processes.

4.4 Determination of the yield of BV assembly and Atto labelling

4.4.1 Yield of BV assembly

The efficiency of BV assembly for the various Agp1 and Agp2 proteins was determined. For Agp1 full-length mutants the percentage of the assembly was calculated using the extinction coefficient of the holo- / apoprotein at 700 nm and 280 nm (Lamparter 2002) as follows:

$$relative\ efficiency\ = \frac{A_{700\ nm}}{A_{280\ nm}}$$

The relative efficiency was corrected according to the BV extinction coefficient at 700 nm and 280 nm (Lamparter et. Al 2002) using the following correction factor (CF), which corresponds to 100% assembly.

$$CF\ for\ the\ BV\ assembly\ \% = \frac{\varepsilon_{BV\ at\ 700\ nm}}{\varepsilon_{BV\ at\ 280\ nm} + \varepsilon_{Agp1\ at\ 280\ nm}}$$

The percentage of the BV assembly is then determined by dividing the relative assembly with the CF assembly.

On the other hand, the ε_{Agp2} at 755 nm is not known yet therefore only the percentage of the relative efficiency was calculated using $A_{755\ nm}$ and $A_{280\ nm}$.

The extinction coefficients at 280 nm for the used Agp1 PCM, Agp2 full-length and Agp2-PCM were calculated from the corresponding protein sequence using the ProtParam tool – ExPASy.

Table 19: Extinction coefficients of the used proteins at the corresponding wavelength

Components	**ε_{prot} $M^{-1}cm^{-1}$**
Agp1 with BV, 700 nm	90000
Agp1, 280 nm	99935
BV, 280 nm	10000
Agp2, 280 nm	81290
Agp1-PCM, 280 nm	78567
Agp2-PCM, 280 nm	58307

4.4.2 Degree of the Atto labelling

For the labelled holoproteins Agp1 and Agp2, the efficiency of the BV assembly and the relative degree of the Atto labelling (DOL) were determined.
The DOL refers to the dye-to-protein ratio using the measured absorption spectra and applying the Lambert-Beer law.

The concentration of the dye will be then $C_{dye} = A_{max} / \varepsilon_{max} \times d$, where ε_{max} is the extinction coefficient of the dye at its maximum absorption A_{max} at 495 nm.

The DOL, which represents the average number of the dye molecules coupled to the protein molecule is defined as $DOL = C_{dye} / C_{prot}$

However, there should be a correction factor (CF) for the contribution of the dye to its absorption at 280 nm, which is given as A_{max} x CF_{280}, where each Atto dye has a definite correction factor and an extinction coefficient. The corresponding properties for Atto495 and Atto565 are presented in the table below:

Table 20: *Optical properties of Atto495 and Atto565 (Atto catalogue 2007-2008)*

Atto dye	MM, g/mol	λ_{max}, nm	ε_{max}, $M^{-1}cm^{-1}$	CF_{280}
Atto495	574	495	8.0 x 10^4	0.39
Atto565	733	563	1.2 x 105	0.16

The correct absorption of the protein at 280 nm will ben then calculated as follows:
$A_{prot} = A_{280} – (A_{max}$ x $CF_{280})$, where A_{280} is the initial absorption of the labelled protein at 280 nm and its concentration as $C_{prot} = A_{prot}/ \varepsilon_{prot}$ x d
ε_{prot} is the extinction coefficient of the corresponding Agp1 or Agp2 protein at 280 nm *(Table 19).*

Replacing the above equations, the DOL will be than calculated as:

$$DOL = \frac{A_{max}\ x\ \varepsilon_{prot}}{(A_{280} - A_{max}\ x\ CF_{280})\ x\ \varepsilon_{max}}$$

Since the extinction coefficient of the dye with its conjugated π-electron system, when it is bound to the protein, is frequently different from the free dye, a relative error up to 20% could be expected (Atto-tec GmbH, Atto catalogue 2016-2018). Nonetheless, this method was used to get an estimation of the degree of labelling and to obtain a correction factor for the FRET measurements that compensates for the varying yields of labeling.

4.5 FRET measurements

In the following project, intermolecular FRET was examined, with the aim to study protein–protein interactions between the labelled Agp1 and Agp2 proteins.

Fluorescence emission spectra were recorded with a Jasco FP-8300 fluorometer. The excitation wavelength and split width were fixed to 470 nm and 2.5 nm, respectively and the emission spectra were then recorded between 480 and 700 nm.

For these experiments, the dark-adapted form was mainly used. Agp1 in the Pr and Agp2 in the Pfr form, were therefore prepared under green light and all the measurements were also performed in darkness.
The fluorescence of Agp1 and Agp2 were first measured separately as a control having A_{703nm} and A_{750nm} ~ 0.1. Afterwards equal volumes of Agp1 and Agp2 solutions with A_{703nm} and A_{750nm} ~ 0.2, respectively, were mixed prior to measurements, to reach final absorptions at the respective wavelengths of 0.1. Since measurements were performed under green light, Agp1 and Agp2 should be expected in their dark-adapted forms in the mixture. This corresponds to the Pr – Pfr forms of Agp1 and Agp2 respectively *(see §5.3.1, Figure 32c)*.

However, in the case of FRET studies using different light conditions, Agp1 and/or Agp2 were irradiated using either R or FR light, Figures 15 and 16 illustrate the experimental steps of this Approach.

In the first scheme, proteins were illuminated separately, each with the respective light – Agp1 with R and/or Agp2 with FR. Afterwards, they were mixed, and emission spectra were measured. Therefore, four combinations were possible according to the respective form of Agp1 and Agp2 *(Figure 15):*

- Pr-Pfr designates the mixture of the dark-adapted states of the proteins
- Pr-Pr, when only Agp2 was illuminated with FR
- Pfr-Pfr, when only Agp1 was illuminated with R
- Pfr-Pr, when Agp1 was illuminated with R and Agp2 with FR

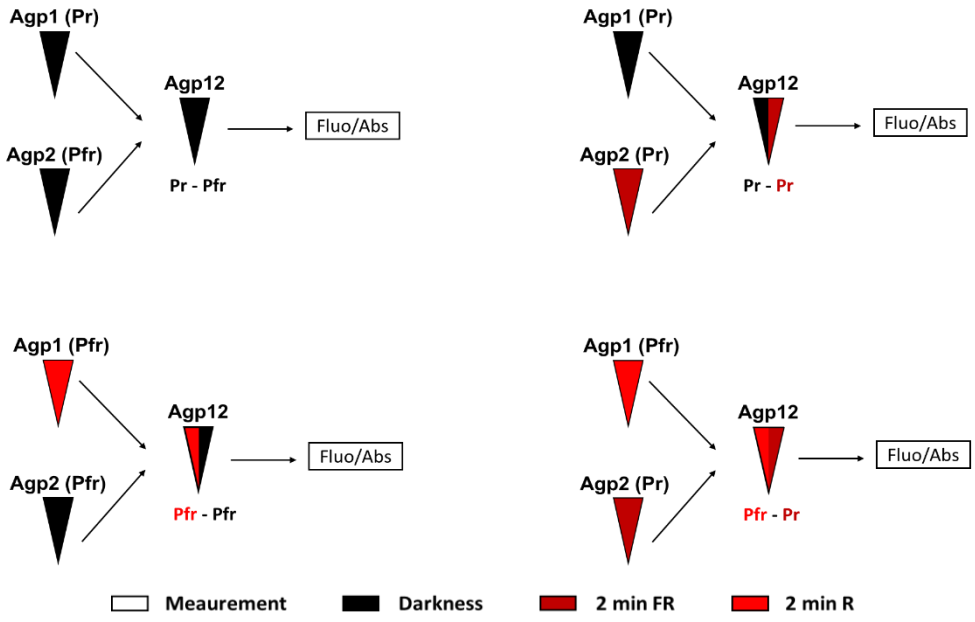

Figure 15: Schematic illustration of the FRET measurement using different light conditions: *In this case Agp1 and Agp2 samples were illuminated separately and then were mixed together, where the emission and Absorption spectra were measured. The Pr or Pfr represent the predominant form of the respective protein in the mixture.*

In the second scheme, proteins were mixed first as they are in their dark-adapted states, having therefore Pr-Pfr for Agp1 and Agp2, respectively.

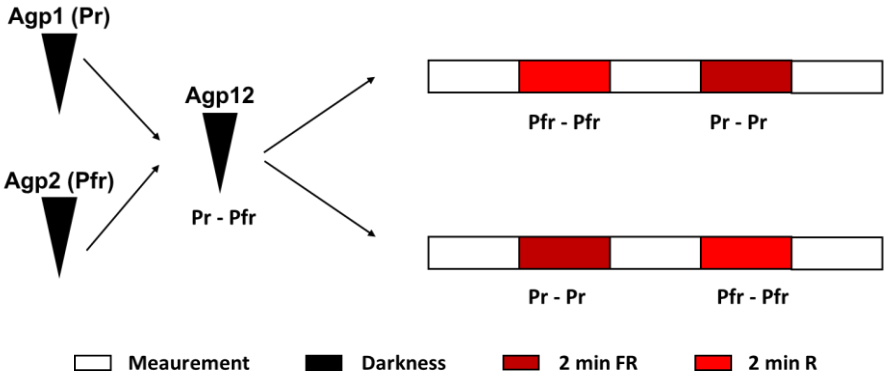

Figure 16: Schematic illustration of the FRET measurement using different light conditions: *In this case Agp1 and Agp2 samples were first mixed and then illuminated either with R followed by FR (D-R-FR) or FR followed by R (D-FR-R)*

After their mixing, they were irradiated with R to obtain Pfr-Pfr, followed by FR to obtain Pr-Pr for Agp1 and Agp2, respectively. In the case of the illumination with FR first, the proteins had first Pr-Pr and then switched to Pfr-Pfr after R illumination.

FRET measurements were repeated at least 4 times and the average results of the E_{FRET} are illustrated in § 5.4.5.

4.5.1 Determination of the distance "r" between the molecules

As mentioned previously (§ 1.5.1) the Förster theory shows that the FRET efficiency (E_{FRET}) varies with the sixth power of the distance "r" between the molecules, in this case between the fluorophores bound to Agp1 and Agp2 proteins.

The following equation was used for this purpose (Gayrard and Borghi 2016; Lakowicz 2006b):

$$E_{FRET} = \frac{1}{1+(r/R_0)^6} \qquad \textit{(Equation 1)}$$

The Förster-Radius R_0 is the characteristic distance between the two fluorophores, when the FRET efficiency is 50% in this case between Atto495 and Atto56. According to the manufacturer, R_0 between these Atto dyes corresponds to 50 Å, which corresponds to 5 nm (Atto-tec GmbH, Atto catalogue 2016-2018) and the effective range of energy transfer is below 10 nm.

For FRET measurements a standard fluorimeter with a continuous excitation light source was used, thus the donor quenching could also be measured and used for the calculation of the E_{FRET}.

In this case E_{FRET} is directly related to the ratio between the fluorescence intensity (FI) of the donor in the presence of the acceptor (I_{DA}) and the FI of the donor in the absence of the acceptor (I_D), which is the measure of donor quenching, according to the following equation (Gayrard and Borghi 2016):

$$E_{FRET} = 1 - \frac{I_{DA} * A_D}{I_D * A_{DA}} \qquad \textit{(Equation 2)}$$

Therefore, it was relevant to measure the FI of the donor (Agp2) with and without acceptor (Agp1), which enables the quantification of the FRET efficiency.

First E_{FRET} was calculated according to equation (2) and then applied in equation (1) to calculate the distance between Agp1 and Agp2.

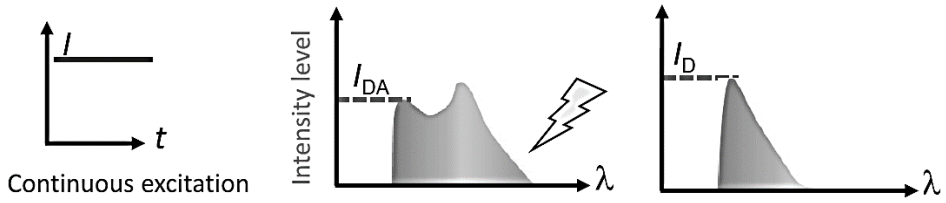

Figure 17: Illustration for the calculation of FRET efficiency according to the donor quenching and acceptor photobleaching*. The graphic in the middle shows the FI of the mixed donor and acceptor, where I_{DA} refers to the donor FI in presence of the acceptor after its continuous excitation. The right figure shows the I_D of the donor alone. Figure is adopted from (Gayrard et al. 2016)*

- **Correction factors used for the calculation of the FRET efficiency**

To minimize the pipetting error and the error that could be caused by the difference in the DOL two CFs were used.

The first CF was the reduction of the pipetting error, by monitoring the measured absorption spectra, and using the following equations system:

$$K_1\, A_{A(570nm)} + \; K_2 A_{D(570nm)} = A_{M(570nm)}$$

$$K_1\, A_{A(505nm)} + \; K_2 A_{D(505nm)} = A_{M(505nm)}$$

A_A corresponds the absorption of the acceptor alone, A_D is the absorption the donor alone and A_M is the measured absorption of the mixture of Agp1 and Agp2 that is detected at the same wavelength used of the donor and acceptor, 505 nm and 570nm respectively. K_1 and K_2 are the consequent CF for Agp1 and Agp2 respectively.

Using these equations both CFs can be then calculated as follows:

$$K_1 = \frac{A_{M(570nm)}\, A_{D(505nm)} - A_{M(505nm)} A_{D(570nm)}}{A_{A(570nm)} A_{D(505nm)} - A_{A(505nm)} A_{D(570nm)}}$$

$$K_2 = \frac{A_{A(570nm)} A_{M(505nm)} - A_{A(505nm)} A_{M(570nm)}}{A_{A(570nm)} A_{D(505nm)} - A_{A(505nm)} A_{D(570nm)}}$$

These CFs, K_1 and K_2 were then used to correct the single absorption spectra and the corresponding fluorescence spectra of Agp1 and Agp2. Then the *corrected* E_{FRET} was calculated according to equation 2.

The second CF was the DOL of the Agp1 proteins, where the final E_{FRET} (see § results) was calculated according to:

$$E_{FRET} = corrected\ E_{FRET} * \frac{1}{DOL\ of\ the\ corresponding\ protein}$$

4.6 Fluorescence anisotropy measurements

Various Agp1 mutants were used to study the fluorescence anisotropy decay with the fluorophore at a definite position in the protein. For this purpose, the required proteins were expressed, purified, assembled with the chromophore BV and finally labelled with Atto488 as described previously (§ 4.3.3, § 4.3.5 and § 4.3.6).

An ultrafiltration step was performed prior to the start of each measurement to ensure that there were no free Atto molecules in the sample, that could affect the anisotropy measurements.

An additional check for the absence of free atto molecules, was achieved using SDS gel electrophoresis where the gels were checked for the presence of the fluorophore under UV light.

The time resolved anisotropy measurements were performed using the MicroTime 200 microscope (Picoquant) by measuring the time correlated single photon counting (TCSPC) and the fluorescence correlation spectroscopy techniques (FCS).

For a proper detection of fluorescence using these techniques the concentration of the proteins had to be reduced to ~ 10 nM to obtain approximately 10 molecules in the irradiated area. For the measurements, 30 µl of the sample were dropped on a microscopic cover slide.

For this approach a short pulsed linearly polarized 488 nm laser was used with a Pulse width of 50 ps.

Furthermore, the configurated system consists of two single photon counting detectors for the detection of the parallel and perpendicular emission intensities. In addition to the photon counting unit Picoharp 300 (PicoQuant) with a 50 µm pinhole, a bandpass filter with a focal point of 525 nm and a width of 50 nm and a polarizing beam splitter were used.

The sample was illuminated by a focused laser beam, with a fixed laser power at around 426 a.u, whose optical axis was perpendicular to the surface of the sample and polarized along the x axis.

The fluorescence emission was collected by the same objective, filtered spatially by the pinhole, and spectrally by the emission bandpass filters and finally was split into two beams *via* the polarizing beam splitter with orthogonal polarizations (x and y axis). Each of the beams was focused onto its single photon counting detector, so that it could be detected and finally registered by the photon counting unit, by the use of the time-tagged time resolved (TTTR) data format (Jiang et al. 2016).

These data obtained were then read out with the program Symphotime, exported, calculated with the software MATLAB and depicted with help of the software OriginPro.

The anisotropy measurements were performed at the institute for applied physics of Prof. Dr. Ulrich Nienhaus, with the help of Dr. Guigas.

4.6.1 Determination of the anisotropy decay r(t)

By use of time-resolved anisotropy measurements, it is possible to quantify the depolarization and the time scale in which the depolarization occurs.

The simplest approach to calculate the polarization in terms of fluorescence anisotropy *r(t)* is to use the definition of anisotropy as a function of the measured fluorescence intensities of the polarization along the different axes (Peter Kapusta 2002; Jiang et al. 2016).

$$r = \frac{I_{II} - G.I_{\perp}}{I_{II} + 2.G.I_{\perp}} \qquad \text{(Equation 3)}$$

I_{II} and $I_{\perp}$ correspond to the fluorescence intensities of the parallel and perpendicular polarized emission respectively, after the excitation of the sample with the linear polarized light.

The G factor represents the instrument and wavelength dependent correction factor that compensates the polarization bias of the detection system. The G-factor for Atto488 nm was determined after calibrating the system, initially by measuring a sample of the used dye in the basic buffer without it being conjugated to the protein.

The G factor was determined by measuring the anisotropy of Atto488, and the decays were then collected for the parallel and perpendicular orientations. Based on the fact that the decay of free dyes is close to a mono-exponential decay, the anisotropy decays of Atto488 were then fitted using a mono-exponential fit function to estimate the amplitude of the constant background noise for each detector. This was afterwards subtracted from the intensity decays. To coincide both // and ⊥ decays, the perpendicular decay was then shifted in time allowing the anisotropy to be calculated according to equation (3). The value of the G factor was adjusted iteratively so that the residual anisotropy was equal to zero, after the initial relaxation disappear, which was caused by the molecular rotation.

The Atto488 sample was prepared with a final concentration of 10 nM and stored at 4°C and used each time before starting the anisotropy measurements of the Agp1 mutants.

A similar process was used to obtain the time-resolved anisotropy decays for Agp1 mutants, using equation (3) after measuring the parallel and the orthogonal fluorescence intensities upon excitation. Nonetheless, the value of the G factor was in this case a constant as obtained from the calibration procedure (Jiang et al. 2016).

- **Rotational correlation time analysis**

The degree of the emitted fluorescence polarization is expressed as time-resolved anisotropy, which can be obtained by measuring the anisotropy as a function of time:

$$r_{(t)} = r_{(\infty)} + r_0 \exp(t/\tau) \qquad \textit{(Equation 4)}$$

By means of the software OriginPro it was possible to calculate a double or two-phase exponential fit decay function (ExpDec2), which corresponds to the following formula, and is based on the equation 4:

$$y = y_0 + A_1\, e^{-(x-x_0)/t_1} + A_2\, e^{-(x-x_0)/t_2}$$

y corresponds to the time offset value of the fluorescence anisotropy as a function of time (x), y_0 is the time offset of the residual fluorescence anisotropy at t=20 ns, A the amplitude of the coresponding kinetic phase, and it reflects the extent of the rotational diffusion for the given anisotropy decay component (Kim et al. 2012). x_0 corresponds to the x offset of the time measurements, and finally t_1 and t_2 correspond to the decay time constants or the correlation time of the first an second kinetic phases (see § 5.3.3).

- **Determination of the hydrodynamic radius in Pfr**

Furthermore, using the FCS technique it was also possible to detect the diffusion coefficient in aqueous solution, based on the recorded correlation function and the Stokes-Einstein relationship *(Equation 5)*:

$$D = \frac{k\,.\,T}{6\pi\,.\,\eta\,.\,R_h}$$

D is the diffusion coefficient, *k* is the Boltzmann constant (1,3807 x 10^{-23} JK^{-1}), T refers to the temperature in Kelvin, and *η* is the viscosity, which also depends on the temperature 8.90 × 10^{-4} Pa·s at 25°C or 9,321 × 10^{-4} Pa·s at 23°C (Peter Kapusta 2010). The use of this equation allows the calculation of the hydrodynamic radius of the measured Agp1 mutants.

4.7 Kinase assay of Agp1 mutants

In this approach, Agp1 mutants used in the time-resolved fluorescence anisotropy measurements were used to test the impact of the introduced mutations on the autophosphorylation mechanism, particularly on transmission of the signal between the Pr and the Pfr form. Experiments were carried out in the isotope laboratory, because of the used radioactive ATP, γ-^{32}P ATP.

In addition to the Agp1 mutants, Agp1-wt was also tested as a control, in order to compare the phosphorylation yield of the mutants in comparison to the wt. Agp1-wt was used as a control each time the phosphorylation was performed, in order to have a reference for each experiment on the basis of which the differences in the phosphorylation yield of the mutants could be detected. The labelled proteins were used and tested for both forms the Pr (in darkness) and the Pfr, which is obtained by irradiating the samples for 2 min using the R light. The setup of the autophosphorylation reaction is presented in table 21.

Table 21: *Phosphorylation reaction*

Components	Final concentration [mM]
Tris/HCl pH 7,8	25
$MgCl_2$	5
β-Mercaptoethanol	4
H_2O	
KCl	50
Ethylenglycol	5 %
γ-^{32}P ATP	50 µM, containing 0.37MBq
Protein	0.25 µM

The phosphorylation assay was stopped after adding 3x loading buffer to the radioactive mixture causing the denaturation of the proteins and then transferred onto a PVDF membrane (§ 4.3.2). After blotting, the membrane was wrapped in cellophane preventing the formation of air bubbles and placed on a FujiFilm Imaging plate Bas-1500, where it was incubated for about 30 minutes in the cassette, before the

measurements of the radioactive signals using the Phospho-Imager FujiFilm FLA-2000 (Fuji photo Film, Düsseldorf) took place.
The analysis of the phosphorylation intensities of the obtained protein bands, were extracted using the software ImageJ and subsequently analysed with the software OriginPro.

4.8 Conjugation assay

In this attempt the role of the TraA gene on the conjugation mechanism was tested, in addition to the impact of the phytochromes Agp1 and Agp2 and of light on this process. Therefore, the TraA gene located in the pTi was knocked out from the donor cells used in the experiments. The conjugation experiments were performed with one type of recipient strain, which was the *A. fabrum* without pTi and pBin-Gus. This strain has and Amp resistance. Various donor strains were used, to test the effect of both phytochromes.

4.8.1 Preparation of *A. fabrum* TraA knockout strains

The donor strains used for this purpose were the wt, Agp1^{-}, Agp2^{-} and Agp12^{-} strains including pTi and the mobilizable pBin-Gus. The pBin-Gus was already transformed by means of electroporation into the different strains mentioned above. As a result, they acquired a Kan resistance and included both pTi and pBin-Gus (Bai et al. 2016).

Nevertheless, the pTi was used for the homologous recombination to knock out its TraA gene and pBin-Gus was used for the conjugal transfer.

For the additional knockout of TraA, the following scheme was performed to obtain the pTi without the TraA gene.

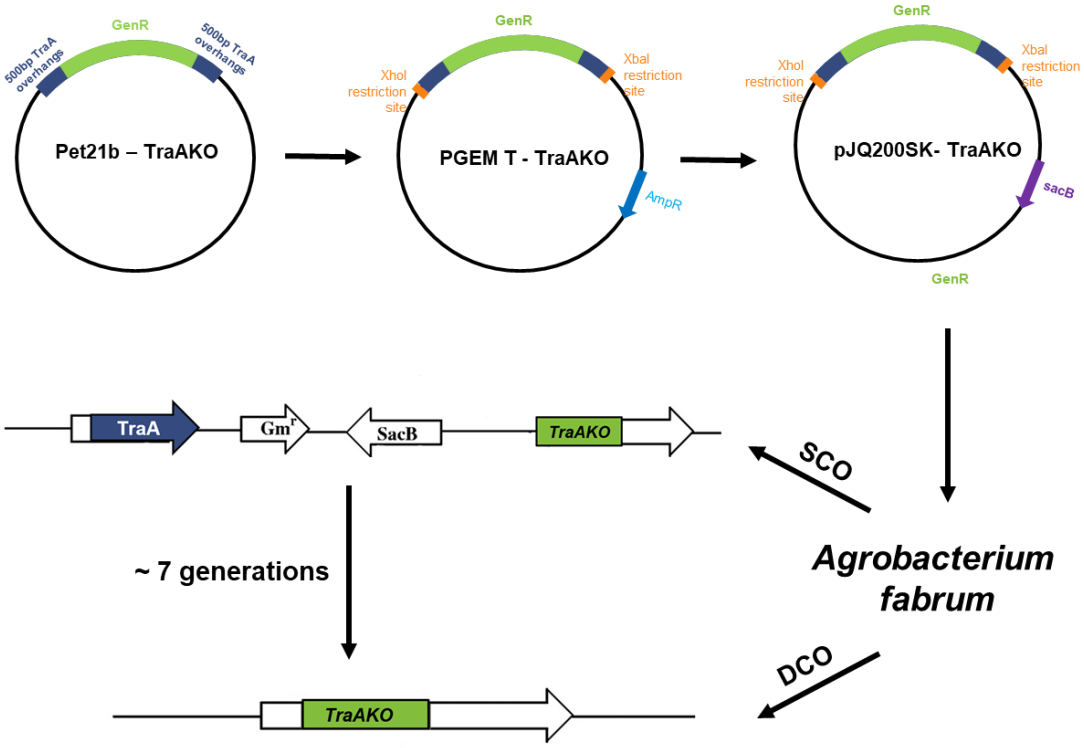

Figure 18: Illustration of the TraA knockout scheme: *It starts with the TraA expression vector up to the transformation into A. fabrum, where a single cross over (SCO) occurred that is followed by a double cross over (DCO) after at least 7 generations.*

First the TraA gene was amplified from its expression vector pET21b, leaving 500 bp at the end and the beginning of the segment. This segment was then ligated to a gentamycin resistance cassette, which was amplified from the pJQ200SK *via* its phosphorylated primers, to ensure a specific binding of the resistance cassette.

The ligation product was afterwards introduced into the pGEM T easy vector. For this insertion, the construct was first amplified by help of primers containing restriction enzymes sequences of XbaI and XhoI. PGEM-T vector was used because of its T overhangs that ease the ligation of PCR products and make it more efficient. Furthermore, it is considered as a high-copy-number vector and allows a blue-white selection on IPTG-Amp-XGal LB plates, enabling the determination of the ligated insert.

In the next step a double digestion occurred for the construct pGEM-TraA$^-$ and pJQ200SK with XbaI and XhoI to ligate the TraA$^-$ construct into the suicide vector

pJQ200SK *via* the restriction sites. This plasmid permits gene replacement and allows a positive selection for this integration, when it is cultivated in a media that contains 5% sucrose. The construct pJQ200SK-TraA$^-$ will enable the homologous recombination with the TraA gene presented in the pTi, in the various strains of *A. fabrum*.

In this last step of the transformation, either a single cross over (SCO) could occur, where both vectors will consolidate and a SacB and a Gen resistance will be presented, or a double cross over (DCO), where the TraA gene in the pTi will be completely replaced by the knocked-out construct. The DCO can be finally selected using a saccharose plate.

4.8.2 Conjugation experimental steps

The conjugation assay involves three steps and takes in general about five days to reach the final results of the grown colonies under the premise that the DNA transfer was successful.

Step 1: Preparation of cultures

In the first step, different overnight cultures were prepared. This includes the wt recipient strain and the four donor strains, where the TraA gene was knocked out. The inoculation was performed in liquid LB medium with a low concentration of the corresponding antibiotic, 50 mM Amp and 25 µM Kan respectively, and then incubated at 28°C. The wt recipient exhibited an Amp resistance, whereas all the donor strains had a Kan resistance caused by the Kan cassette on pBin-Gus (Bai et al. 2016).

Step 2: Co-cultivation

2 ml of the overnight culture were respectively centrifuged for 1 min at 10000 x g and the pellet was twice washed using 1 ml ABMM and centrifuged respectively at 10000 x g for 1 min. Finally, the pellet was dissolved and mixed with 2 ml ABMM.

The recipient and donor strain cultures were then diluted 6-fold (100 µl culture with 500 µl ABMM) and the OD_{600} was then measured.

For the co-cultivation a mixture of ABMM, the wt recipient and the respective donor strains were prepared in a total volume of 800 µl, where they had a final OD_{600nm} = 1 in the mixture.
Afterwards, the prepared samples were incubated at 26°C overnight for 24h, without shaking and under different light conditions, such as in darkness, under R and FR light.

For the red light, an 80 × 80 cm array of 650 nm light emitting diodes (LEDs) was used with an intensity of 50 µM m^{-2} s^{-1} and for the far-red light a 25 cm x 21 cm array with 730 nm LEDs was used with the similar intensity of 50 µM m^{-2} s^{-1}.

Step 3: Dilution and double resistance selection

On the third day, a serial dilution was prepared respectively 1:20 to get a final dilution of 1:8000, from which 100 µl were used and dropped on agar plates containing both Amp and Kan antibiotics and incubated at 26°C for three nights under the same light conditions as in the co-cultivation step. The plating was always for three replicates for each tested donor strain and the assay was repeated 3-4 times.

The last step consists of the evaluation of the conjugation efficiency, which was determined by the number of colonies that had grown on the agar plates. The detection of colonies was realized by using Safe Imager Transilluminator to photograph the plates under white light.

5 Results

The main focus of this work was to study the biological function of phytochromes in *Agrobacterium fabrum,* to further understand its signal transduction mechanisms, and how these phytochromes are involved in this process.
For this purpose, different approaches were pursued to examine if and how Agp1 and Agp2 phytochromes are involved in the signal transduction process, hence influencing other cellular mechanisms.

Initially, it was shown how both phytochromes act with each other, influencing the conjugation mechanisms (Bai et al. 2016). Additionally it was revealed that they could affect other mechanisms such as the phosphorylation or chromophore assembly and biological responses such as plant infection and cell growth (Xue et al. 2019).

A first approach to gain more insight into the signal transduction in *A. fabrum* took place *in vitro* using various Agp1 mutants, where dynamics and mobility studies were implemented. The aim was to investigate changes in the mobility within defined regions of the Agp1 protein upon photoconversion from the Pr active form to the Pfr inactive form. These experiments were performed using the time-resolved fluorescence anisotropy.

Furthermore, interaction studies were performed using Agp2 wt and various Agp1 proteins either in their full-length version or just using the PCM- region (see § 5.4.1 and 5.4.2) with the intention to figure out, how this interaction occurs and if the histidine kinase could play a role in this putative interaction. To assess where this interaction takes place, the different mutants of Agp1 were used for this purpose (see § 1.2.2), in addition to the Agp2 single site mutations that were tested for altered interactions with one of the Agp1 mutants (see § 5.4.4). This allowed to gain more detailed information on how this possible interaction occurs. Besides that, it was also important to elucidate, if the fluorescent dye can bind equally to the cysteines along the Agp2 protein, as well as the degree of labelling of Agp1 mutants, for the correct evaluation of the FRET efficiency.

As a last approach to study the interaction, further investigations were performed to detect the influence of red light on the interaction between these phytochromes (see § 5.4.5).

The used Agp1 mutants were also tested regarding their kinase activity, through the evaluation of their impact on the autophosphorylation signal upon photoconversion. The main motivation was to have a control experiment, in order to verify the significance of the FRET and time-resolved fluorescence anisotropy results, obtained using these mutants.

A last approach was the performance of conjugation assays *in vivo*, with the aim to test if the TraA protein located in the pTi, could be involved in the conjugation reaction cascade (see § 5.5). Therefore, the TraA gene, located on the pTi plasmid of *A. fabrum*, was knocked out in the donor strains prior to testing their capability of DNA transfer into the recipient *A. fabrum* cells.

5.1 Preparation of the holoproteins and their labelling

In order to perform the FRET measurements, time-resolved anisotropy and autophosphorylation assays, it was necessary to purify the proteins to be used, so that the subsequent assembly with the chromophore BV and the labeling with the fluorescent dyes Atto could take place.

Several variants of Agp1 and Agp2 proteins were used in the course of this research, either in their wild-type form or as mutants where a mutation was introduced at a site of interest.

5.1.1 Agp1 and Agp2 protein mutants

In the first part of the interaction studies, many Agp1 mutants were used. Each of these mutants had undergone a single mutation *via* SDM, to introduce a cysteine residue within a specific region of the protein. These mutants were the same as the mutants used in the work of Kacprzak et. al 2017.

Figure 19 shows the positions of the cysteines that were introduced for the spin labelling test for the PELDOR experiments already published (Kacprzak et al. 2017).

The chosen amino acids for the mutations were: S122C, which corresponds to the amino acids located in the link between the PAS and GAF domain, A362C located in the β-sheet region of the PHY domain, K517C positioned on the helix connecting the PHY and HK domain, R535C and K554C located at further positions in the HK and finally R603C situated in the ATP-binding domain of the HK.

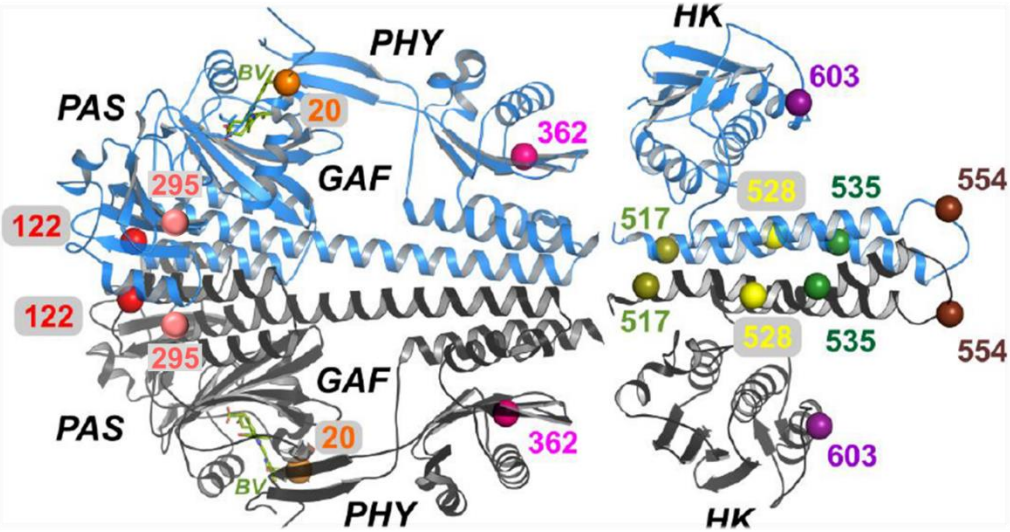

Figure 19: Location of mutations sites in the Agp1 phytochrome: *Crystal structure of the Agp1-PCM in parallel arrangement, with a homology model histidine kinase dimer. The shown carbon atoms represent the mutated positions to cysteines (coloured spheres with the position number), as well as of the functional Cys-20 (Kacprzak et. al. 2017).*

These mutants were used in the first part of the FRET measurements, for the time resolved fluorescence anisotropy measurements and for the autophosphorylation assays (see later).

In the second part of the FRET measurements, Agp2 mutants were prepared, where in each variant a single cysteine was replaced by a serine residue *via* SDM. The aim was to gain more detailed information on the labelling mechanism, since Agp2 has in total eight cysteines, of which C13 in the PAS domain is reserved for the covalent binding of the chromophore BV.

The remaining cysteines are found at positions 29, 33 and 47, which are also located in the PAS domain, whereas positions 249, 277 and 353 are found in the GAF domain (*Figure 20).* The final cysteine residue at position 647 is in the HK domain.

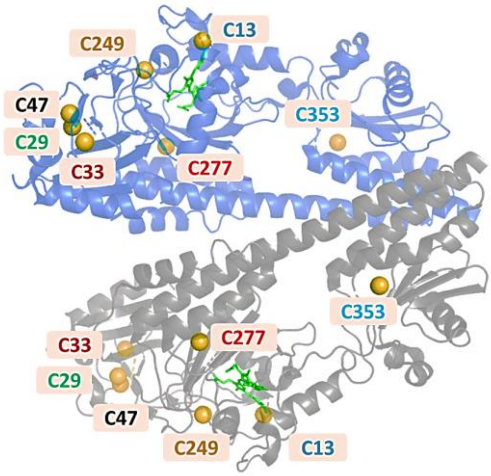

Figure 20:*PCM Structure of Agp2 with the positions of the native cysteines that are used for the SDM. PDB code 6G1Y*

The aim of these mutations was to figure out, which cysteine could possibly bind the fluorophore, since it is not clear, which position is preferentially labelled. In contrast, Agp1 has only 2 additional cysteines which were mutated in order to have only one cysteine residue at the above-mentioned positions.

Furthermore, the Agp2 mutants were also used, to investigate their impact on the interaction studies with Agp1 protein.

The corresponding Agp2 mutants were designated as followed: C47S, C249S, C277S, C353S and Agp2 PCM, which lacks the HK and therefore does not have a cysteine at position 647.

5.1.2 BV assembly of phytochromes and Atto labelling

The designated Agp1 and Agp2 proteins were expressed and purified as described in detail previously. Afterwards, they were assembled with the chromophore BV and then labelled with the appropriate fluorescence dye, depending on the experiments they were used for.

For the FRET experiments, it was necessary to generate a donor and an acceptor protein. Therefore, two types of fluorophores were used that served this purpose. The donor protein used was Agp2-wt in the first series of experiments and later, the Agp2 mutants, which were labelled with the fluorescence dye Atto495. Thus, the acceptor Agp1-wt protein and its various mutants, served as acceptor proteins and were labelled with Atto565.

In case of time-resolved fluorescence anisotropy, Agp1 mutants were labelled with Atto488. However, the BV assembly and the labelling process was the same for all the experiments.

Figure 21 shows the typical absorption spectra of the assembled and labelled Agp1-wt and Agp2-wt phytochromes, which are also similar to the used mutants. From these spectra several peaks could be recognized that refer to the different components presented in the samples.

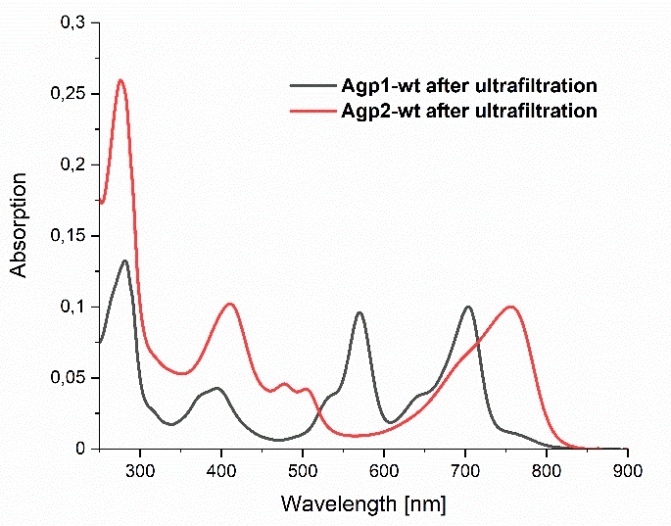

Figure 21: Example of the absorption spectra of the labelled holoproteins Agp1 and Agp2: *Agp1-wt spectrum (black) and Agp2-wt (red) after their assembly with BV and their labelling with the corresponding Atto dye. Starting from 900 nm the* absorption maxima *are identified as follows:* Q-band *at 755 nm for Agp2, or 703 nm for Agp1, Atto565, Atto495, BV absorbing in the blue range designated as* Soret band*, and the overall amount of molecules absorbing at 280 nm, such as the apoprotein and Atto.*

The dark adapted Agp1 and Agp2 proteins show their characteristic Q-band absorption maxima at 703 nm and 755 nm respectively, followed by the absorption of the fluorophore Atto565 at ~ 570 nm and Atto495 at ~ 500 nm. The peaks at 395 nm and 410 nm correspond to the Soret-band of BV that absorbs in the blue light range and is blue-shifted in case of the Pfr form of Agp2. The absorption band with a maximum at about 280 nm can be attributed to the absorption of aromatic side chains of the total protein, including the apoprotein, and any other aromatic molecules, *i.e.*, the fluorescence dyes.

5.1.3 Efficiency of BV assembly and Atto labelling

Tables 22 and 23 show the calculated assembly percentage of the BV and the DOL for the used Agp1 and Agp2 proteins in the FRET experiments.

Comparing the assembly of Agp2-wt with Agp1-wt, as well as with Agp1 mutants, Agp2 always exhibited a lower assembly efficiency either with BV or with the Atto fluorophore. The relative efficiency of the BV assembly was approximately 40 - 50% for Agp2 and 60 – 90% for Agp1. The degree of labelling of the different Agp1 mutants was also not similar (*Table 22).*

Table 22: Assembly percentage with BV and the DOL for the used Agp1 proteins in the FRET measurements

Agp1 Proteins	rel. efficiency of BV assembly	% of BV Assembly	DOL
S122C	82%	100%	100%
Wt	85%	104%	69%
A362C	82%	100%	81%
A362C-PCM	87%	85%	77%
K517C	83%	101%	100%
KR535C	68%	83%	52%
K554C	69%	84%	61%
R603C	75%	92%	76%

Similarly, the different Agp2 variants were also tested for the yield of chromophore assembly and the degree of fluorophore labeling.

Figure 22 shows the results of the assembly and the Atto labelling of the different Agp2 mutants, which were compared to the Agp2-wt.

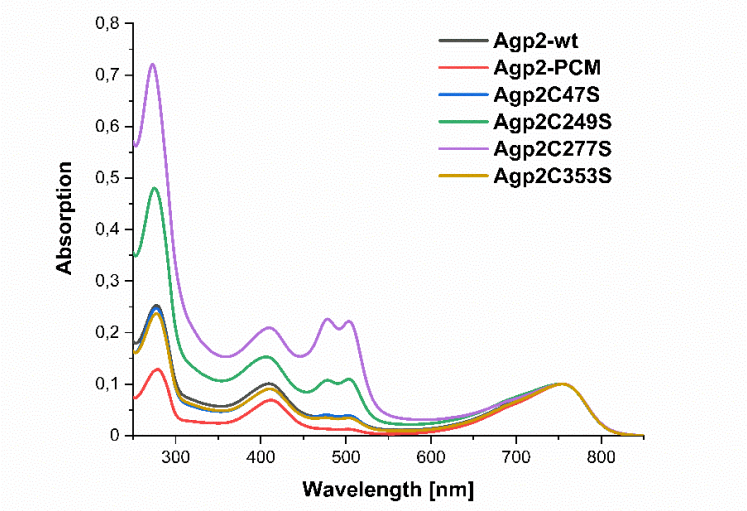

***Figure 22: BV assembly and DOL of Agp2 mutants**: For a better comparison, the Absorption spectra were set to $A_{750\ nm}$ =0.1. Agp2-wt, C47S and C353S show a similar BV assembly efficiency and DOL, whereas Agp2-PCM has a higher BV assembly but a lower DOL. On the contrary C249S and C277S show a lower yield of BV assembly and a higher DOL.*

As visible from the spectra in figure 22 and from table 23, the single mutations have affected not only the degree of labelling but also the efficiency of the chromophore assembly. The absolute percentage of the BV could not be calculated since the ε_{BV} at 750 nm for Agp2 is not known.

Table 23: Assembly percentage with BV and the DOL for the used Agp1 proteins in the FRET measurements

Agp2 Proteins	rel. efficiency of BV assembly	DOL
Agp2-wt	44%	20%
Agp2-PCM	79%	9%
Agp2 C47S	42%	20%
Agp2 C249S	24%	29%
Agp2 C277S	17%	43%
Agp2 C353S	45%	18%

For instance, the mutants C42S and C353S exhibited a similar behaviour as for the Agp2-wt, where they show a similar DOL and efficiency of the BV assembly. This suggest that the mutation of these cysteines neither affect the overall labelling efficiency nor the BV assembly; hence they are probably not involved in the labelling process or are somehow difficult to be labelled.

Agp2-PCM shows possibly a better BV assembly, nonetheless a lower DOL by approximately the half, suggesting that the cysteine located in the HK can be easily labelled. This could lead to the possibility that the HK maintain the PCM domain in a definite structure, which makes it difficult for the BV molecules to bind to its cysteine.
On the contrary, the mutations C249 and C277 have altered the DOL and lowered the assembly efficiency, suggesting that these cysteines could also be involved in the labelling process, nonetheless one cysteine could be more labelled than the other one.

Finally, in order to know, which cysteines were involved in the labelling process, the apoprotein Agp2 and the labelled holoprotein were analysed *via* MALDI-TOF.
The prepared protein samples were sent to the “Institut für funktionelle Grenzflächen” (IFG) at KIT Campus Nord, where the experiment was performed by Dipl. – Ing. Frank Kirschhöfer, who provided the final results.

***Table 24**:Illustration of the cysteines found either in the apoprotein or in the labelled holoprotein via MALDI-TOF*

	C13	C29	C33	C47	C249	C277	C353	C647
Apoprotein	■	■	■	■	■	■	■	■
Holoprotein + Atto	■	■	■	■	■	■	■	■

■ Cys not found ■ Cys found in the apoprotein ■ Cys found in the holopoprotein

The results show that C29, C33, C47 and C249 could be found in both forms of Agp2. This suggests that these cysteines did either not bind the fluorophore at all or that the labeling was incomplete. On the contrary, which would be consistent with the covalent

attachment of BV to C13 and the successful labeling of C647 with the fluorophore. C277 and C353 were neither found in case of the apo- nor in the labelled holoprotein. This is due to the fact that usually not all the peptide fragments obtained after the proteolytic digestion can be detected by this method, thus indicating the limitations of this approach.

5.2 Kinase activity of Agp1 mutants

The aim of this project was to examine the autophosphorylation activity of the histidine kinase using the same Agp1 mutants used for the PELDOR experiments *(Figure 17)* to analyse changes of the distances in the homodimer upon photoconversion (Kacprzak et al. 2017).

This assay was performed, by checking if these mutants can affect the phosphorylation activity either in the Pr or in the Pfr form. Therefore, the autophosphorylation activity was measured by using a radioactive γ^{-32}P ATP and the resulting bands were detected *via* the Phospho-Imager and are presented in figure 23.

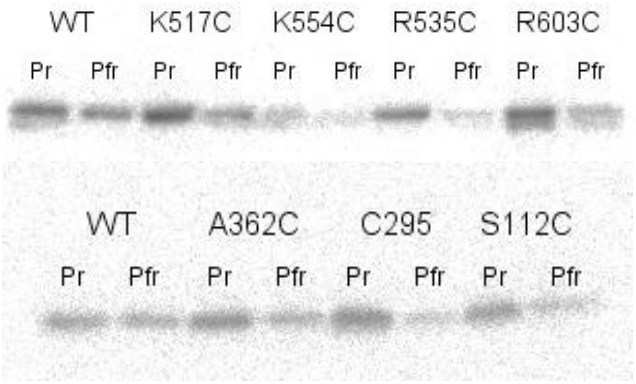

Figure 23: *Western blot membrane showing an example of the protein bands after the kinase assay. Different intensities can be seen between the Pr and Pfr form, as well as between the different mutants of Agp1*

Results were first detected from the bands of the phosphorylated samples after their transfer onto the western-blot PVDF membrane. Depending on the degree of the autophosphorylation activity, the resulted bands showed either a strong or a weak intensity. These differences could be seen either depending on the mutant used or whether Agp1 was in the Pr or Pfr form.

This kinase assay was performed with the help of a master student – Latifa Hourani – under my supervision and repeated 3-4 times. The quantification of the autophosphorylation activity is shown in figure 24.

5.2.1 Comparison of the phosphorylation activity in Pr and Pfr

The software ImageJ was used to assess the kinase activity, by analysing the intensity of the bands, detected on the western blot membrane.
To maintain a comparable yield of experiments, the protein samples were prepared with the same concentration, according to A_{703nm} = 0.1.

When comparing the kinase intensities *(Figure 24)*, the Agp1-wt in the Pr form showed a higher autophosphorylation activity than in the Pfr form, as previously published (Noack and Lamparter 2007; Ibrahim Njimona 2011; Lamparter et al. 2002). All the Agp1 mutants showed a higher activity as well in the Pr form as for the wt.

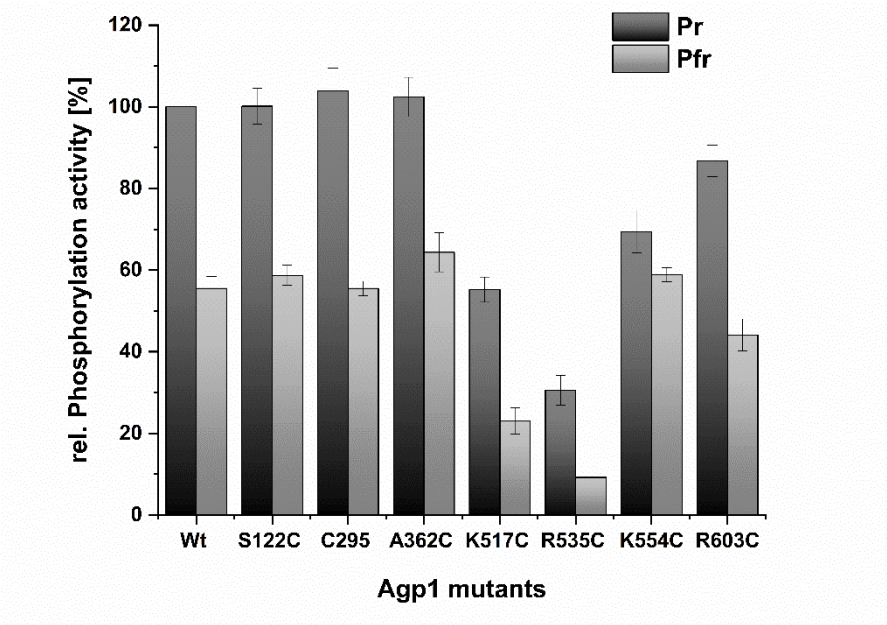

Figure 24: Average results of the HK autophosphorylation activity using different Agp1 mutants *in comparison to the wt, which was set to 100%. The autophosphorylation is also light regulated, where it is higher in the Pr (dark bars) than in the Pfr form (light bars).*

Interestingly the wt and the mutant proteins, where positions within the PCM were mutated *i.e.,* S122C, C295 and A362C exhibit a higher autophosphorylation yield in

the Pr form than the mutant proteins, where positions within the HK module were mutated *(Figure 24).* This suggests that the former mutants have only a slight influence on the autophosphorylation activity of the histidine kinase.

However, the mutants K517C, R535C, K554C and R603C exhibit a lower autophosphorylation activity in the Pr form in comparison to the Agp1 wt, suggesting that the mutated positions could affect the function of the protein, but only in a slight manner and could be probably involved in the autophosphorylation process, hence also in the signal transduction pathway. Nonetheless, the autophosphorylation activity is basically still preserved, and these mutants are still suitable for further experiments.

Furthermore, it can be clearly seen that the autophosphorylation activity of all the tested mutants has decreased and it is half as strong as in the Pfr than in the Pr form for almost all the mutants of the PCM domain, except for some mutants of the HK module. On the contrary, the kinase activity of the mutants K517C and R535C decreased a bit more than half in the Pfr form and for K554C it was third as strong as in the Pfr than in the Pr form.

Therefore, it can be concluded that the autophosphorylation is not only down regulated upon photoconversion but is also slightly affected if any changes or mutations occur in the HK module. Nonetheless it is barely influenced, upon mutations in the PCM.

This approach served as a control, to test whether the transmission of the signal is affected by the mutations upon photoconversion and if the mutated proteins are still functional and thus suitable for further analyses using the fluorescence- based methods by means of time-resolved fluorescence anisotropy or FRET.

5.3 Time-resolved fluorescence anisotropy

Since Agp1 mutants were proven to be functional for further analysis, studies of the dynamics at definite positions in the protein were performed, to further understand the involvement of phytochromes in the signal transduction process.

Therefore, the influence of the Pr and the Pfr form on the dynamics of Agp1 domains was studied *via* time-resolved fluorescence anisotropy, in addition to the examination of the differences in the dynamics between the various Agp1 mutants.

5.3.1 System calibration

Before the start of each fluorescence anisotropy measurement, the system had to be calibrated by measuring a sample of the fluorescent dye Atto488, which was dissolved in basic buffer to the final concentration of 10 nM. The same procedure was applied for the subsequent measurements of the Agp1 mutants.

The used Atto dye is isotopically polarized (Jiang et al. 2016) and its anisotropy decay results were obtained with r(∞) ≅ 0. *(Figure. 25 b)*

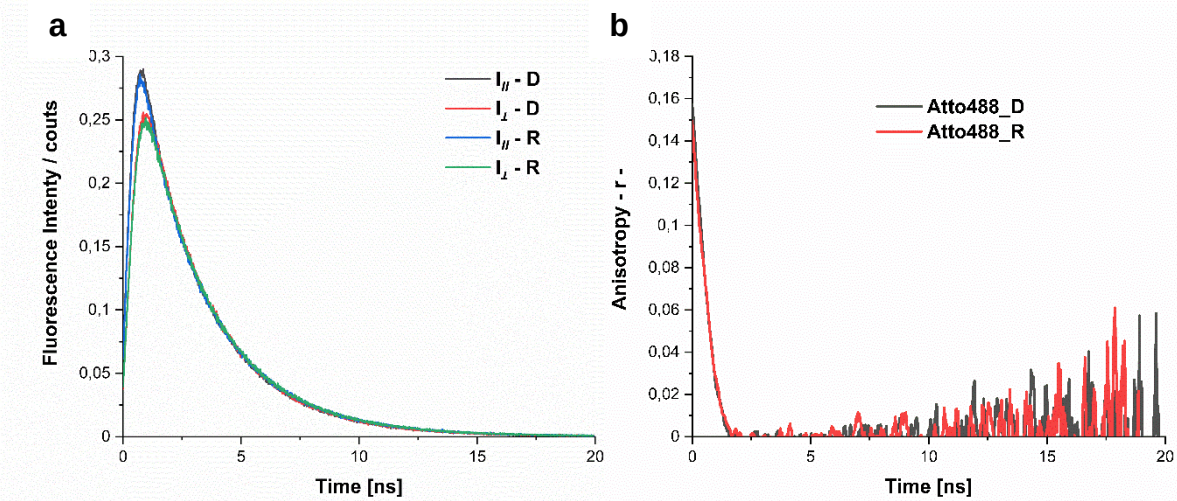

Figure 25: Fluorescence Anisotropy and counts for Atto488 in darkness (D) and after 2 min with R illumination (R): *(a) represents a measurement example of the fluorescence intensity/ counts measured either in a parallel direction (II) or a perpendicular one (⊥). (b) represents the anisotropy decay that is calculated using the data of the fluorescence counts. As a control-test, Atto488 was measured in the same way as the protein samples, to check if the red light could affect the anisotropy of the free Atto.*

The time-resolved fluorescence anisotropy was measured by TCSPC technique (time correlated single photon counting). This enabled the determination of the anisotropy decay, *via* the intensities of the detected depolarization emission in the parallel and orthogonal direction to the polarized incident light *(Figure 25a*).

These fluorescence data were then used in equation (3) for the calculation of the anisotropy decay *(Figure 25b).*

The G factor corresponding to the instrument and wavelength dependent correction factor, was empirically determined for every measuring series, to compensate the bias of the polarization of the detection system. The values obtained varied between 0,95 and 1,066.
As shown in figure 25b, the anisotropy of the free Atto decays very fast and reaches 0 after ~ 1,5 ns and shows no differences between the anisotropy performed in darkness and after irradiation with R. This trial was carried out in the same way as the protein samples, only as a control-test, to determine if the anisotropy of the free Atto is influenced by light.

5.3.2 Anisotropy decay of Agp1 mutants

The same procedure used for the anisotropy detection of the fluorescence dye, was also performed for testing the Agp1 samples, where the parallel and perpendicular depolarized emissions were detected, and the obtained data were used for the calculation of the anisotropy.

The fluorescence anisotropy decays were not only compared for each mutant between their Pr and Pfr form, but also the decay differences between the single mutants used, which also showed differences in the decay behaviour.

Samples measurements were repeated at least 4 times and the anisotropy decay was fitted, using a double exponential function for each measurement.
Furthermore, FCS data were recorded, which enabled the calculation of the hydrodynamic radius for each used mutant (§ 5.3.4).

Observing the fluorescence anisotropy decay of Agp1 mutants, it can be deducted that the shape of this decay differs from the one of Atto488 and does not reach 0 after 20 ns *(Figures 26 – 28)*. These decays consist of a first rapid phase where the anisotropy decays fast between 0 ns – 2 ns, corresponding to the mobility and dynamics of the Atto dye bound to the protein. The second slow phase can be detected starting from 2 ns, represents the mobility of the inner domains of the protein’s subunits.

- **Agp1 mutants of the PCM**

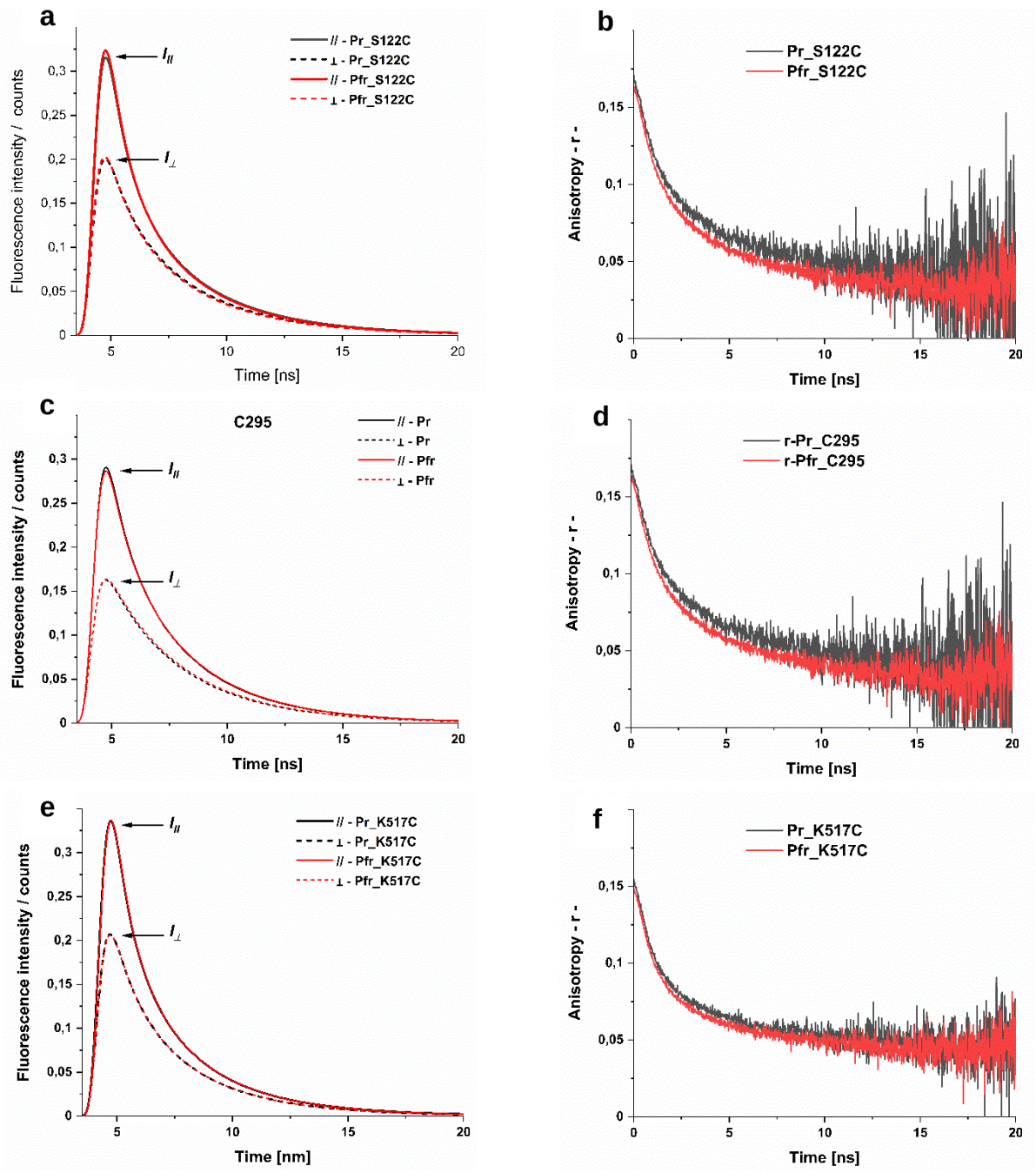

Figure 26: Fluorescence intensity and anisotropy decay of mutations in the PCM domain: *a, c, e) show an example of the fluorescence intensities or counts for the parallel ($I_{//}$) and perpendicular ($I_{\perp}$) depolarisation in the Pr (black) as well in the Pfr form (red).*
b, d, f) show the average of anisotropy decay of 4 measurements derived from the fluorescene count values.for the different mutants between the Pr (black decay) and Pfr (red decay) forms. Minimal differences between the Pr and Pfr form could be seen in the different anisotropy decay, despite the signal-to-noise ratio.

Further anisotropy measurements were performed using other Agp1 mutants, where another position in the PCM was mutated, mainly the position 362 of the β-sheets of the PHY domain, either in its full-length or just using the PCM part *(Figure 27).* This enabled additionally the comparison of the anisotropy decay between the full-length and the PCM protein

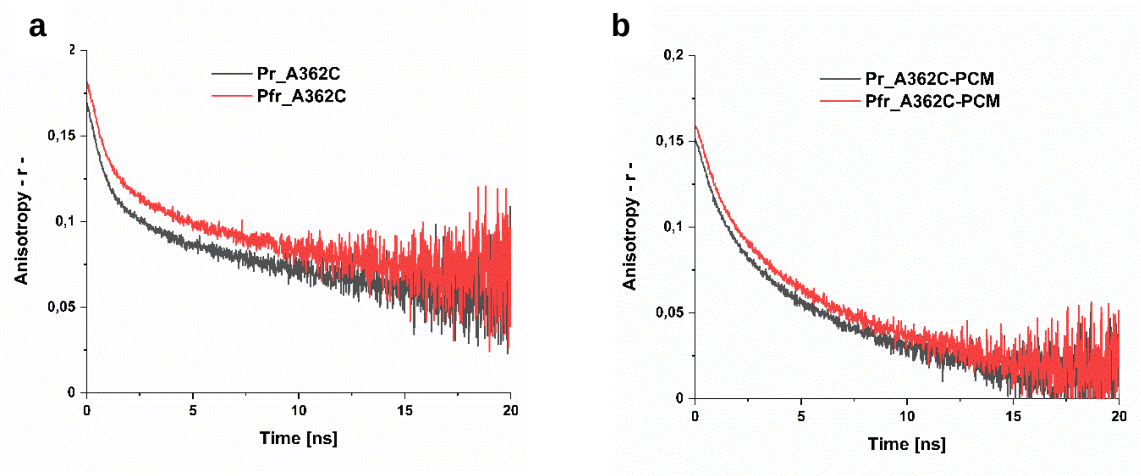

Figure 27: Average of the fluorescence anisotropy decay of A362C full-length and A362C- PCM, (n=4): *a) shows the difference of the anisotropy decay at position 362 of the full-length protein in Pr (black) and Pfr (red) and b) the anisotropy differences in the PCM variant upon photoconversion. The decay in the PCM is faster than in the full length and differences in the dynamics between Pr and Pr can be seen.*

The comparison of the fluorescence anisotropy decays of both the PCM and the full-length protein, reveals that anisotropy decay of the specified domain change upon photoconversion, where both Pfr curves show an upward shift.

Furthermore, a clear difference in the decay behaviour can be seen between these mutants. The comparison of the Pr decays or Pfr decays show that the fluorescence anisotropy of the PCM protein decays more rapidly and r_∞ seems to reach zero faster than the full-length mutants. This suggests thus that the dynamics of the protein at this region is more flexible or faster in the PCM version than in the full length, where the HK is attached *(Figure 28 a & b).* Moreover, since the PCM protein is smaller, it rotates faster, thus the fluorescence anisotropy decays faster and the third phase is reached faster than the full length.

- **Agp1 mutants of the HK module**

Further mutations located in the HK module were also tested, where the autophosphorylation site H528 was mutated into a cysteine in addition to positions R535, K554 and R603 in the ATP binding domain, were also mutated.

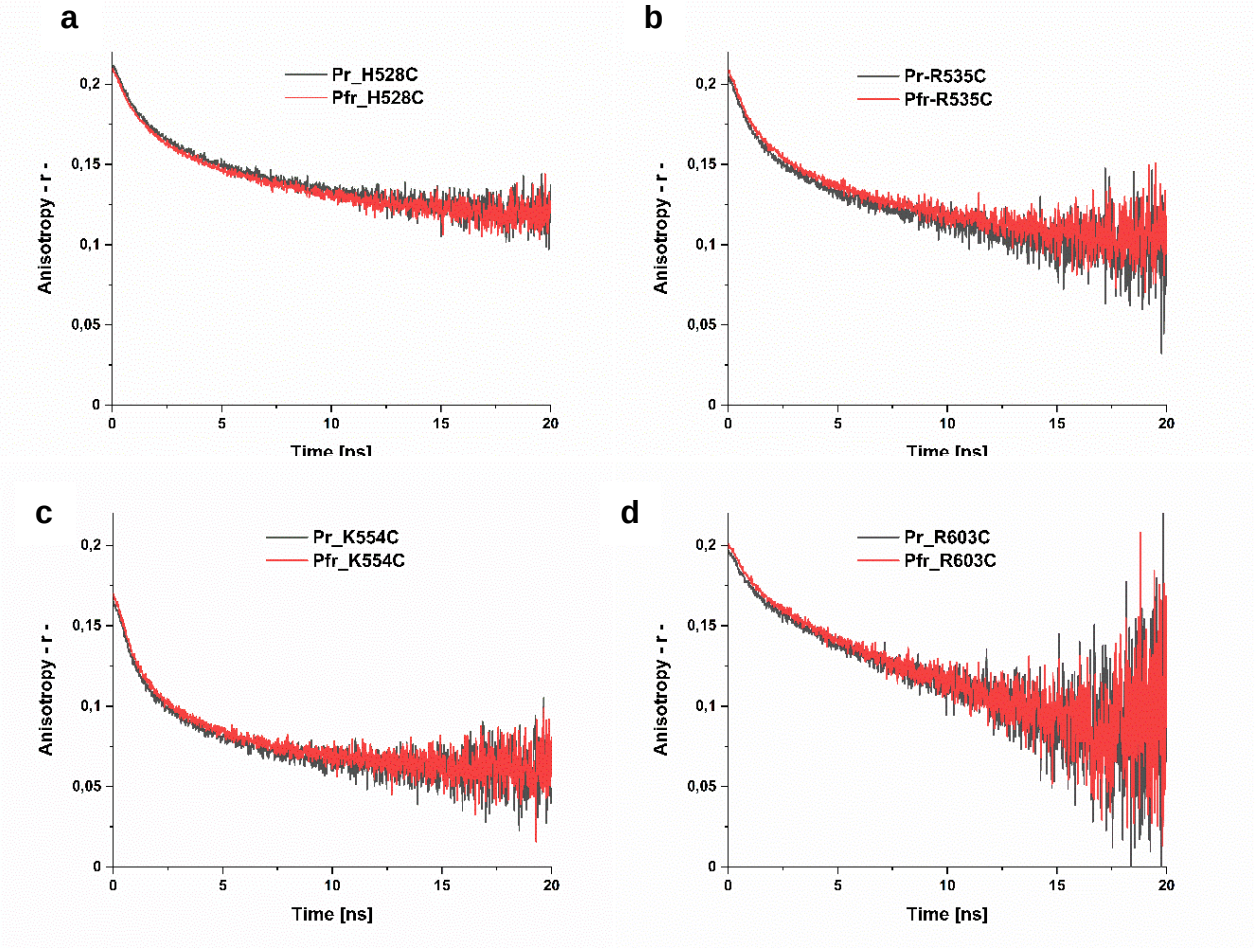

Figure 28: Average of the fluorescence anisotropy decay of H528C, R535C, K554C and R603C (n=3-4): *Different anisotropy decay behaviour can be seen for the different mutants among themselves or in relation to the Pr and Pfr form. Minimal differences of the dynamics upon photoconversion can be seen, despite the intense noise signal*

As shown in figure 28, a very slight shift of the anisotropy decay between the Pr and Pfr form occurs for R535C and R603C, whereas almost no changes can be detected for K554C and H528C. However, these slight differences should not be neglected.
For all these results, the signal-to-noise ratio is remarkable, mostly starting from ~12 ns presumably either due to some fluorescence quenching or to half lifetime of the fluorophore 4.1 ns, which resulted in noisy fluorescence anisotropy profiles. However,

similar anisotropic behaviour could be seen for S122C, C295, A362C and K517C suggesting that the mobility at these positions or domains is faster than the mobility at the positions 528, 535, 554 and 603. In addition to the fact that a noticeable dynamic change in the PCM region could be identified, nonetheless these changes seem to decrease or disappear at the HK domain.

For a better comparison and understanding of the anisotropy decay results, and in order to determine, whether information about the domain movements can be extracted from the data, a double exponential fit function was adapted, which was then used for further analysis and quantification.

5.3.3 Rotational correlation time analysis

As mentioned (§ 4.6.1), a double or two-phase exponential fit decay function was used. This approach enables a more precise quantification of the kinetic components and a better comparison of the anisotropy decay between the Pr and the Pfr form, by comparing the lifetime constants of the decay curves.

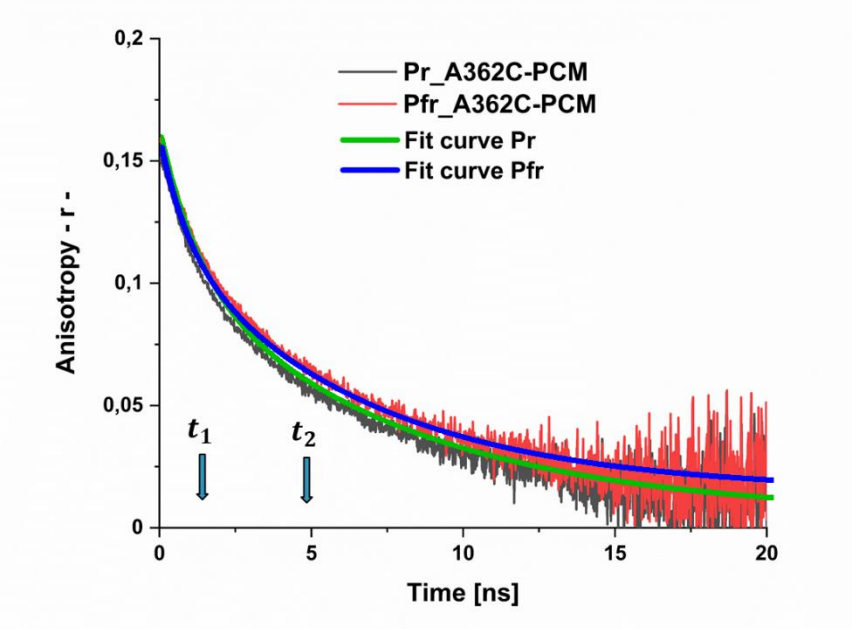

Figure 29: Example of a fluorescence anisotropy decay and the corresponding double exponential fit and time constants. *t_1 refers to the fast phase of the dynamics of the fluorophore Atto488, which is ~ 1 ns. t_2 refers to the dynamics of the domains in the probed protein at the defined label-position starting from ~ 5ns.*

Analyzing the fit curve, three anisotropy decay components could be established and assigned as follows. The first phase corresponds to the fast motion of the attached dye at ~ 0,6 ns. The second slower phase corresponds to the movements of the inner domains at the tested position at the one nanosecond timescale; the last phase which is the slowest phase, corresponds to the overall tumbling of the whole protein (Schröder et al. 2005). This phase depends on the molecular mass and radius of the probed molecule, *e.g.* for serum albumin (66 kDa), this phase was observed at 41.7 ns (Lakowicz 2006b). Hence based on the molecular weight of the Agp1 homodimer ~ 160 kDa, it is expected that the movement of the homodimer corresponds to a kinetic phase with a time constant of ~100 ns, making the third phase very slow.

Therefore, the double exponential fit was sufficient to determine the first two phases with the corresponding kinetic components that are described by the respective time constants. The first time constant (t_1) refers to the rapid phase and the second time constant (t_2) refers to the next slower decay phase of the measured anisotropy *(Figure 29).*

Analysing the results of the lifetime constant t_1 of the rapid phase, all mutants exhibit higher t_1 values than the *decay lifetime* of the measured free Atto, which corresponds to ~ 0.6 ns resulted from the single exponential fit function. Only R603C shows somehow a similar rapid phase, suggesting that at this position the fluorophore is the most flexible, as a free Atto molecule *(Figure 30 a).*

Furthermore, minimal differences can be seen in the first phase upon photoconversion, however these changes are supposed to be insignificant according to the T-Test results, in spite of some mutants *(Table 25).*
The T-Test was carried out, since it serves as a type of inferential statistic and can be used to determine if there is a significant difference between the means of compared groups. In this case, the results of the T-Test refer to the difference between the Pr and Pfr form of the corresponding lifetime constant. These differences are significant, as long as the value of the T-Test $\leq$ 5%

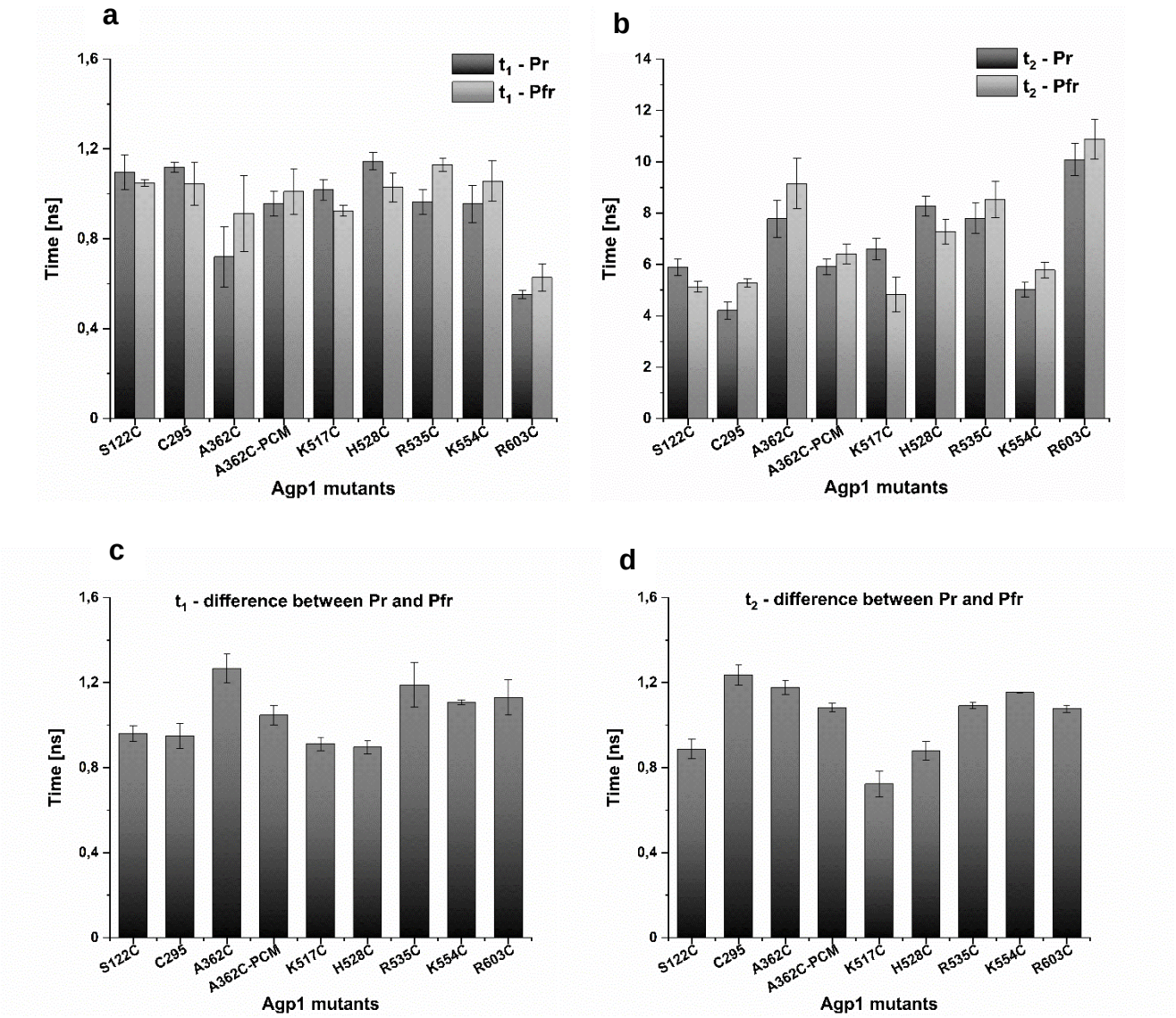

Figure 30: Correlation time constants from the double exponential fit: *The rapid decay phase t_1 (a) and the slower decay phase t_2 (b) for the different Agp1 mutants show a difference of the anisotropy behaviour in both Pr and Pfr form. Nonetheless the significance is more likely to be seen in the second phase, corresponding to the dynamics of the inner domain of the protein. A) and b) represent the average of 4 measurements for Pr and Pfr respectively, whereas c) and d) represent the average difference between Pr and Pfr for t_1 and t_2.*

Nonetheless, these slight differences between Pr and Pfr should not be overlooked at these regions of the protein. Therefore, it was relevant to check the second slow phase, which is described as t_2 value and corresponds not only to the dynamics of the inner domain of the tested Agp1 protein, but also to the different sizes of the tested domains or segments, where the Atto dye is attached to.

Analysing t_2 results of the slower phase decay *(Figure 30 b)*, in addition to results of the calculated T-Test, a significant difference in the dynamics can be seen between the Pr and the Pfr form at the different tested positions. This suggests that the mobility of the domains at these positions in the proteins do change after the photoconversion, however in a different manner. At most positions, the decay in the Pfr became slower having a higher t_2 value in the Pfr than in the Pr, whereas it became faster in the Pfr at positions 122, 517 and 528.

Table 25: *T-Test results for the determination of the difference's significance between Pr and Pfr of both calculated lifetime constants t1 and t2*

Mutants	**T-Test – t1**	**T-Test – t2**
S122C	17.83 %	4.7 %
C295	21.97 %	0.7 %
A362C	2.94 %	0.6 %
A362C_PCM	15.5 %	1.1%
K517C	4.5 %	1.0 %
H528C	2.0 %	3.4 %
R535C	6.4 %	0.6 %
K554C	0.7 %	0.1 %
R603C	9.7 %	1.4 %

From the fitted double exponential function, it was also possible to determine the amplitudes, which are a measure of the motional freedom of the respective component. The average values of these amplitudes in addition to the average values of the correlation time constants represented in figures 30a and 30b are tabulated in the table 26.

Table 26: *Average values of the rotational correlation times and amplitudes resulting from the double-exponential fit decay. The error of the amplitude values, ranged from 0.001 to 0.005*

Agp1 mutants	A_1		A_2		t_1		t_2	
	Pr	Pfr	Pr	Pfr	Pr	Pr	Pr	Pfr
S122C	0.07	0.07	0.07	0.07	1.1	1.0	5.8	5.1
C295	0.07	0.08	0.07	0.06	1.1	1.0	4.3	5.3
A362C	0.06	0.06	0.06	0.06	0.7	0.9	7.8	9.2
A362C-PCM	0.04	0.04	0.11	0.11	1.0	1.0	5.9	6.4
K517C	0.07	0.06	0.04	0.05	1.0	0.9	6.6	4.8
H528C	0.04	0.03	0.06	0.06	1.1	1.0	8.3	7.3
R535C	0.04	0.04	0.08	0.07	1.0	1.1	7.8	8.5
K554C	0.05	0.06	0.06	0.06	1.0	1.1	5.0	5.8
R603C	0.02	0.02	0.11	0.12	0.6	0.6	10.1	10.9

Comparing the amplitudes of the second phase, mutants showed almost similar values, except for Agp1 mutants A362C-PCM and R603C.

Thus, Agp1 mutants exhibit different anisotropy decays for both Pr and Pfr form with almost the same initial anisotropy value r_0 but a different residual anisotropy value, depending on the decay rate. In addition to the time constant values of the second slow phase, it can be concluded, that some mutants exhibit a similar fast anisotropy decay rate, such as S122C, C295, A362C PCM, K517C and K554C. Whereas A362C full-length, H528C, R535C and R603C show a slower decay, where R603C has the lowest decay rate of them all in both Pr and Pfr form.

5.3.4 Determination of the hydrodynamic radius in Pfr

By means of fluorescence correlation spectroscopy it was possible to perceive the time correlation function (TCF) of the probes, hence allowing the determination of the mobility or rotation of molecules.

Figure 31a shows an example of the correlation function of the Atto488 used for the calibration of the instrument which was measured several times. The derived mean dwell time was used to determine the correlation diffusion coefficient and hence the hydrodynamic radius of the molecule. The mean dwell time of Atto was about 88 µs,

therefore any similar results when measuring the protein sample, was a sign of free Atto molecules, which were detected in the laser focus and were not considered in the analysis.

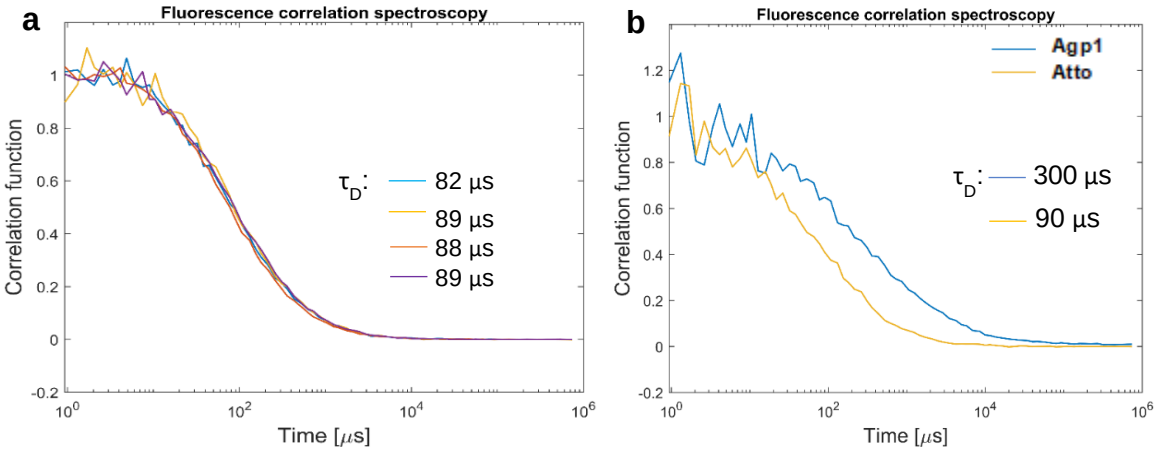

Figure 31: *Illustration of the measured correlation function of the fluorescence dye Atto, which show a mean dwell time at an average of 88 µs (a). b) shows the difference between a free Atto molecule and an Agp1 protein, which shows a prolonged dwell time*

On the contrary, proteins, which are already larger than the Atto molecules, exhibit a longer dwell time *(Figure 31b),* and therefore they possess a larger hydrodynamic radius. The radius of the molecule was calculated using equation 5 (see § 4.6.1).

As is shown in *table 27*, the radius of the molecule is not the same if the different mutants are compared. The mutants, where definite positions in the PCM and at the beginning of the histidine kinase (Position 528) were mutated, show almost the same radius value of ~4,7 nm. The radius increases for the mutations located further in the HK domain to almost double in the ATP-binding domain of the position 603. On the contrary the radius of the A362C-PCM was the lowest of them all, due to its reduced molecular weight in comparison to the full-length protein. Hence, the shape and the size of the Agp1 protein is smaller in the PCM than in the full-length, enabling the molecule to rotate faster in the PCM.

These radius values were the same for Pr as well as for Pfr form with an error range of ±0,2 nm and showed no difference upon the photoconversion.

Table 27: Values of the radius and MM of the mutations at different positions in Agp1

Agp1 mutants	R [nm] - Pr	R [nm] - Pfr	Approximate MM (KDa)
S122C	4,7	4,7	170
C295	4,8	4,8	180
A362C	4,5	4,4	150
K517C	4,7	4,9	170
H528C	4,5	4,5	150
R535C	5,8	5,6	320
K554C	6,3	6,2	410
R603C	8	7,9	850
A362C – PCM	3,5	3,5	67

Furthermore, it could be assumed that the shape of the PCM region is different from the shape of the HK domain, which could be wider, or that the mutations in the HK domain alter the conformation of the protein, hence increasing the radius value.

The estimation of the molecular weight according to the obtained radius values, was calculated using of a converter tool. The converter can be found at the following link: https://www.fluidic.com/resources/Toolkit/hydrodynamic-radius-Converter/.

The results showed that the MM obtained from the radius values, which ranges from 4.5 till 4,8 nm, corresponds the MM of Agp1 homodimer. The increased radius for the mutants R535C, K554C and R603C, showed consequently and increase in the MM.

5.4 Förster Resonance Energy Transfer

In this approach the potential interaction between Agp1 and Agp2 phytochromes was analysed. For this purpose, several cysteines were introduced *via* SDM at various positions in Agp1 protein enabling its labelling and then tested for interaction with the Agp2 protein.

In the first trial, the full-length Agp2-wt was used with the various Agp1 mutants used in the Anisotropy studies, in addition to Agp1-wt full length, Agp1-wt-PCM.

In the second trial of the interaction assay, single mutations were introduced into the Agp2 full-length protein, and then tested with the labelled Agp1K517C mutant. The mutations were introduced at each of the native cysteines in Agp2 at positions 47, 249, 277 and 353, which are located in the PCM region. To eliminate the C647 located in the HK region, Agp2-PCM was used.

5.4.1 FRET using Agp2-wt with Agp1 full-length or Agp1-PCM

5.4.1.1 FRET using Agp1-wt full-length or PCM

In this approach, the potential interaction between Agp2-wt and Agp1-wt full length proteins was tested and it was intended to compare it with the possibility of interaction using Agp1-PCM.

Figures 32 shows the FRET results for Agp2-wt with full-length Agp1-wt and Agp1-PCM, respectively. For all FRET measurements the same analysis was performed. First the fluorescence intensity of Agp1 (FI Agp1) was measured *(Figure 32 a & b, black spectrum)*, with final A_{703nm} = 0.1 as well as its absorption spectrum *(Figure 32 c & d, black spectrum)* was recorded. Then Agp2 protein was measured in the same way *(Figure 32, red spectra),* also with a final A_{755nm} = 0.1. Finally Agp1 and Agp2 were mixed to reach the same final concentrations that were used to record the spectra of the single proteins before (0.1), then the fluorescence (*Figure 32 a & b – blue spectrum)* as well as the absorption spectrum of the mixture were recorded (Figure 32 c & d - blue spectrum).

The first aim of this approach was to examine, if there is any sign of FRET after mixing Agp1 with Agp2. Therefore, further calculation had to be done, to determine the existence of FRET. For this purpose, the fluorescence intensity of the directly excited donor (I_D) was normalized to the FI of the directly measured mixture containing donors and acceptors (I_{DA}).

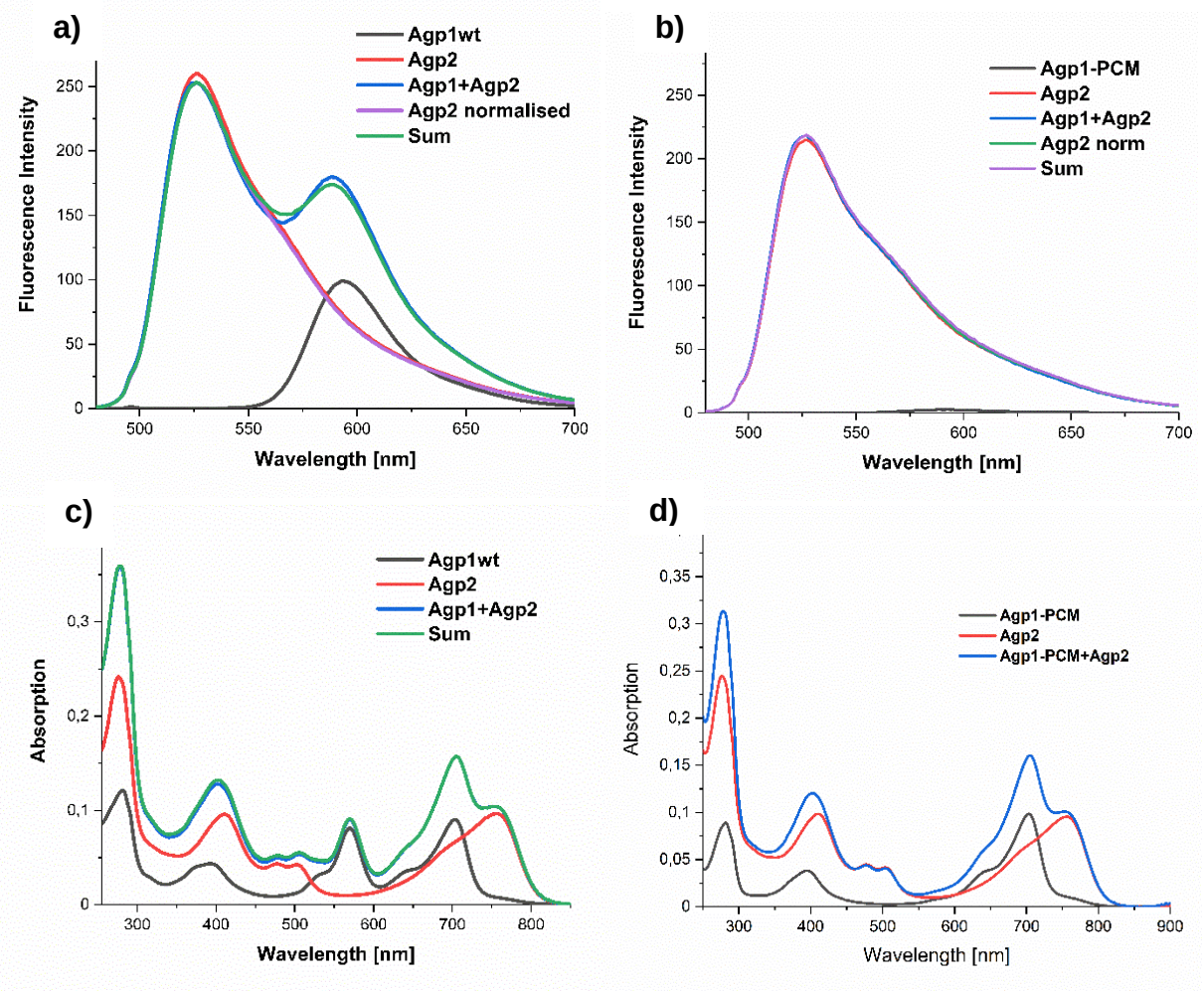

Figure 32: FRET measurements with Agp1wt full-length and Agp1-PCM: *a) & c) represent the emission and absorption spectra of the FRET attempt of Agp2 and Agp1 wt full-length respectively, n=4. b) & d) represent the fluorescence emission and the absorption spectra of the FRET attempt of Agp2 wt and Agp1-PCM respectively, n=1. A slight FRET signal is to be seen using Agp1wt full length, whereas no FRET measurements were possible using Agp1-PCM, due to the unlabelled Agp1-PCM protein.*

Analysing figure 32, the Agp2 spectrum was normalised to its quenched value in the mixtures *(Figure 32 a & b – lilac spectrum, Agp2 normalised)*. Afterwards, the normalised Agp2 spectrum was added to the already measured Agp1 spectrum to get the sum spectrum *(Figure 32 a & b – green spectrum, Sum)*, which corresponds to the likely summed, overall fluorescence intensities emitted by both proteins in case of the absence of interaction, when they are excited separately.

Using this preliminary analysis, it was possible to identify the presence of FRET between the proteins measured, when comparing the fluorescence intensities of the

acceptor in the mixture (blue spectrum) with the calculated sum spectrum (green spectrum) at ~595 nm and corresponds to I_{AD} and I_{AS} respectively. In case of the presence of FRET signal, I_{AD} in the mixture should be higher than I_{AS} of the calculated sum.

Analysing figure 32 a, we can ascertain that Agp2 FI at 525 nm decreases after adding Agp1, whereas the Agp1 FI at ~595 nm increases after the mixture. Furthermore, I_{AD} is higher than I_{AS} of the sum spectrum, suggesting hence the presence of FRET signal between Agp1 and Agp2, however, with a low FRET efficiency.

Comparing now the FRET attempt of Agp1 full length and Agp1-PCM, and since Agp1-PCM could not bind almost any fluorescence dye, Agp1-PCM could not emit any fluorescence as in Agp1-wt, and the spectrum of the mixture has the same shape as Agp2 alone, disabling the determination of FRET using this mutant.
Many other trials were performed to label Agp1-PCM protein using various procedures and changing the used labelling's conditions. For instance, the light conditions were modified, either in darkness or irradiated with red light or even the conduction of the labelling process under normal light, so that if any conformational changes occur, could help the binding of the fluorescence dye. Furthermore, the concentration of the TCEP used was also adjusted, but not more than 20 µM, otherwise the protein would have been damaged and precipitated. Finally, it was also tried to label first the protein instead of its assembly with BV, but all these attempts were condemned to failure and the protein could not be labelled in any way.

5.4.1.1 FRET using full-length Agp1A362C or Agp1A362C-PCM

Since Agp1-PCM could not be labelled and thus the FRET attempt did not lead to a clear statement, another PCM protein version was used, where a mutation was introduced at position 362 and the protein was designated Agp1A362C-PCM.

As shown in figure 33a, the Agp2 FI has decreased at 525 nm and Agp1 FI at 595 nm increased, where I_{AD} is higher than I_{AS}, showing thus the presence of FRET between Agp2 and the mutant Agp1A362C.

On the other hand, by observing the FRET experiment with the protein Agp1A362C-PCM, there is neither a decrease in the Agp2 FI nor is I_{AD} higher than I_{AS}. The absence of FRET can therefore, either be due to the absence of the HK, which seems important for the interaction to occur, or to the lower I_A in Agp1A362C-PCM as in Agp1A362C full-length, which leads to an undetectable FRET signal.

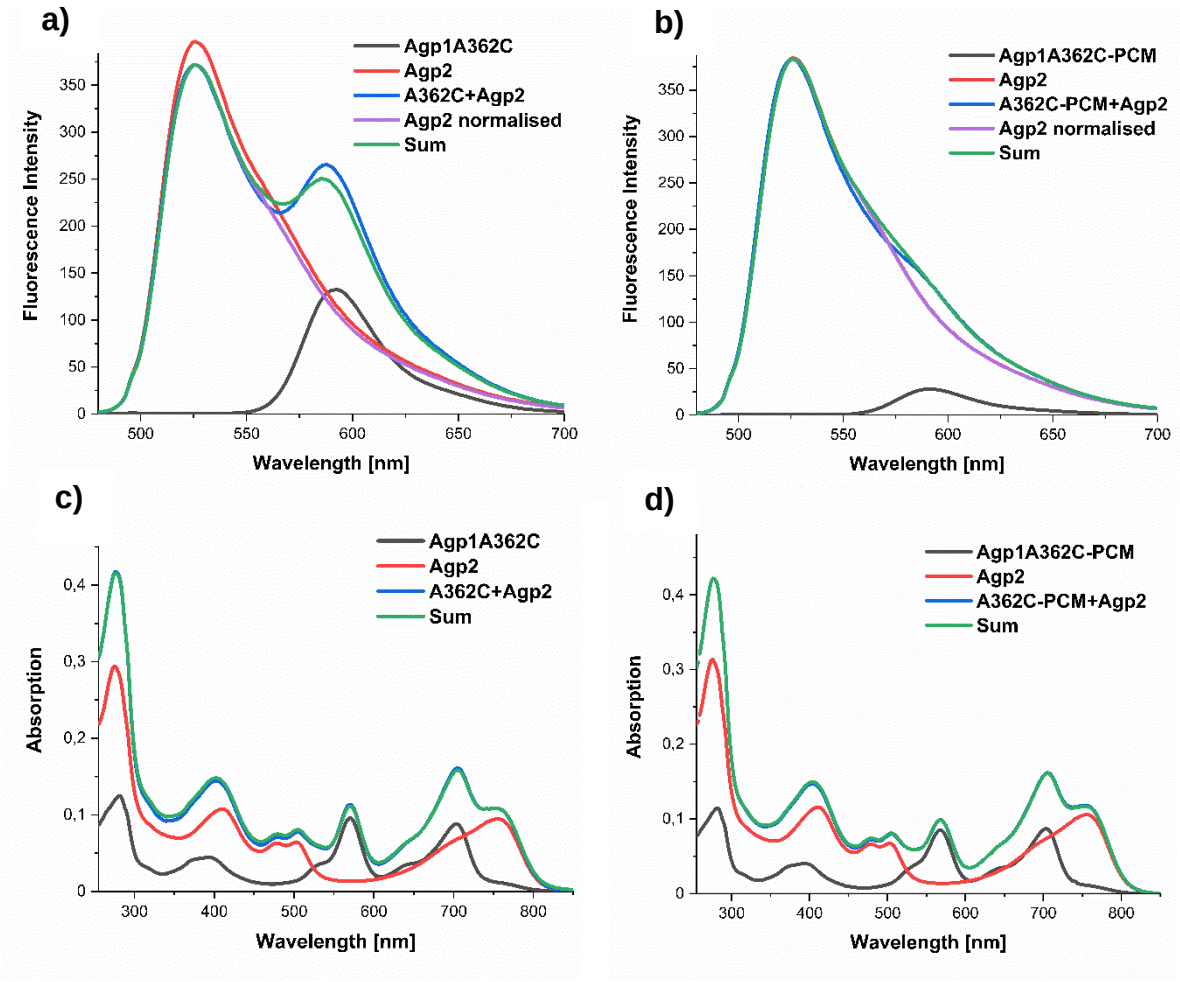

Figure 33: FRET measurements using full length Agp1A362C and Agp1A362C-PCM: *a) & c) represent the average emission and absorption spectra of 4 repeats (n=4) for the FRET experiment Agp2 and full-length Agp1A362C, respectively. b) & d) represent the average fluorescence and absorption spectra of the FRET attempt of Agp2 wt with Agp1A362C-PCM respectively, n=3. A FRET signal can be seen for the full-length protein Agp1-A362C, whereas no FRET signal can be detected if the PCM protein is used.*

5.4.2 FRET using Agp2 with various Agp1 mutants full-length

Based on these results, further FRET experiments series using various Agp1 mutants were performed. These mutants as described previously are either located at the beginning of the N-terminal in the PAS domain, in the HK domain or at the end of the C-terminal of the Agp1 phytochrome protein, in the ATP-binding domain.

5.4.2.1 Mutations in the PAS or ATP-binding domains

Comparing both FRET experiments for the mutants Agp1S122C and Agp1R603C, it can be observed that I_D has decreased after its mixing with Agp1 and I_{DA} is higher than I_{AS}, emphasising the presence of FRET signal between both proteins and therefore clearly indicating that Agp1 and Agp2 do interact with each other.

Nonetheless, the FRET signal using Agp1R603C is a little different in comparison to Agp1S122C or to Agp1-wt and Agp1A362C.This could be due to the respective lower FI of R603C, which is as half as low, since Agp1R603C was not as good labelled as Agp1S122C *(Figure 34), (§ 5.1.3, table 22).*

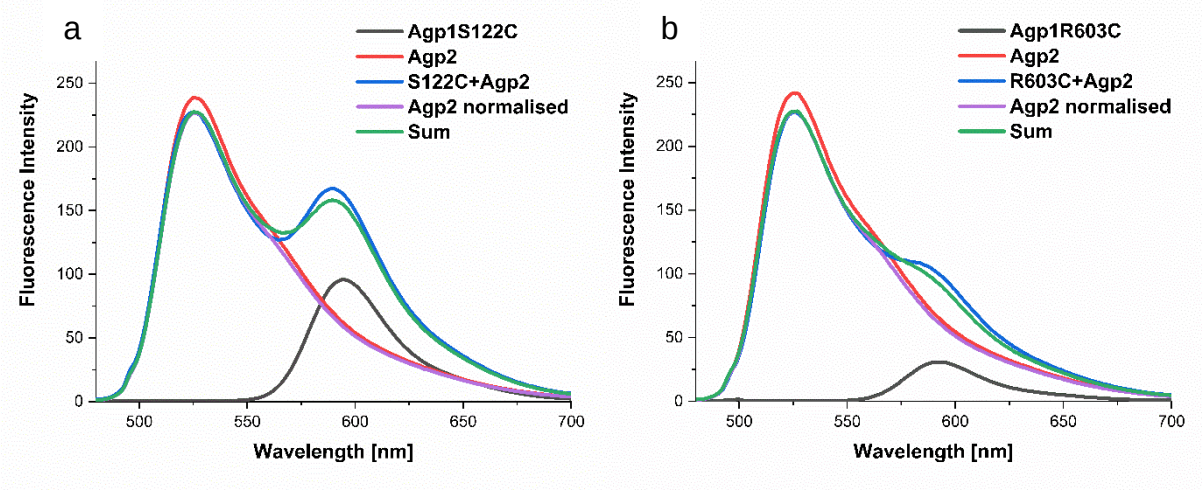

Figure 34: FRET measurement with Agp1S122C and Agp1R603C: *FRET signal can be seen at positions 122 and 603 of Agp1 protein, which is described by the decreasing of I_D and the increasing of I_A, where I_{AD} (blue spectrum) is higher than I_{AS} (green spectrum) at 595 nm.*

5.4.2.2 Mutations along the HK domain

The last FRET measurements using Agp2-wt, were then performed using mutations starting from the helix connecting the PCM with HK domain, at the beginning of the DHp domain (K517C), to other mutations along the HK domain (R535C and K553C).

The FRET results with these mutants showed a different aspect compared to the mutants mentioned above.

Starting from the helix connecting the PHY and the HK domain, FRET at the position 517 was tested. As is shown in figure 35a, a clear decrease of the FI of Agp2 at 525 nm after its combination with Agp1K517C, in addition to the increasing signal of I_A, where the difference between I_{AD} and I_{AS} is clearly higher, than the above mentioned Agp1 mutants. This leads to the conclusion, that the interaction at this position is higher than the other positions tested. Thus, the donor fluorophore of Agp2 is in a closer proximity to the fluorophore attached at position 517.

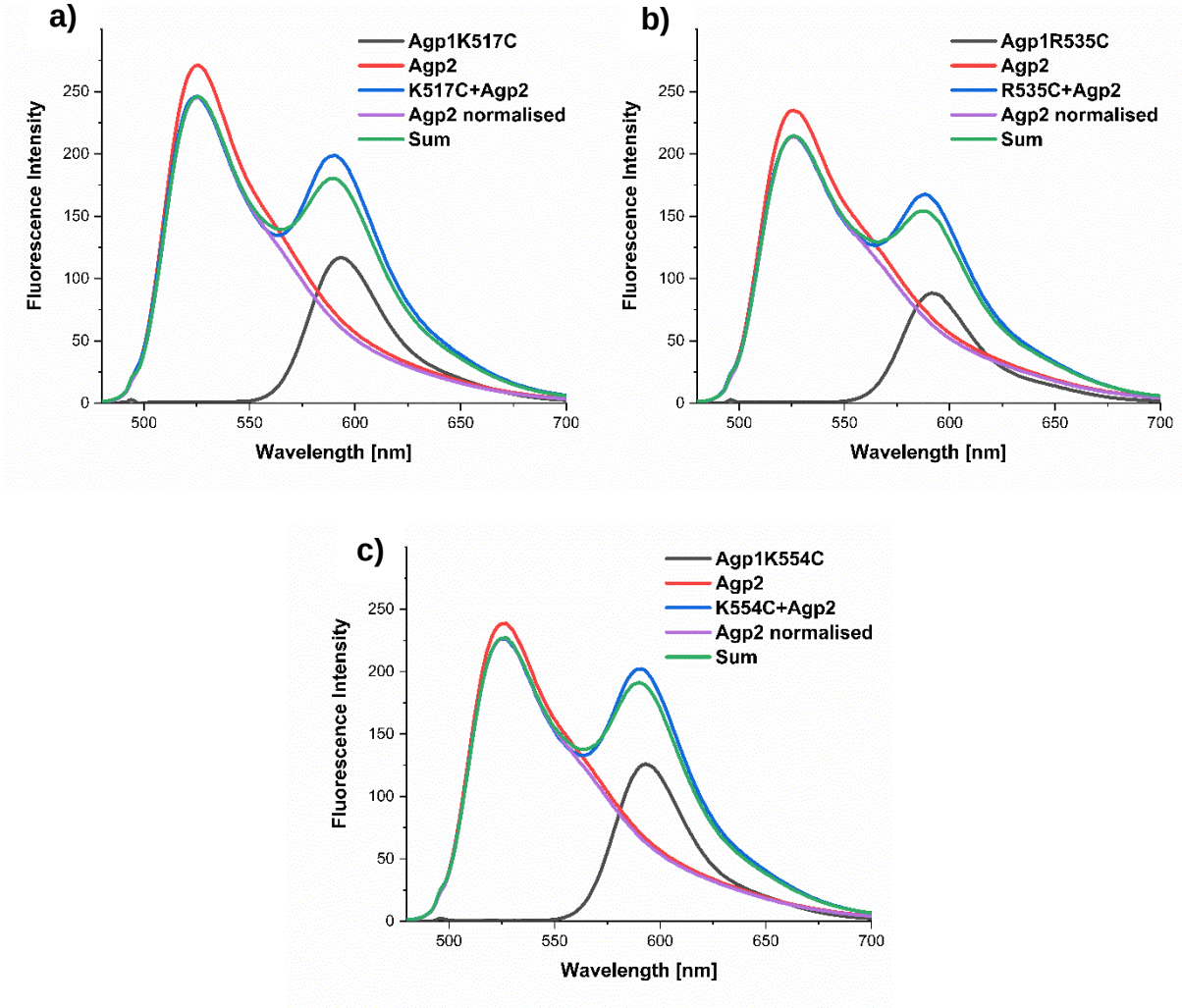

Figure 35: FRET measurement using Agp1K517C, Agp1R535C and Agp1K554C: *these positions are located in the HK domain of Agp1. They all show a FRET signal, however a higher one can be seen at 517 and 535, by comparing the quenching of the donor intensity (I_D). The FRET signal at position 554 seem to be similar to the signal tested using the above-mentioned Agp1 mutants.*

Furthermore, a FRET signal was also detected when using the mutations at position 535 and 554 of the HK domain, however with a different FRET efficiency *(Figure 35 b & c).*

5.4.3 FRET efficiency and distance between Agp1 and Agp2

Based on the above-mentioned results, the presence of a FRET signal can be clearly seen, hence an interaction between Agp2 and the different Agp1 mutants. It was therefore relevant to determine the FRET efficiency E_{FRET} and the derived distance between the donor and acceptor fluorophores, with the aim to see if this interaction can be modelled on the molecular level. As mentioned previously the Förster theory shows that the E_{FRET} varies with the sixth power of the distance *r* between the centre of the molecules according to the equations below *(see also § 4.5.1).*
In the experiments presented here these molecules are the donor and acceptor fluorophores attached to Agp2 or Agp1 protein, respectively.

$$E_{FRET} = \frac{1}{1 + (r/R_0)^6} \qquad E_{FRET} = 1 - \frac{I_{DA} * A_D}{I_D * A_{DA}}$$

Nonetheless, it is important to point out that the calculation of the relative distance could only be correct if there is exactly one donor and exactly one acceptor fluorophore. This is, however, not the case for Agp1-wt, having two cysteines, nor for Agp2 full-length, which could be at least labelled at two different positions (§ 5.1.3). Consequently, the r values were only used to have an overview on the possible distancing.

The extracted I_{DA} and I_D values from the fluorescence emission spectra and the extracted A_A and A_{AD} values from the absorption spectra were used to determine E_{FRET} and the derived spacing between each variant of Agp1 and Agp2. Furthermore, the DOL value of Agp1 proteins was used as CF for the E_{FRET} values since Agp1 had always a higher DOL than Agp2 (§ 4.5.1).

Comparing the calculated E_{FRET} and the relative *r* results, it can be clearly determined that the FRET efficiency was not the same for all Agp1 mutants and consequently also the distances vary respectively between Agp2 and the different Agp1 mutants.

***Table 28: Determination of the average of E_{FRET} and the estimated relative distance**, n=4 at least.*

Agp1 mutants	E_{FRET}	r [Å]
S122C	**0,037**	**86**
Agp1-wt	**0.017**	**98**
A362C	**0.043**	**84**
A362C-PCM	**0.009**	**109**
K517C	**0.137**	**68**
R535C	**0.117**	**70**
K554C	**0.061**	**79**
R603C	**0.045**	**83**

For example, the highest E_{FRET} was seen at the label position 517 of Agp1, followed by E_{FRET} at the label position 535. This suggest that the distance between the attached fluorophore at these positions and the one(s) attached to Agp2-wt are the closest in comparison to the other labelled positions of Agp1 *(Figure 36).*

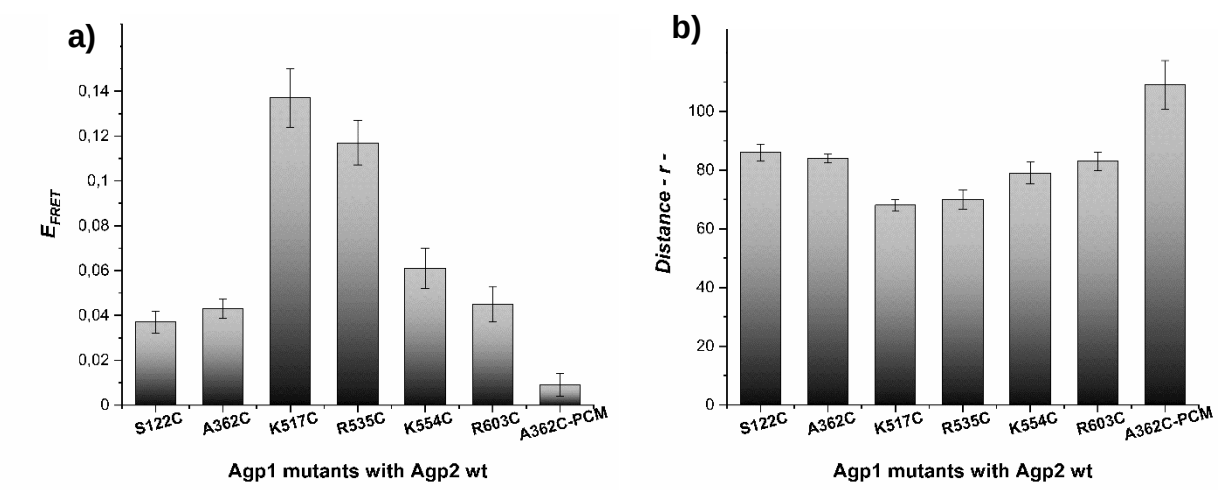

***Figure 36: Average of the E_{FRET} (n=4) and the derived relative distance between Agp2-wt and Agp1 different mutants:** A) show the FRET efficiencies between the donor fluorophores and the acceptor fluorophores labelled at a definite position in Agp1. The highest efficiency was found at position 517, this E_{FRET} decreases either towards the N-Terminus of the PCM (122) or towards the HK domain/ ATP-binding domain. However, no FRET could be detected using the PCM protein B) shows the relative distance separating the bound fluorophores, which is the reverse result as the E_{FRET}. Positions 517 and 535 seems to be the nearest to the donor fluorophores bound to Agp2*

On the other hand, the E_{FRET} between the labelled positions 122, 362, 554, 603 and Agp2 seems to be similar. This suggest that the interaction occur in a way that both phytochromes are positioned, where these positions have almost the same spacing toward the labelled positions of Agp2 involved in this interaction. With the fluorophore labels attached to the native cysteines at positions 279 and 295 in Agp1-wt the lowest FRET efficiency of full-length Apg1 with Agp2-wt is observed. Interestingly, Agp1A362-PCM exhibits a far lower FRET efficiency than Agp1A362, indicating that the interaction of Agp1-PCM with Agp2 is different than the corresponding interaction involving full-length Agp1. This suggests a particular role of the HK module of Agp1 in the interaction with Agp2.

5.4.4 FRET using different Agp2 mutants with Agp1K517C

Based on the results obtained from the FRET measurements between Agp2-wt and the different Agp1 mutants, it was obvious that FRET occurs mainly with the N-terminal helix (DHp domain) of the HK module of Agp1. Nonetheless, it was still not clear how this FRET occurs in Agp2 or where the interaction between both proteins took place. Especially since Agp2 has in total seven free cysteines, but probably only few of them potentially bind the Atto dye, whereas all the Agp1 variants tested have one cysteine, except for Agp1-wt that has 2 cysteines at positions 279 and 295.
For this reason, it was useful to first test the labelling efficiency, by mutating one cysteine residue each time at a specific position in the protein, to determine if this mutation could induce any changes in the degree of labelling, giving thus some hints about the cysteine residue that could mostly bind the fluorescence dye.
Furthermore, it was relevant to test the FRET efficiency using Agp1K517C and Agp2 mutants that enabled to perceive which domain of Agp2 is involved in this interaction.

E_{FRET} and the derived calculated distance between the interacting fluorophores have shown almost similar results *(Figure 37, Table 29)*. The corresponding fluorescence spectra are all listed in §8, Appendix A.

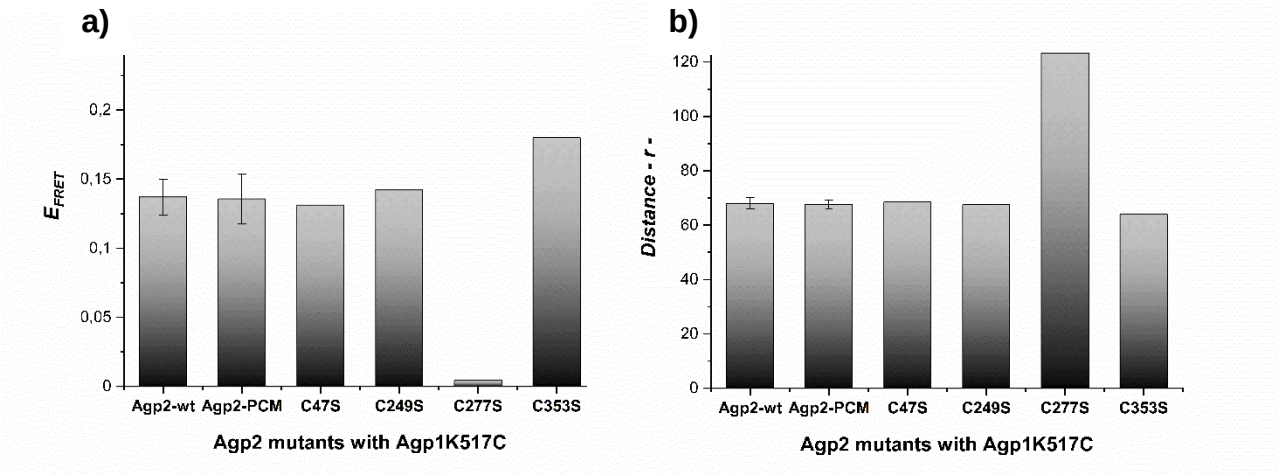

***Figure 37*: FRET efficiency and the resulting distance between Agp1K517C and the corresponding Agp2 mutants used:** *A) E_{FRET} was almost the same using the mutations at positon 47 and 249, in addition to the PCM mutant. On the contrary, it decreased drastically if the mutant C277S is used and increases lightly in case of C353S. B) represents the relative distance between the interacting fluorophores of the corresponding protein, where the distance seems to stay the same, but for the mutation at position 277.*

Table 29: E_{FRET} and the relative distance between Agp1K517C and the different Agp2 mutants

Agp2 mutants	Agp2 wt	Agp2-PCM	Agp2-C47S	Agp2-C249S	Agp2-C277S	Agp2-C353S
E_{FRET}	0,137	0,135	0,131	0,141	0,004	0,18
Distance, r [Å]	68	68	69	67	123	64

The results show that even when the histidine kinase is absent (Agp2-PCM), FRET can occur with Agp1K517C, since for this protein E_{FRET} is almost the same as Agp2-wt is used as the donor. This suggests that the interaction between Agp1 and Agp2 occurs possibly between the HK region of Agp1, starting from the helix of the DHp and the PCM domain of Agp2. Nonetheless, the orientation of these proteins towards each other, is still not clear.

The mutations of the cysteine residue either at the position 47, 249 or 353 of Agp2 led almost to the same efficiency results, suggesting hence that these cysteines are not that relevant for the FRET signal to occur or precisely they are not involved in the FRET with Agp1K517C.

On the contrary the deletion of the cysteine at position 277 has led to the drastic decrease of the $E_{FRET,}$ suggesting thus that FRET occurs mainly *via* the label bound to C277.

Unfortunately, no FRET experiments could be made using mutations at positions 29 and 33 of Agp2, due to lack of time for the generation of these mutations *via* SDM, which seem to be a bit difficult to execute. Additionally, the FRET experiments with C47S, C249S, C277S and C353S could only be performed once.

5.4.5 Light effect on the FRET of Agp2-wt with Agp1K517C

The last series of FRET experiments that was considered in the course of these interaction studies of *A. fabrum* phytochromes, was to test if the illumination with red light R or far-red light FR have an effect on the interaction between both phytochromes. In other words, it was intended to see if the photochromic state of the phytochromes and the the conformational changes resulting from photoconversion, can affect the efficiency of this interaction.

Therefore, one of the Agp1 mutants, Agp1K517C, was used for this purpose in combination with Agp2-wt.
Experiments were then carried out following two different schemes, as previously described *(§ 4.5, Figures 15 & 16).* The results obtained from the analysis of the effect of the light conditions on E_{FRET} are represented in figure 38.

The results show that when both phytochromes are in the Pr form (Pr-Pr) the FRET efficiency decreases and therefore the spacing between the donor and acceptor fluorophores is higher than in their dark-adapted forms; Pr for Agp1 and Pfr for Agp2. When both are in the Pfr form, E_{FRET} increases and therefore the relative distance between the two attached fluorophores decreases. Additionally, when Agp1 is in the Pfr form and Agp2 in the Pr form, there are almost no changes in the E_{FRET}.

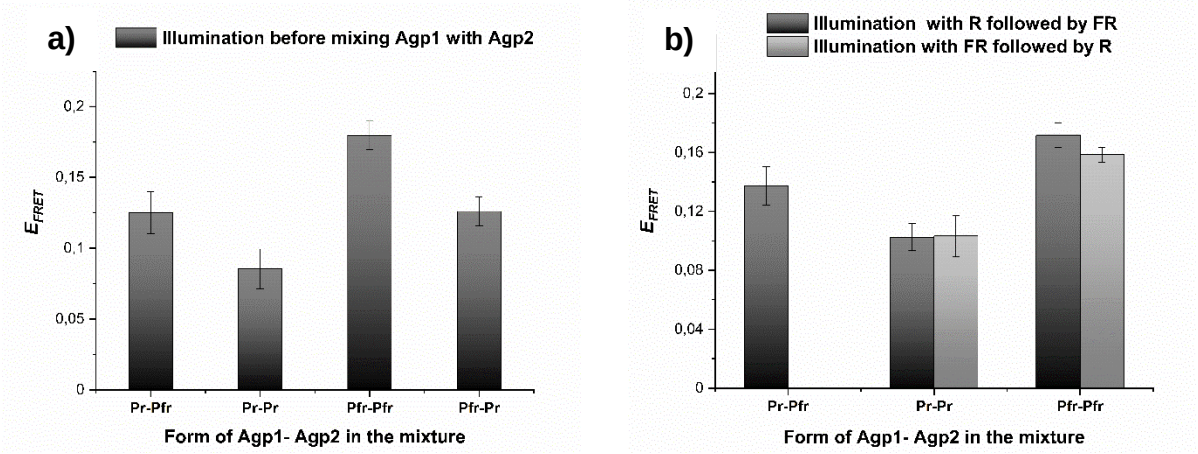

Figure 38: Comparison of E_{FRET} under different light conditions: *A) shows the results illuminating the two proteins separately before mixing them. When Agp1 was illuminated with R, both proteins are predominantly in the Pfr form and E_{FRET} obviously increased. On the contrary, when Agp2 was irradiated with FR and both proteins are predominantly in the Pr form, E_{FRET} decreased. Additionally, when they were both irradiated such that Agp1 was predominantly in Pfr and Agp2 in Pr (Pfr-Pr), E_{FRET} was almost the same as when both proteins were in their respective dark-adapted states (Pr-Pfr). B) shows the resulting E_{FRET} that were obtained if the two proteins were illuminated after mixing. Similar results were obtained from the experiments which followed the two different schemes in A and B.*

These results indicates that the interactions or the structures of the complexes between Agp1 and Agp2 are different in the various cases, suggesting that in the Pfr form both phytochromes are closer to each other. Similar results could be seen, when Agp1 and Agp2 were illuminated after they were mixed in their dark-adapted states.

Table 30: *Relative distance between the label positions of Agp1 and Agp2 after R or FR irradiation, before and after the mixing. Results were rounded to the nearest whole number.*

	Pr – Pfr	**Pr – Pr**	**Pfr – Pfr**	**Pfr – Pr**
Irradiation before mixing	69 Å	74 Å	64 Å	69 Å
Irradiation after mixing, D-R-FR	-	72 Å	65 Å	-
Irradiation after mixing, D-FR-R	-	71 Å	66 Å	-

Since not all absorption spectra were available, as in the case of the FRET using different Agp1 mutants, only the correction factor of the labelling was used in this case and compared to the FRET of Agp1 and Agp2 in their dark-adapted, which was calculated similarly.

5.5 Conjugation studies after TraA knock out

The last approach in the course of the studies of the bacterial signal transduction, was the investigation of the role of the TraA protein in the conjugal transfer of *A. fabrum,* the one encoded by the pTi. The reason for this approach is mainly because Tra genes are supposed to be involved in the signal transduction pathway v*ia* the conjugation mechanism, where TraA is supposed to be the first protein interacting in this process, having the relaxase function that induces the conjugal transfer (Kurenbach et al. 2002; Kopec et al. 2005). Furthermore, first conjugation experiments were performed after the knockout of the whole pTi, resulting in an alteration of the conjugation rate and showing that the conjugation is controlled by the phytochromes (Bai et al. 2016).

For this purpose, the conjugation experiments were performed after the knockout of one of the TraA genes of *A. fabrum*, which is located in the pTi and then the conjugation activity was tested without the presence of the TraA gene, and thus also without the protein TraA that is encoded by this gene.

The conjugation experiments were carried out using different donor strains of *A. fabrum* and using different light conditions. Results show the average of 3 repeats, where each time 3 replicates of the donor strains were prepared.

5.5.1 Preparation of *A. fabrum* donor strains

In order to knock out the TraA gene from the pTi of the *A. fabrum* cells, a pET21b-construct was prepared, containing the two outer ends of the TraA gene with approximately 500bp from each end, surrounding a gentamycin resistance cassette, instead of the original gene sequence.

The construct containing the knocked-out TraA gene was then inserted in the pjQ200SK plasmid, thus enabling the homologous recombination, after the transformation of the plasmid into the various *A. fabrum* donor cells by means of electroporation. As a result, the TraA gene of the pTi was replaced by this TraA knockout construct, making the TraA gene unfunctional. It should be noted that the bacteria needed time to perform the double crossover that takes place during the homologous recombination. Although the single crossover was established rapidly

during the transformation, the double crossover required several generations of cultivation to be accomplished. It was advantageous to subject the cloned bacterial strains to selection pressure so that the DCO is carried out more quickly.

Until the DCO was completed, the phytochromes knock-out mutants of *A. fabrum* donor required six to seven generations, while the wild-type knock-out mutant even required nine generations.

The various donor cells that have already completed the DCO, namely the desired TraA knockout mutants (TraA$^-$), could also grow on kanamycin, since the Kan cassette was introduced in the pBinGus plasmid. The recipient strain that lacks the pBinGus, could only be cultivated in Amp medium. Therefore, if any conjugation occurred, cells must have had both the Amp and the Kan resistance to grow on the plates with double selection, due to the transfer of the DNA having the Kan resistance.

5.5.2 Conjugation assay using different *A. fabrum* donor strains and different light conditions

The conjugal transfer with the different TraA$^-$ donor strains was performed in order to investigate not only the influence of the TraA gene on the DNA transfer but also to investigate the role of Agp1 and Agp2 in this process, in addition to the effect of light.

Hence the conjugation was performed involving donor strains that had both phytochromes (TraA$^-$), or one of these phytochromes (TraA$^-$/Agp1$^-$, or TraA$^-$/Agp2$^-$) or had neither of these phytochromes, which corresponds to the strains (TraA$^-$/Agp12$^-$).

To investigate the effect of light on this conjugal transfer process, the conjugation assay was also performed either in darkness, during R and also during FR irradiation.

The experimental procedures of this approach were performed with the help of a master student – Latifa Hourani – under my supervision.

The conjugation results were quantified according to the number of colonies that grew on the Amp/Kan plates, and are represented in the graph *(Figure 39)* as colony-forming unit per ml (cfu/ml). When analysing the conjugation results, it can be clearly seen that no conjugation occurred when the TraA was knocked out from *A. fabrum* pTi, no matter if the phytochromes Agp1 and Agp2 both were both present or both absent in the cells. Furthermore, for the same cells no conjugation was observed, using different light conditions

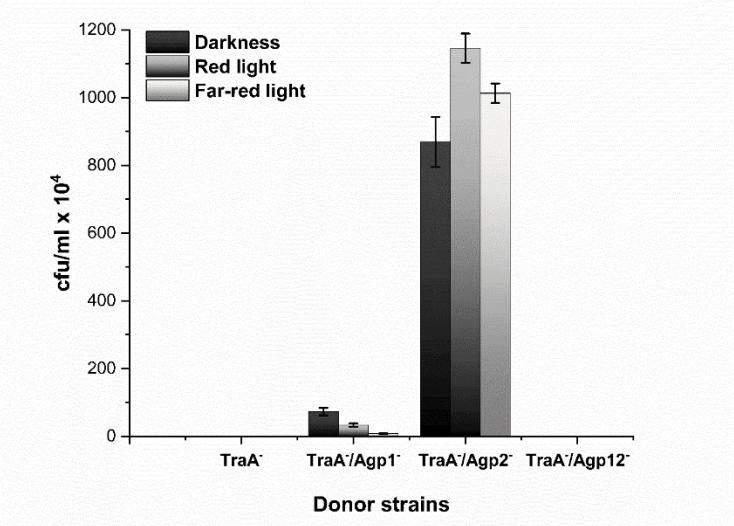

Figure 39: Conjugation results after TraA knockout: *Comparison between the cell density of the conjugation performed in various donor strains with the wt recipient, under different light conditions. The conjugation could not be performed when the TraA gene was knocked out in presence or absence of both phytochromes. Nonetheless, the conjugal transfer occurred if either one of these phytochromes were presented in the cell, however at a different conjugation rate.*

These results lead to the conclusion that TraA is indeed involved in the signal transduction of this DNA transfer process among *A. fabrum* cells.

On the other hand, the conjugation in the Agp1$^-$ cells of *A. fabrum* could take place even without having the TraA gene located in the pTi (TraA$^-$/Agp1$^-$), but with a very low efficiency compared to the conjugation with Agp2$^-$ donor strains that also lack the TraA gene of the pTi (TraA$^-$/Agp2$^-$).

This could mean that the absence of the Agp1 phytochrome in the *A. fabrum* cells, has an influence on the conjugation, in addition to the fact that the light conditions have influenced the conjugation rate without TraA. The highest conjugation rate in the absence of Agp1 could be seen in darkness and the lowest during irradiation with FR.

Moreover, the conjugation using the Agp2$^-$ cells of *A. fabrum* could also take place without the TraA gene, however with higher conjugation efficiency than in the case of TraA$^-$/Agp1$^-$ donor strains. The highest conjugation rate using the TraA$^-$/Agp2$^-$ donor strains could be seen during R irradiation and had almost the same rate in the darkness as under FR light, which is a little bit higher.

These results could lead to the assumption that when one of the phytochromes is not present, the other phytochrome can be activated enhancing thus the DNA transfer by activating the TraA genes encoded by the pAt and the linear chromosome. On the contrary, when both phytochromes are present, they interact with each other, hence inhibiting the activation of the other two TraA genes and thus the conjugal transfer.

6 Discussion

In order to study the signal transduction in *A. fabrum* several approaches were used. On the one hand, fluorescence-based experiments were performed *in vitro* and on the other hand *in vivo* signal transduction studies were carried out, focusing on the conjugal transfer mechanism in *A. fabrum.*

Signal transduction studies were previously performed to determine whether the bacterial phytochromes Agp1 and Agp2 are involved in the transmission of the signal after light absorption by the PCM. Recent research has shown that these phytochromes are relevant and interdependent for some mechanisms in *A. fabrum*, such as conjugation in addition to the alteration of other cellular processes such as cell growth, in addition to the BV assembly and autophosphorylation (Xue et al. 2019)

For further studies on the signal transduction pathways in *A. fabrum*, different approaches were followed. First FRET measurements were carried out, in order to assess whether there is an interaction between Agp1 and Agp2 by using either wild type proteins or mutants, followed by the investigation of possible light effects on this interaction. Furthermore, time-resolved fluorescence anisotropy was used, to test whether the dynamics of the protein differs between the Pr and the Pfr form of the protein Agp1, which was tested by labelling the protein(s) at different positions. Moreover, the autophosphorylation assay was conducted using the same Agp1 mutants as in the previous experiments, which was used as control experiment, to test the functionality of the used Agp1 mutants. A final approach was to study the effect of the protein TraA encoded by the pTi on the conjugation of *A. fabrum in vivo*.

Agp1 mutants that were used for this purpose, were originally prepared to be suitable for spin-labelling so that these could be examined by means of pulsed EPR techniques. They were already generated by Ibrahim Njimona *via* SDM and exploited to gain more information about the distances within the dimer protein upon photoconversion at these positions, by means of pulsed electron-electron double resonance (PELDOR) measurements (Kacprzak et al. 2017). Nonetheless, results have not shown significant differences between the Pr and the Pr. Hence raising the question if not the dynamics of the protein that changes upon photoconversion.

For this purpose, these mutants were again used, since they are distributed at characteristic positions across the whole structure, allowing to study the influence of these mutations on the autophosphorylation activity of the histidine kinase, the dynamics changes at definite domains of the protein and figure out how the interaction occurs between Agp1 and Agp2 on the molecular level.
In addition to the Agp1 mutants mentioned above, two other proteins were used. Agp1 wt, which already contained all the native cysteines and the mutant termed C295, where only the native cysteine at position 279 was mutated to serine, leaving C295 as the only labelling position.

6.1 Preparation of the holoproteins and their labelling

Usually, TCEP was used as reducing agent to reduce the formation of disulfide bonds and prevent the emergence of other oxidative products of the SH group with the aim of ensuring the following labelling. In the process of the BV assembly, the first gel filtration did not only get rid of the residual BV molecules but also from the applied TCEP. In its absence the reduced SH groups slowly get re-oxidized and therefore reformation of disulfide bonds that inhibit the binding of atto and therefore the degree of labelling is dependent on the amount of SH groups left to bind. Not to mention, that the position of the cysteine residue within the protein can also affect the degree of labelling.

Furthermore, a strong maximum at 280 nm was sometimes identified, which refers not only to the amount of proteins in the sample but also to the amount of every aromatic amino acid presented in the sample characterized through the absorbance at this wavelength. The latter can either be found in the protein itself, the BV or even in the applied fluorescent dyes. In addition, disulfide bonds that can also contribute to the absorption at this wavelength, however not as significant.

Depending on the sample, it can be observed a variation in the binding efficiency of chromophore at C20 of the Agp1 phytochromes wt and mutants. The yield of the chromophore assembly has typical values of 83 -100 % for the protein presented here. Consequently, unoccupied C20 could be accessible for other reagents (Borucki and Lamparter 2009) and presumably for the Atto dye. Therefore, it could be possible that

both cysteines, the introduced one *via* SDM and also to some extent the C20 were available for either a covalent or a non-covalent linkage of the dye in each of the samples (Kacprzak et al. 2017).

When comparing all labelled Agp1 mutants, one can observe that the labelling efficiency also differed from one mutant to the other, depending on the location of the cysteine residue and on the type of the protein and whether it is a full-length or just a PCM protein. The cysteine residue can either be exposable and bind easily the fluorescent Atto dye or embedded within the molecule and is therefore inaccessible to other molecules. For instance, Agp1-wt full-length could bind Atto freely, whereas the Agp1-PCM could not bind enough Atto dye (§ 5.4.1). Based on the three-dimensional structure of the PCM of an Agp1 mutant (PDB code 5I5L, or 5HSQ), it is evident that the two native cysteines C279 and C295 are deeply buried in the protein and not easily accessible for various labels (Borucki and Lamparter 2009). Hence suggesting in this case that the histidine kinase could affect the conformation of Agp1 or pull the PCM region, rendering some amino acids unreachable for other molecules. On the contrary the presence of the HK enables the Atto molecules to penetrate and bind easily.

Furthermore, according to the DOL results, A362C-PCM exhibited a lower labelling efficiency as well as a lower BV assembly than the full-length A362C, leading hence to its lower FI. Nonetheless, this low FI of A362C-PCM could be also due to the absence of the HK, which normally induces the protein to assemble as a homodimer. Hence, it could be possible that the absence of the HK has ruined the formation of the dimer and consequently A362C-PCM is presented as a monomer in the solution. This could reduce the FI, since half of the amount of the dyes are bound for the same concentration. Not to mention, the conformational changes of the PCM in comparison to the full-length, which could also have probably induced a quenching in the FI of Agp1.

In addition to the pipetting error, these differences in the DOL or BV assembly could also influence somehow the E_{FRET}, by influencing the amount of quenching of the donor fluorophore. For this reason, correction factors were used, to minimize their effect as much as possible.

Based on the BV assembly and DOL results of Agp2 and its mutants, differences could be seen among them. For instance, Agp2 PCM showed a higher yield of BV assembly but a lower labelling efficiency, suggesting that the cysteine in the HK is more exposed than the other six cysteine residues located in the PCM and is therefore mainly involved in the labelling process. Additionally, it emphasizes the role of the HK in the assembly process and shows again that the PCM region exhibit conformational differences between the PCM region in the PCM protein and in the full-length protein. Thus, making some position of the molecule more flexible or exposed for other molecules such as BV to bind more efficiently.

The mutation of the cysteines at the positions 42, and 353 showed a comparable DOL and BV assembly as the Agp2-wt, assuming that their elimination did not affect the labelling as in the PCM mutants. Therefore, it could be possible that these cysteines do not bind that much atto molecules or even can't be labelled, leaving thus the hypothesis, that Atto binds mostly in the HK, at position 249, 277 and probably also in the PAS domain at the position 29 and 33. Unfortunately, the mutation of these last two cysteines could not be performed due to the lack of time.

The results of the DOL and the BV assembly after elimination of the C277 and C249, suggest that possibly the cysteines at these positions are involved in the assembly process of the BV on the C13. Possibly by stabilizing its binding at the C13, due to their near displacement to the C13/ the chromophore BV *(Figure 40),* and the removal of one or the other cysteine could have rearranged the binding pocket, where BV can be embedded in.

On the contrary, the mutation of one of these cysteines seemed to accelerate the binding of the fluorophore dye, leading to the assumption that upon removal of one cysteine, the other cysteine could be more exposed and possibly they are not able to compete to bind the Atto molecules.

Positions 29, 33 and 47 are also very close to each other *(Figure 40).* Besides the labelling or the assembly at the position 47 were not influenced by the mutation, it could be possible that the cysteines at 29 and 33 act the same way as C47 and probably Atto cannot or hardly attach to these positions since they are in a close proximity *and* seem to be deeply buried.

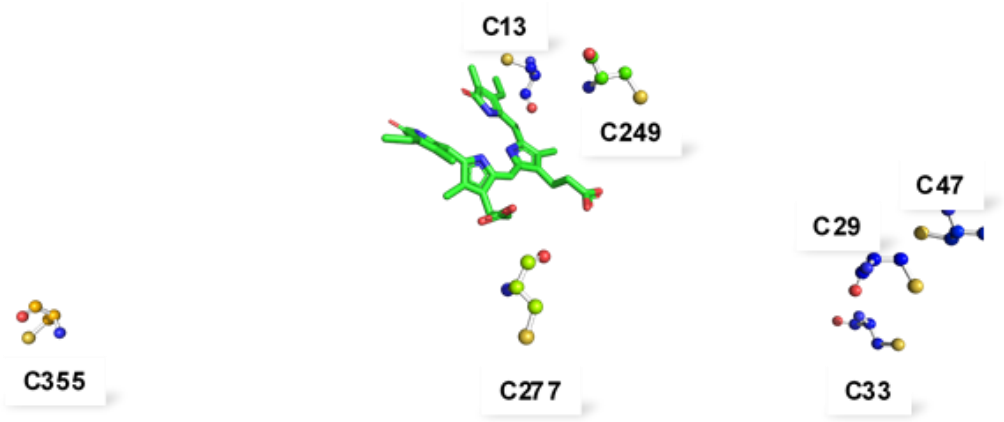

***Figure 40**: **Illustration of all the cysteines positions based on the PCM domain structure of Agp2** Showing the cluster of the positions in the PAS domain (C29, C33, C47), the near distance of C249, C277 to C13 and the far location of C353 towards the other cysteines*

According to these results and the results of MALDI-TOF, it could be concluded that the main cysteines involved in the labelling process are presumably C249, C277 and C647 and that C277S has a significant different conformation than the wildtype.

6.2 Kinase activity of Agp1 mutants

In the course of this project the signal transduction pathway in the photoactive *A. fabrum was* first investigated *in vitro via* autophosphorylation studies of the HK in Agp1. The aim of this approach was to see if mutations in Agp1 protein at different positions, could affect the signal transmission by influencing the kinase activity, and mainly to reveal possible alterations upon photoconversion. Since strong differences using the single mutants would be a problem for the informative value of the fluorescence-based experiments.

As previously reported the autophosphorylation reaction of Agp1 wt occurs preferably in the Pr state but it decreases after red light illumination (Lamparter et al. 2002). Autophosphorylation results for all the used mutants have also shown differences in the kinase activity upon photoconversion, where the yield decreases in the Pfr form compared to the Pr form *(§ 5.2, Figure 20).* The differences indicate only minor variation in the autophosphorylation activity, which is hence advantageous for the usability of the mutants for the other experiments.
Considering the fact that a RR is involved in the phosphorylation reaction (Multamäki et al. 2020), it will receive a phosphate from Agp1 during the phosphotransfer reaction, however, this phosphotransfer seems to be altered upon photoconversion.

This emphasize the fact that phytochrome photoactivation comprise large-scale of structural changes in the photosensory module upon photoconversion, which are then passed on to the output HK domain (Burgie and Vierstra 2014; Burgie et al. 2016; Takala et al. 2014) These conformational changes are mainly in the so-called tongue and in the DHp bundle, which likely include rotation, bending, or changes in register of the constituent helices (Möglich 2019). Therefore, these conformational transitions could indeed alter the interactions and/or enzymatic activity of the output HK domain, no matter where the mutations were introduced.

Furthermore, differences in the autophosphorylation activity between the different mutants could be seen. The kinase activity decreased specially for the mutations in the HK in the Pr as well as in the Pfr form, in comparison to Agp1 wt and the mutations located in the PCM domain.
Due to the remarkable reduced kinase activity of the mutants at positions 517, 535, 554 and 603, it can be assumed that the signal transmission becomes more difficult after mutating the mentioned amino acids of the HK domain. Leading to the hypothesis that the respective amino acids K517, R535, R554 and R603 are also somehow involved in the kinase activity and transmission of the signal.

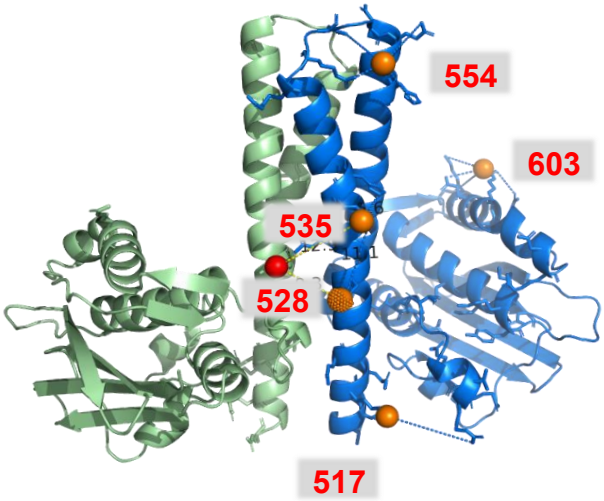

Figure 41: Agp1 Histidine kinase from the homology model T. maritima (4JAU): *showing the positions 517, 535, 554 and 603, where a cysteine was introduced.*

On the other hand, mutations in the PCM domain exhibit a slight difference in the kinase activity when compared to Agp1 wt. Consequently, it could be deduced that an improved signal transmission at 362 can be detected when the alanine is mutated to a cysteine, emphasizing the hypothesis that the so-called tongue of the PHY domain is also involved in transmitting the signal from the PCM to the HK domain.

Moreover, position 603 is located on the ATP-binding part of the histidine kinase, which is why a reduction of the histidine kinase activity can be explained here by a more difficult ATP binding possibility. The amino acid Arg, contains a long-chain residue with a guanidine group, which was replaced by the amino acid cysteine, containing a thiol group. The same hypothesis can be concluded for the mutants K517C and R535C, which also show a particularly low phosphorylation activity and can also be related to their direct positioning in the HK near the autophosphorylation site H528, and points to their subtle influence on the local structure and probably the dynamics of the protein. A similar argument could be made in the case of R603C of the ATP-binding domain. Thus, these amino acids with their long chains and probably their engagement in salt bridges or hydrogen bonds with other amino acids, can play a significant role in the structure formation and stabilization of the phytochrome and hence in the signal transmission since the absence of the described amino acids in this process can

change the flexibility of the protein, which is due to the lack of or the presence of new interaction between the amino acid residues.

Furthermore, other studies of phosphorylation in *Deinococcus radiodurans (DrBphP),* showed that the Arg in the H+7 position participates in the interactions with its RR active site, which is involved in the phosphatase reaction (Multamäki et al. 2020). This thus leads to the conclusion that R535 of Agp1 (H +7) is involved in the signal transduction, due to highly reduced kinase activity in the dark-adapted state Pr.

As a conclusion, mutations in the HK region could slightly affect the kinase activity, probably a phosphatase activity too, or both activities (Hsing et al. 1998), nonetheless they do not affect the whole main autophosphorylation activity of the protein, thus also do not affect its functionality. Hence the structural changes due to the photoconversion or the elimination of one of the mentioned amino acids, specifically in the HK domain, reduces the autophosphorylation yield. It could simply alter a structure that inhibits the access of ATP to the histidine or make it difficult, inhibit or reduce the interaction with the RR, disable the PCM to transduce the signal to the HK effector effectively, or finally decrease the activation of the HK module (Multamäki et al. 2020).

6.3 Time-resolved fluorescence anisotropy

Knowing how a bacterial signal transduction is operated through phytochromes has gained much importance in the research nowadays. In previous research (Xue et al. 2019; Bai et al. 2016; Rottwinkel 2011), the function of *A. fabrum* phytochromes in modulating different cellular mechanisms was elaborated. As for other bacteriophytochromes, this starts by the isomerisation of the BV chromophore upon photoconversion, which is also accompanied by conformational rearrangements that propagate throughout the entire PCM domain (Möglich et al. 2010). It was postulated that these changes pull the PHY domain apart along with the long helix. These rearrangements are then traced from the long helix of the PCM, *via* the linker helices of the HK domain and into the DHp effector module, resulting in a downstream transmission of the signal in case of *D. radiodurans* (Möglich et al. 2010; Takala et al. 2014; Burgie et al. 2016).

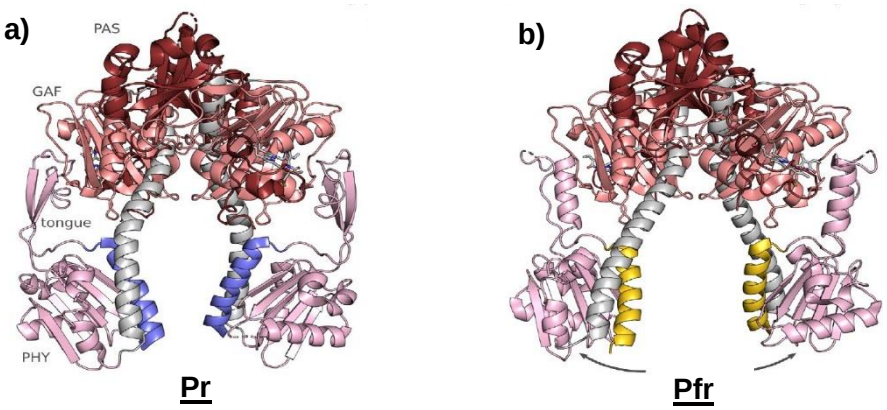

Figure 42: Structure and signaling of bacteriophytochrome histidine kinases*: A) shows the structure of the PCM in the Pr from und b) in the Pfr form, where the long helix (grey) has straightened and pulling apart the PHY domain and causing the rearrangement of the PCM and hence the output helices of the HK (yellow). Figure adopted from (Möglich 2019)*

Nonetheless, PELDOR experiments investigating the distance between the dimer upon photoconversion of Agp1 have not revealed any changes in the distance upon Pr-Pfr conversion (Kacprzak et al. 2017). Both findings do not concur with each other and it is therefore still unclear how phytochromes modulate their biochemical output activity structurally, when absorbing light (Björling et al. 2016).

Based on these circumstances and on the fact that the transmission of the signal is indeed affected after the photoconversion into the Pfr form in case of Agp1 (§ 5.2, and § 6.2), another hypothesis was deployed, suggesting changes of the flexibility or the mobility of the protein domains upon photoconversion, rather than the changing of the distance between the protein dimers. This was based on the unpublished structure results of P. Sheerer, T. Lamparter and N. Krauß et al. and on the Agp1-PCM structures, which are assembled with the locked chromophore 15Za – PDB files 6R27 and 6R26.

To check this hypothesis, experiments using time-resolved fluorescence anisotropy measurements were performed, with the main goal of clarifying the dynamics of protein of the inner domains of Agp1 and changes in these dynamics that may occur upon photoconversion.
Remarkably, these kinds of measurements do not depend on the concentration of the fluorophore, thus on the intensity of the detected signal (Picoquant).

6.3.1 Anisotropy fluorescence decay of Agp1 mutants

As already shown *(§ 5.3.1, Figure 21),* the anisotropy of Atto488 decays very fast reaching zero, which implies the randomly distributed polarization dipoles of the Atto molecules existing without preferable orientation (Jiang et al. 2016). This decay is a characterization of free Atto molecules, that can move freely and rapidly in the sample, owing this to their small size and free mobility.
Comparing the decay of the free Atto and the ones of the labelled protein, it was possible to distinguish that the decay r(t) remained mostly constant and did not reach zero that fast indicating a prolonged depolarization of the emission as a characteristic of the movement of the protein and not the free Atto anymore.

The fluorescence anisotropy decays for the different Agp1 mutants were analysed and compared between the Pr and the Pfr form to see, if any changes in the dynamics occur upon this photoconversion.
For more precise comparison of the fluorescence anisotropy decay between the Pr and the Pfr form, the correlation time or time constant was calculated using a double exponential decay fit function (§ 5.3.3).

Based on the fit results, the decay consisted of two types of phases, that refers to two different correlation time constants. t_1 refers to the rapid phase that corresponds the movement of the Atto dye, whereas t_2 refers to the slower phase decay, and corresponds to the dynamics of that portion or segment, as well as the dynamics of the inner domain of the protein, where the fluorophore is attached to. Therefore t_2 is the correlation time constant of interest (Bucci and Steiner 1988; Kim et al. 2012).

Comparing the fluorescence anisotropy decay of the different Agp1 mutants in the Pr and Pfr form (see § 3.5.2) and the results of the second phase lifetime constant t_2 *(see § 5.3.3, Figure 25b)*, significant differences between the Pr and the Pfr of the different mutants could be deducted, where the dynamics in the Pr seems to be faster or flexible than in the Pfr, at most of the positions of the protein. These changes in dynamics are not only seen in the PCM domain but also in the effector HK domain.

Based on the previous finding, the crystal structure of Agp1-PCM showing how the long helix can rotate about a hinge *(Figure 42)* and exhibiting some flexibility in the Pr form and disappear in the Pfr form (Nagano et al. 2016). These different conformations could also influence the one of the HK. This correlates with the changes in the dynamics that are detected at the position 517 located at the DHp domain, where the dynamic of this this domain is faster in the Pr form in comparison to the other tested positions of the HK module.

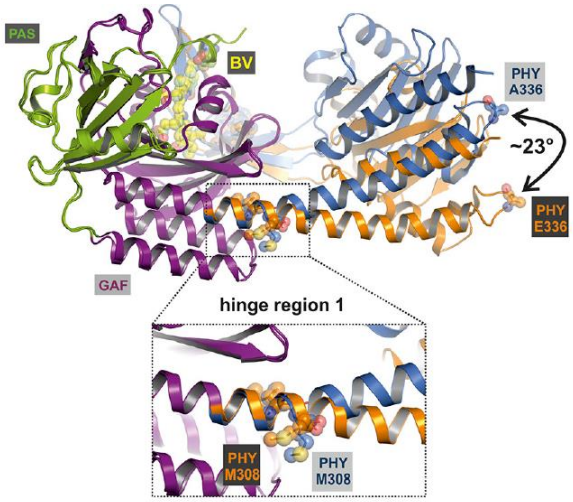

Figure 43: PCM Structure of the SER13 mutant of Agp1: *showing the hinge region, and the possible conformations that this helix could adopt around this hinge. Figure adopted from (Nagano et al. 2016)*

Furthermore, dynamic changes upon photoconversion could also be observed at positions 295 and 122 which are located at the beginning of the long GAF-PHY-connecting helix and a linker loop connecting PAS and GAF domains, respectively. This suggests that these conformational changes around this hinge could be bidirectional and probably propagate through the whole helix, or presumably that this flexibility of the helix could also induces some flexibility at its opposite end. These changes are then accompanied by dynamics changes at its opposite end. Nonetheless the dynamics at these positions is faster, due to their location at the of the helix (C295) and at a linker loop (S122C) and probably the moving segment or inner domain is smaller, leading to the fast dynamic.

Moreover, the position 362, which is located in the tongue connecting the PHY with the GAF domain, shows differences in the dynamics in the full-length as well as in the PCM

mutant. This is due to the isomerisation of the chromophore causing the repositioning of the tip of the tongue and inducing in turn its secondary structure changes and refolding (Takala et al. 2014). These domain motions upon these rearrangements hence influenced the dynamics of the respective domain.

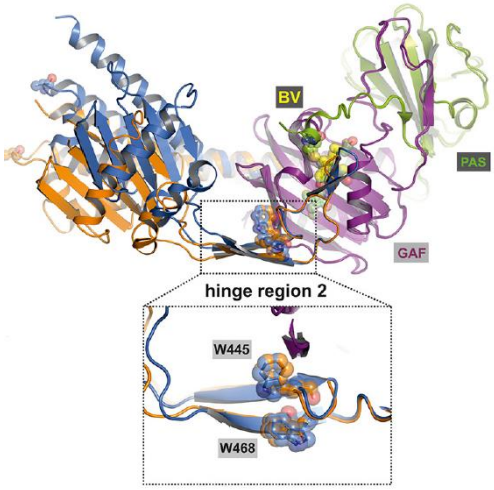

Figure 44: PCM Structure of the SER13 mutant of Agp1: *different orientation of the same structured showed in figure 43, but here showing the second hinge in the middle of the tongue of the PHY domain, which undergoes secondary structure changes upon photoconversion. Figure adopted from (Nagano et al. 2016)*

Moreover, the dynamics of the tongue in the PCM mutant seems to be faster than in the full-length, when comparing the dynamics of Agp1 having the label at position 362. Emphasizing hence, that the protein in the PCM is more flexible, leading to the assumption that the HK plays a role in the structure stabilisation of the Agp1, troubling thus the mobility and flexibility of the PCM domains.

Further observations of the fluorescence anisotropy decay were carried out using Agp1 proteins with mutations in the HK module. The different mutations in the HK domain, located at the position 528, 535, 545 and 603, exhibited slower dynamics in comparison to the PCM except for the position 554. This could be due to its location on the surface of a linker loop, easing hence its dynamics *(§ 5.1.1, Figure 19).*
Furthermore, these slower dynamics also shows that the label in these cases is in a larger segment that is related to the movable domain.

These changes in the dynamics along the HK domain, suggest that the output domain also undergoes various rearrangements upon photoactivation of the HK, thus regulating diverse signalling processes. Therefore, the transfer of the phosphate from the ATP of the ATP-binding domain to the histidine residue, could then modify the conformation of the protein and consequently its function.

According to previous studies in similar bacterial phytochromes *(D. radiodurans),* various speculations on these rearrangements were proposed. First, they could either include a closure or opening of the active-site cleft, packing of the activation loop, and rotation of the helix between the kinase domains (Grant et al. 2010) or they could lead to an opening of the dimers at some positions in the HK domain (Björling et al. 2016)

On one hand, other studies have speculated that the dimer interface of the output domains can break after its photoactivation upon light absorption, where the crystal structure of a near–full-length phytochrome revealed an open conformation (Björling et al. 2016). On the other hand, crystal structures of bacterial histidine kinases pointed out that the dimer of the output domain stays intact upon its activation in a full-length protein, considering the presence of an additional dimer between the DHp domains of the full-length phytochrome. The last possible suggestion based on x-ray solution scattering implied a rotational motion close to the phosphoaccepting histidine, which was also supported by the quaternary arrangement of the protein (Björling et al. 2016).

6.3.2 Determination of the hydrodynamic radius in Pfr

In this approach it was also possible to determine the hydrodynamic radius of the used protein by means of the fluorescence correlation spectroscopy technique available on the system at the same time as the TCSPC. This technique enabled to perceive the time correlation function (TCF) of the probes, which allowed the observation of the molecular movement and the determination of the hydrodynamic radius of the molecule at each labelled position.
Logically no matter which mutant was used, the same radius should be obtained, since the same protein was used, which is the Agp1 full-length protein. However, large differences in the molecular radius were observed specifically for the examined Agp1

mutants R535C, K554C, R603C of the HK module, in addition to the mutant A362C-PCM.
Usually, differences in the hydrodynamic radius can be only observed, when a protein either has a different mass, as in the case of A362C PCM which showed a smaller radius than the full-length or shows changes in the conformation or structure of the protein. Therefore, any alteration in the radius, will affect either the mobility or the rotational movement of the probed molecule (Schwille and Haustein).

Based on the results of the calculated R_h, the radius of the protein was similar for most of the mutants used, nonetheless it seems to increase for the mutations located next to H528 of the HK domain, where it reaches its maximum at position 603.
This suggests that the conformation of the protein seems to be different for this domain, after the mutation of the arginine at positions 535, 603 and the lysine at position 554.
This leads to the following speculation for the observed differences in the radius values of the HK. The amino acid arginine of R603 has an amphipathic side chain and contains a positively charged guanidium group at the end of the chain.
Based on the hydrophobic interior and the hydrophilic surface of the protein structure, arginine residues are found on the outside part of the protein, enabling the hydrophilic head group to interact with a polar environment, by forming either hydrogen bonding or salt bridges. These interactions could possibly occur either with a neighbouring lysine (K), arginine (R), Aspartate (D) or glutamate (E), maintaining hence the structure of the protein and stabilizing its native folding. If these bonds are broken, **e.g.,** upon their mutation with a cysteine residue, this probably leads to conformational changes and a refolding of the native protein structure either on the monomer level or also the homodimer level. Thus, these conformational changes could have altered structure of the protein and hence its radius e.g., in case of the mutations at the positions 535 and 554, which were formerly an arginine and a lysine residue, respectively.

Nonetheless, it could also be possible, that free cysteines still exist in the sample, that could not bind the fluorescence dye Atto. This would leave these residues free to interact with other free cysteines allowing the formation of disulfide-bonded dimer of the homodimer protein. Leading thus to conformational changes and formation of protein aggregates, specifically if the cysteine residue is exposed, easing hence the

bonding of additional molecules to form possibly a tetramer, i.e., in case of the mutant Agp1R603C or also Agp1K554C. Nevertheless the analysis of FCS curves is prone to artifacts that may lead to erroneous size determination (Sherman et al. 2008).
Nonetheless, comparing the radius values between the Pr and the Pfr from, no significant differences can be concluded. Hence, emphasizing that the dimer does not pull apart upon photoconversion.

Based on the above-mentioned speculations about the rearrangements of the HK domain and the above-mentioned results, the following hypothesis could be also formulated. The two monomers of the HK are coiled around each other and it seems that the mutations at H+7 and H+26 modifies its degree of coiling by somehow altering the existing bonds between the amino acids that maintain the dimerization of the HK. Hence, it could be possible that these changes in the radius at these positions have also altered the phosphorylation yield *(§ 5.2.1, Figure 20),* since the angular orientation of the coiled coil linker is crucial for kinase functionality and also their dynamics (Björling et al. 2016).
Moreover, based on computer molecular simulations (Kacprzak et al. 2017; Dago et al. 2012), it was also suggested that the activation of the HK involves a rotation of the ATP binding sites, by approximately 90° around the helix bundle axis of the kinase (Björling et al. 2016; Dago et al. 2012). It could be thus possible that this rotation is affected by the mutation, influencing hence its conformation and therefore the radius and the autophosphorylation yield accordingly.

6.3.3 Parameters influencing anisotropy measurements

Different challenges were confronted during the anisotropy measurements. Therefore, it was important to assess some parameters that could have affected the measurements and the derived results.
When preparing the samples, the aim was to achieve a final concentration of the labelled holoprotein ~ 10 nM based on the absorption measurements at 703 nm. However, depending on the value of the laser power, which was maintained constant, it was necessary to either dilute further or concentrate the already prepared sample. This led to different final concentrations for the probes as well as different amount of

protein molecules in the probe. The reason A_{703nm} was used for the assessment of the concentration, was to ensure the same the amount of the holoprotein necessary for the photoconversion. Therefore, the assembly was optimized, to obtain the maximum yield of holoprotein. Nonetheless, it could be still possible that the laser hits an apoprotein molecule that is labelled, which will not perform any photoconversion, altering thus the overall yield of the anisotropy decay.
Furthermore, usually the irradiation of Agp1 leads to the formation of only 80% of the Pfr form. Therefore, if for instance only 80% of the protein was assembled with BV, that will lead to ~ 64% of all the molecules that could actually undergo a photoconversion to Pfr form (Kacprzak et al. 2017).

On the technical level, it is possible that the equipment polarization bias, which can derive from the detectors and monochromators, could have affected the measurements. This may show bias for one plane of polarization over another. In this case it could be possible that more counts were detected on the // detector than on the ⊥ one, nonetheless, this polarisation effect was tried to be reduced by measuring the G factor.
Interestingly, another experimental bias could have been introduced, due to the hindered rotation of the fluorophore or the mobility of the protein, which was the adhesion of the protein to the surface of the cover slip. For this reason, the sample was incubated ~ 10 – 15 min on the cover slip in order to enable the protein to adhere uniformly prior to the measurement, which could decrease the aggregation during the measurement, reducing thus the different molecular brightness caused by the fluorescence quenching rate that could be encountered during the measurements. This is mainly due to a changed environment of the chromophore, or the fluorescence enhancement of single particles due to aggregation effects.

6.4 Interaction studies of Agp1 and Agp2 phytochromes

Previous findings regarding the possibility of interaction between Agp1 and Agp2, show that e.g., the conjugation in *A. fabrum* is not only light regulated but also mediated by both phytochromes Agp1 and Agp2 (Bai et al. 2016). The fact that Agp1 and Agp2 can

act together influencing hence other mechanisms, such as the BV assembly to the phytochrome, the autophosphorylation mechanism or even cell growth (Xue et al. 2019), made it necessary to test the protein-protein interactions between both phytochromes.
For the purpose of understanding more about these phytochrome interaction possibilities, *in vitro* FRET studies were carried out. Using diverse approaches, the interaction of the phytochromes was analyzed, mainly elucidating, which regions of the two proteins are in close proximity to each other in the putative complex.

Therefore, FRET was first tested using Agp2-wt as a donor and several Agp1 mutants in their full-length form or just their PCM part as an acceptor. Then Agp2 mutants were tested with Agp1K517C and finally, the light effect on this interaction was also tested.

6.4.1 FRET using Agp2-wt with Agp1 full-length or Agp1-PCM

Since Histidine kinases are involved in the signal transduction pathway, *via* their autophosphorylation mechanism, thereby regulating various biological processes, the role of the HK module was assessed in this part of the present work. FRET studies were therefore applied, to test, whether the HK is involved in this interaction between Agp1 and Agp2 phytochromes.
For this purpose, FRET experiments with Agp1 full-length were first performed and compared with the FRET experiments using Agp1-PCM, which lacks the HK module.

Agp1-wt and Agp2-wt display, as previously mentioned, different amounts of cysteines located at different positions within the protein. Consequently, leading to a different labelling pattern.

Comparing the FRET results of Agp1-wt full-length and its PCM version, Agp1-wt full-length has resulted in a FRET signal, leading to the assumption that both phytochromes interact with each other. On the contrary, Agp1-wt PCM could barely be labelled, thus no FRET signal could be detected.

Since the comparison of the full-length Agp1-wt with the PCM has not led to an assertion regarding the function of the HK in this FRET approach, the same experiment was applied using a mutant of the Agp1 protein. In this regard, Agp1-A362C mutant

was used either in its full-length or just using its PCM part. The reason for this selection, is that each position in the protein differs from the others and can be presumably influenced differently in the presence or absence of the HK, and the HK module seems to be important for the interaction of Agp1 with Agp2.

Comparing the FRET results of the full-length Agp1A362C and its PCM variant, a decrease in the donor intensity at 525 nm could be clearly noticed, leading to presence of a FRET signal in the full length, emphasizing that Agp1 and Agp2 could interact with each other. On the contrary, the absence of the FRET signal in the PCM variant could either be due to the absence of the HK, which seems to keep Agp1 and Agp2 in a nearer distance, enabling the formation of the interaction complex, or due to the low FI of the acceptor.
Nonetheless, in order to get as complete information as possible about the spatial arrangement of the interacting proteins, further interaction possibilities were tested, using different label positions in the Agp1 protein.

6.4.2 FRET using different Agp1 and Agp2 mutants

Considering the calculated FRET efficiencies obtained from experiments where Agp2-wt was combined with the different Agp1 mutants *(Table 27 and Figure 36)*, it is clear that the lowest efficiencies are to be seen for those Agp1 mutants where the fluorophore was bound to positions in the PCM, *i.e.,* positions 122 and 362. This efficiency increases, when moving further along the protein towards the HK domain, where the highest efficiency was recorded at the label position 517, followed by 535, 554 and finally at the position 603 of the ATP-binding domain. This leads to the conclusion that both phytochromes do interact with each other, in addition to the assumption that these positions are the nearest to the label position of Agp2, where the interaction mostly took place.

Furthermore, the hypothesis of the role of the HK can be formulated again, that the HK of Agp1 is involved in the interaction mechanism with Agp2, based on its ability to enhance the interaction, by reducing or maintaining the distance between the two proteins, when present. This interaction mainly occurs at the beginning of the DHp-

Domain of the HK, where the positions 517 and 535 are involved in this interaction process and the PAS-GAF domain is more distant.

Nonetheless, it is still not clear, if the observed FRET was due to interactions of both proteins, involving the cysteine residue of HK domain of Agp2 or the cysteines located in the PCM. This leads to two possible interaction scenarios, that involves probably either a parallel or an anti-parallel orientation of the molecules.

In the interest of resolving this ambiguity regarding the Agp2 phytochrome interaction site, with the aim to to acquire more data for defining suitable boundary conditions for modelling of the protein-protein interface *via* molecular modeling approaches, further experiments were performed by combining various Agp2 mutants with Agp1K517C, since the highest E_{FRET} was obtained using Agp1K517C in combination with Agp2-wt.

Since E_{FRET} after mixing Agp2-PCM with Agp1K517C was almost the same as for the one performed with the full-length protein, this leads to the conclusion that Agp1 interacts with the HK domain, whereas the PCM of Agp2 is mostly involved.

Additionally, whether this interaction with Agp2 occurs *via* its PAS domain, *via* its GAF or its PHY domain is still not clear, besides that the possible orientation of these molecules, such as an anti-parallel orientation, or a most likely shifted parallel orientation, or even a definite displacement angle between both, is still not clear.

Therefore, the replacement of a single cysteine each time at a definite position in Agp2, was essential to gain more details. According to the E_{FRET} results using the Agp2 mutants, the absence of the label at position 277 has drastically altered the FRET signal with Agp1K517C, suggesting that almost no interaction was possible and therefore that mainly the nearest label positions of Agp2 to the position 517 of Agp1 is probably the position 249 or the position 277.

Furthermore, the E_{FRET} increases slightly after the elimination of the cysteine at position 353, causing probably some conformational changes in the protein, allowing the presumed positions 277 or 249 to converge more towards Agp1, making the label at position 517 nearer to the one of Agp2. Moreover, this increase of the E_{FRET}, could theoretically be due to the fact that the Atto dye at position 353 does not contribute to

FRET, *i.e.,* if it is missing the donor quenching is more effective, emphasizing that presumed labelled positions are candidates for FRET.

Based on these results it can be concluded that Agp1 and Agp2 interact with each other, influencing thus biological processes in *A. fabrum*. This interaction occurs mainly between the DHp domain of the HK in Agp1 and with PCM of Agp2.

6.4.3 Light effect on FRET between Agp2-wt and Agp1K517C

As mentioned previously, phytochromes undergo conformational changes upon photoconversion, which are responsible for spectral changes, modulation of the kinase activity and differences in the interaction with other proteins or probably affect the interaction between them.

Accordingly, and as last attempt in the course of this FRET project, it was of interest to examine the influence of the photochromic states of the phytochromes on the ability of Agp1 and Agp2 to interact with each other.

The results showed that when both phytochromes are in the Pfr states, the interacting fluorophores are somehow closer to each other, showing hence a slightly higher E_{FRET} than when only one of the phytochromes is in the Pfr state.

Going back to the conformational changes of phytochromes upon photoconversion, the long helix connecting the PHY and GAF domains is bent and flexible in the Pr form but stretched in the Pfr, in addition to the conclusion, that Agp1 helix at position 517 interacts with the PCM domain of Agp2 phytochrome, it is then possible, that in its stretched form, the helix, is closer to the PCM / GAF domain of Agp2, than in its bent flexible form. Noteworthy, E_{FRET} *decreases,* when Agp2 was irradiated with FR, gaining thus the Pr form. This leads to the assumption, that when both phytochromes are in their Pr form, the conformational changes in the PCM and at the helix, which is bent in both phytochromes, increases the spacing between them, reducing hence the interaction efficiency.

Comparing now the light effect after mixing Agp1 and Agp2 in their dark-adapted state, slight differences could be seen. Nonetheless, the same behaviour was observed, leading to the conclusion, that the Pfr form plays an important role in the interaction of

these phytochromes and that the flexible Pr form induces the phytochromes to diverge from each other. In this case, the effect of these phytochromes influencing cellular processes may be higher in Pfr than in Pr.

Furthermore, it can be concluded, that the interaction between these phytochromes has not influenced their conformational changes upon photoconversion, since the switch between the Pr and Pfr form was still possible, according to the recorded absorption spectra *(Appendix C, Figure A4)*

The difference in this case, is that both phytochromes were irradiated with the same light. For instance, to obtain the Pfr-Pfr form for both phytochromes 3 possibilities were used; only Agp1 was illuminated with R (irradiation before mixing), which shows the higher E_{FRET} than after illuminating the mixture first with FR and followed by R (D-FR-R) or illuminating it by R. In the latter case, not only Agp1 was illuminated with R but also Agp2. According to the absorption spectra *(Appendix B, Figure A2),* the Pfr form is lower in this case. the mixture switches from Pr-Pfr to Pr – Pr and finally Pfr -Pfr.

One difference is that the Pr – Pr or Pfr-Pfr states have slightly changed after irradiating the mixture. This might be the cause of the amount of the Pr and Pfr ratio, which is still in the sample. After irradiation with R, not only Agp1 was irradiated, but also Agp2, which showed a slight decrease in its Pfr form *(Appendix B, Figure A3).*

However, the switch from the already bent form to the stretched form is not that prevented, since the irradiation of the mixture with FR then R has shown that the distance decreases slightly when both are in Pfr form *(Figure 38b) (Appendix C, Figure A4).*

Summarizing these results, Agp1 and Agp2 do interact with each other, where the HK of Agp1 interact with the PCM of Agp2. This interaction is also regulated by light, where the Pfr form seems to increase the efficiency of this FRET signal and therefore presumably have a higher influence on cellular processes. Moreover, it can be concluded that conformational changes still occur even when both phytochromes are already interacting.

Nonetheless, in the signalling pathways, the interactions between proteins are often weak. Additionally, the efficiency and the reversibility of information transfer are of key

importance (Delaforge et al. 2016). Moreover, different processes could have influenced the FRET efficiency. For instance, the rotational correlation time of the chromophores, or the fluorescence lifetime of the donor, in addition to the intramolecular dynamics of the molecule probed by the fluorophores (Schuler 2013).

6.5 Conjugation studies after TraA knock out

In the last exploration of the signal transduction of *A. fabrum* in the course of this research, a different approach *in vivo* was investigated.
It is believed that the proteins encoded by the Tra genes play an essential role in the conjugation pathway and that this cannot take place without these genes, since they are either involved in the formation of the pilus or involved directly in the DNA transfer such as TraA gene (Bai et al. 2016; Gillespie et al. 2010).
TraA is believed to be the first interaction protein in this process and plays a role as a relaxase, initiating thus the conjugal transfer. Moreover, previous conjugation studies were performed without the pTi, which encodes for one of the three TraA genes of *A. fabrum*, showing that the conjugation influenced by its absence and regulated by the phytochromes and light (Bai et al. 2016).
For this purpose, the role of the TraA gene on the pTi and its encoded protein was examined, by knocking out this gene from the pTi. The aim was to see, if this TraA gene influences the conjugal transfer in *A. fabrum* and if both phytochromes also regulate this process after the knockout of the TraA gene.

When observing the results, it is immediately apparent that neither the TraA$^-$ cells nor the Agp12$^-$/TraA$^-$ cells were capable of performing the conjugation, no matter what light conditions they were exposed to.
Based on the domain homology of the relaxases from other organisms, it is assumed that TraA plays the role of the relaxase during conjugation (Cho and Winans 2007). The fact that no conjugation could occur without the TraA gene on the pTi, can lead to the conclusion that this TraA is indeed involved in the conjugation mechanism, inducing the conjugation more efficiently than the other TraA encoded by the pAt and the linear chromosome. Hence, suggesting that this TraA could possibly perform the presumed relaxase function.

In this case, if the relaxase is not present, the OriT can neither be recognized, nor a break can be generated, so that the single stranded DNA could be transferred to the recipient cells, where it will be replicated. Consequently, the conjugation cannot take place, which will result in an inhibition of the cell growth in the conjugation mixture.

On the contrary, Agp1$^-$/TraA$^-$ and Agp2$^-$/TraA$^-$ cells were able to carry out the conjugation even after the knockout of their TraA gene of the pTi, with a different efficiency though.
This suggests that the conjugation could be performed in the presence of Agp2 (in case of Agp1$^-$/TraA$^-$) but only with low conjugation efficiency, indicating thus the regulatory influence of Agp1 on the mechanism, since its absence had initiated the conjugation.
A similar behaviour could be observed, when using Agp2$^-$/TraA$^-$ cells, where the conjugation could still be carried out without the TraA gene on the pTi, nonetheless with a higher conjugation efficiency compared to Agp1$^-$/TraA$^-$ cells. It can thus also be assumed that Agp2 has a higher down regulatory function, influencing the conjugation in *A. fabrum.*
In these both cases, this may refer to the fact that the TraA genes, which are located on the linear chromosome or on the pAt plasmid, can overtake the role of the TraA as a relaxase and induce the conjugation instead of the TraA gene located on the pTi plasmid. Nonetheless, these TraAs were down regulated by the presence of both Agp1 and Agp2. Therefore, the presence of both phytochromes or their absence would inhibit the conjugation process, by inhibiting the interaction with the TraA genes encoded either by the linear chromosome or the pAt. Thus, emphasizing that Agp1 and Agp2 phytochromes interact with each other, influencing various cellular mechanisms, *e.g.,* the interaction with TraA genes.

Comparing the light effect on the conjugation it can also be determined that the conjugation rate has differed for Agp1$^-$/TraA$^-$ and Agp2$^-$/TraA$^-$. While the conjugation efficiency was the highest in the dark for the Agp1$^-$/TraA$^-$ donor cells, it was the lowest in FR. Whereas for Agp2$^-$/TraA$^-$, the lowest conjugation rate was seen in darkness and the highest under red light *(§ 5.5.2, Figure 39).*
These light effects can be traced back to the Pr and Pfr states of the phytochromes.

In Agp1^{-}/TraA^{-} only Agp2 is present, therefore, the Agp2 has its Pfr form either in the dark-adapted state or under R light. This explains the higher conjugation rate in darkness, which corresponds to the Pfr state and the lowest under FR, which corresponds to the Pr state of Agp2. It can thus be concluded that the Agp2 phytochrome induces the expression of the TraA proteins of the pAt and the linear chromosome in both forms, however, it is stronger in its active Pfr form.
Similarly, this can be observed for the Agp2^{-}/TraA^{-}, where in this case Agp1 is present and controls the activity of the remaining Tra genes. The higher conjugation was observed under R, which confers the phytochrome its Pfr state, and is lower under FR and in darkness – the Pr form. It can thus be concluded that the presence of Agp1 alone also induces the expression of the remaining TraA proteins but mainly in the Pfr form, indicating the importance of the Pfr state in this process.

Summarizing, Agp1 and Agp2 do act together, inhibiting their interaction with the TraAs encoded by the pAt and the linear chromosome, hence down regulating the expression of the respective TraA proteins and inhibiting the conjugal transfer.
On the contrary the absence of one of these phytochromes induces these two remaining TraA proteins, hence the conjugal transfer, even in the absence of the TraA encoded by the pTi. They promote the conjugation more in the Pfr form than in the Pr form though.

7 Conclusion

Agp1 and Agp2 phytochromes of *A. fabrum* exhibit opposite spectral characteristics regarding light-induced and thermal conversion between the red absorbing Pr form and the far-red absorbing Pfr form, inducing conformational changes in the phytochromes. Previous studies showed how these phytochromes may act with each other influencing different cellular mechanism.

The aim of this research was therefore to understand the function of a bacterial phytochrome system and its signal transduction, which involves a series of light induced structural modifications. These range from photoisomerization of the chromophore and its local environment to large-scale conformational changes in the entire protein, in addition to the potential interactions between phytochromes, affecting the output activity of the phytochrome and regulating cellular processes.

Agp1 mutants were first used as a model to investigate the functionality of Agp1 in the signal transmission via its kinase activity. This showed that the autophosphorylation and hence the propagation of the signal along the protein was affected after photoconversion to Pfr, exhibiting a similar behaviour as the wt. Furthermore, the autophosphorylation was also slightly affected by the mutations in the HK domain, but have not influenced the main function of the protein.

Moreover, the changes in the dynamics upon photoconversion at the domains of interest in the PCM as well as in the HK domain, showed that Agp1 is intrinsically dynamic. It exhibits various conformational modes with different amplitude motions, where either local bonds fluctuations are involved or conformational changes, which are required for the function of the protein.
Together with previous findings, the following scheme of the signal transduction pathway in *A. fabrum* could be illustrated. The PHY domain plays a role as a mechanical linker, which couples the photosensory domain (PCM) and the HK output domain. This coupling is mediated by the motif called tongue that connects the PAS-GAF domain and the long helix, connecting the HK domain.

After light absorption by the PAS domain, changes occur within the chromophore-binding domains of the protein, which seem to control the entire structural process of the protein upon this photoconversion.

This isomerisation of chromophore induces several rearrangements and refolding of the tongue, which are also accompanied by changes in the dynamics, nonetheless these dynamics are slower after photoconversion. These rearrangements and dynamics changes, propagate to the output domain along the long helix, which switches from a flexible bent form to a straight form, enabling the transmission of the signal to the output domain involving the amino acid K517 (H -11) of the DHp domain.

This transmission is also accompanied by changes in the dynamics along this helix, where the dynamics at the beginning of the DHp domain speed up in the Pfr form.
At this level, the ATP-binding domain, which changes its binding site, enables the transfer of a phosphate from the ATP, allowing the autophosphorylation of the histidine residue. These changes are due to rotational movements of the domain that could affect its folding. Hence, this will induce further conformational changes of the coiled helices that could uncoil, due to rotational movements, hence influencing the dynamics of the ATP-binding domain, as well as the HK domain. Leading thus to a higher dynamic of the HK module in both photochromic states of than the dynamics of the PCM. However, without inducing an opening at the end of the HK domain, since the radius of this module does not change upon photoconversion. This can hence establish the key elements of the structural photocycle of bacterial phytochromes.

Furthermore, the transmission of the signal is not only light-regulated, but it is also regulated by the interaction of both Agp1 and Agp2. In this interaction, the HK domain, mainly the amino acid at position 517 of the DHp domain is involved with the PCM domain of Agp2, primarily with its GAF domain.
As light induces conformational and dynamics changes in the phytochrome, the interaction between these phytochromes is also light regulated, showing a higher interaction in the Pfr form for both phytochromes and the lowest in their Pr form.

Finally, *in vitro* studies of the signal transduction *via* conjugal transfer have indeed confirmed that the TraA gene of the pTi is involved in the conjugation mechanism and

emphasized the role of Agp1 and Agp2 phytochromes in this process. It shows that both phytochromes do interact together, inhibiting the function of the remaining TraA genes, which are located in the pAt and in the linear chromosome of *A. fabrum*.
Thus, repressing the conjugal transfer since their interaction, inhibit the interaction of the single phytochrome with the remaining TraAs required for their activation. Nonetheless, this mechanism is not only down regulated by both phytochromes, but also by light, hence regulating the expression of the remaining TraA proteins. It seems that also in the conjugal transfer, the Pfr form is the more active form for the interaction of one of the phytochromes with the remaining TraAs, enabling a higher conjugal transfer.

8 Appendix

Appendix A: FRET with Agp2 mutants

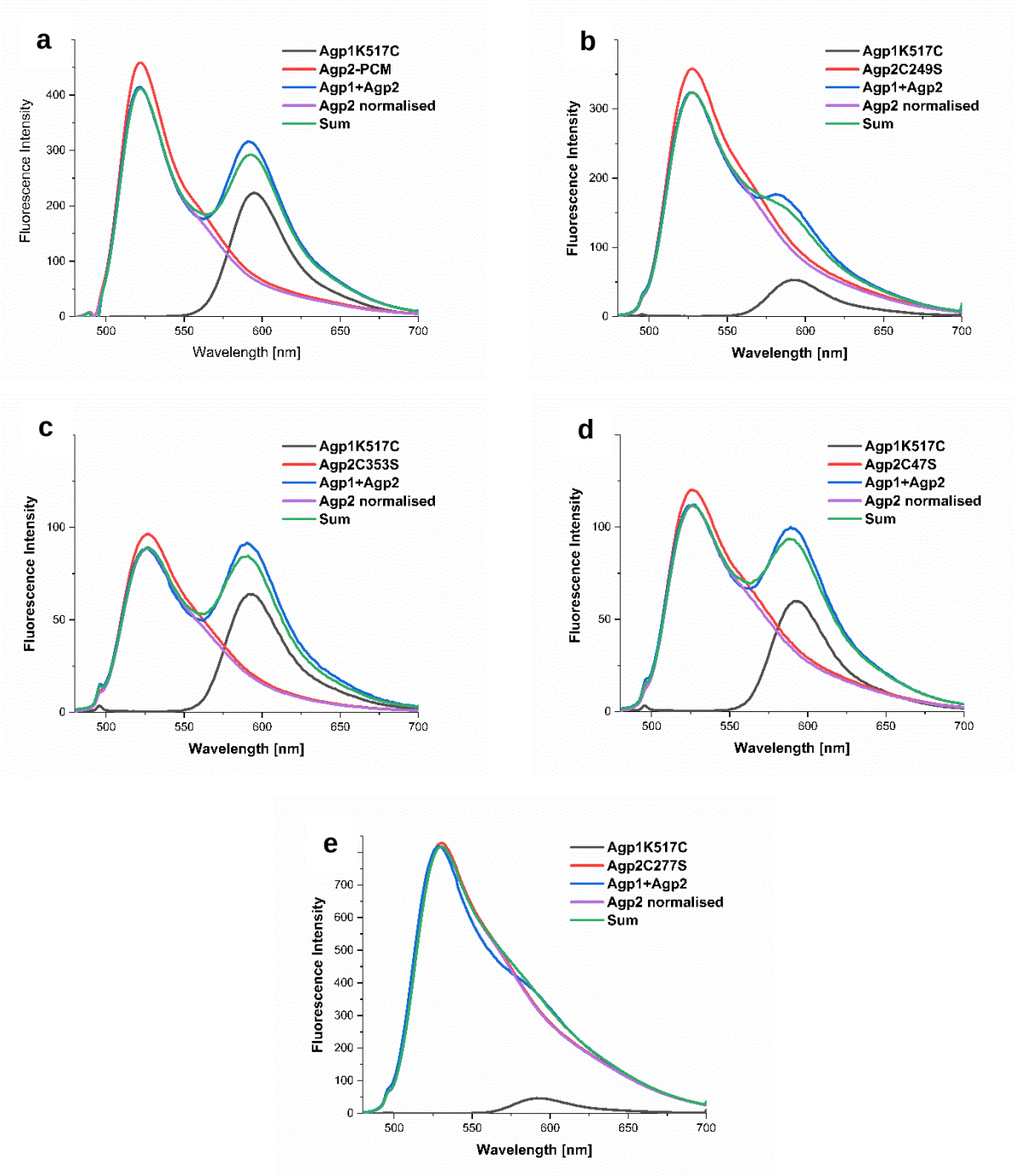

Figure A 1: Fluorescence emission spectra of FRET using Agp2 mutants with Agp1K517C: *In each mutant one cysteine at a definite position was removed, to disable to attachment of Atto dye and test if FRET still occurs. Results have shown that a FRET signal can be seen for all the used Agp2 mutants, expect for the mutant Agp2C277S – For Details see § 5.4, §5.4.4.*

Appendix B: Light effect on the FRET of Agp2-wt with Agp1K517C

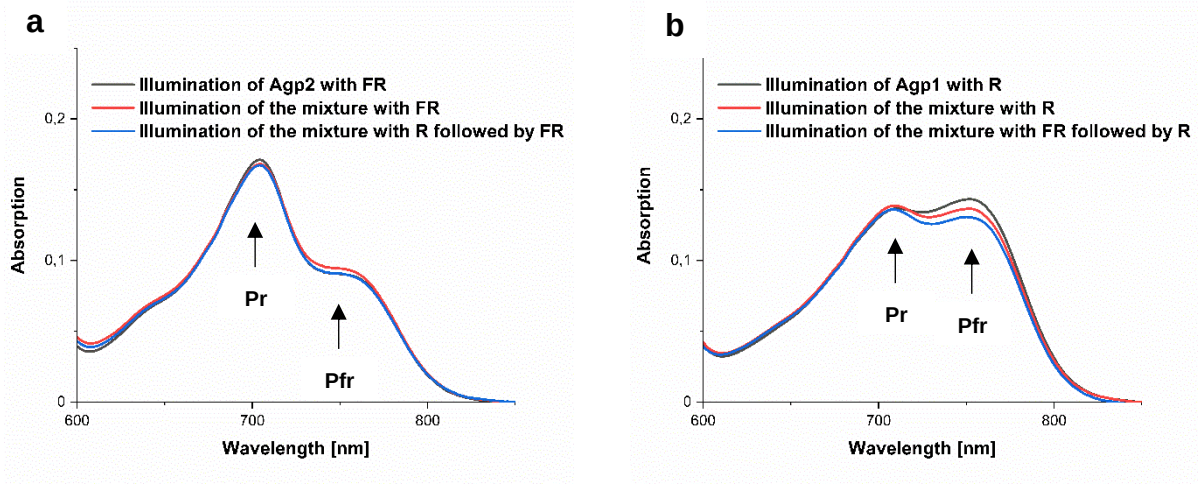

Figure A 2: Absorption Spectra of Agp1 and Agp2 mixture with the respective illumination: *A) shows the different combinations leading to Pr-Pr form of Agp1 and Agp2 respectively either by illumination only Agp2 with FR and then mix it with Agp1 (black spectrum), or illuminating the whole mixture with FR (red) or first R followed by FR. The spectra show almost no difference in case of the different Pr-Pr forms. B) show the similar illumination process but using R to illuminate Agp1 alone (black), then illuminate the mixture with Pr or with FR followed by R, to get the Pfr-Pfr form – For details see § 4.5. In this case, it seems that the amount of the Pfr form at A_{755nm} differs according to the way of illuminating the sample (§ 5.4.5 and § 6.4.3)*

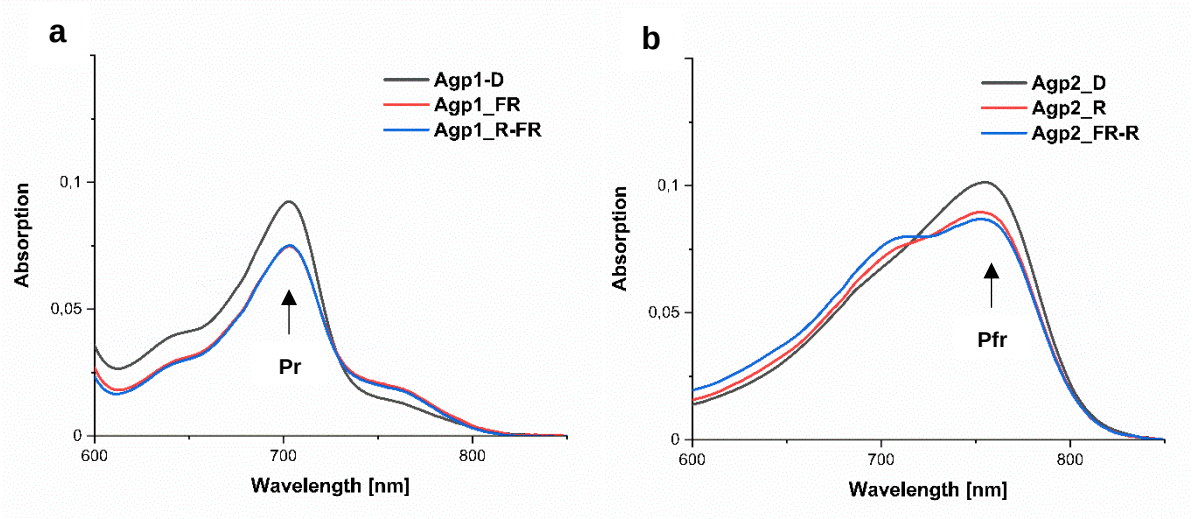

Figure A 3: Absorption spectra of Agp1 and Agp2 (600 nm – 850 nm) showing the differences upon light illumination: *Agp1 has the R absorbing Pr form, after its illumination with FR or R followed by FR the amount of Pr seemed to slightly decrease. On the other hand, the FR absorbing form of Agp2 (Pfr) also decreased after R illumination or FR followed by R and a slight increase of the Pr form could be seen (§ 5.4.5 and § 6.4.3)*

Appendix C: Light effect on the FRET of Agp2-wt with Agp1K517C – Absorption spectra of the illumination after the mixture and before the mixture of both proteins

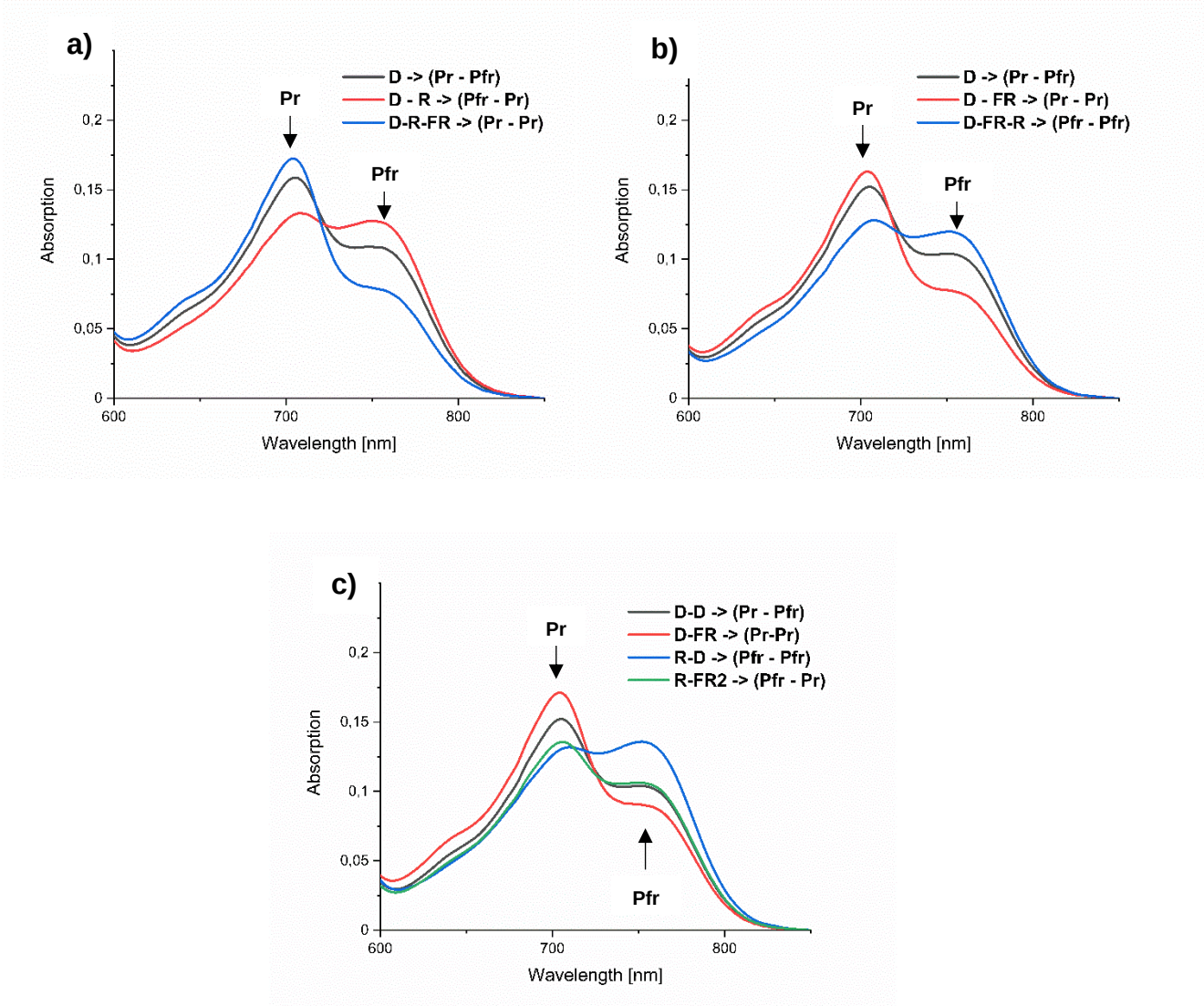

Figure A 4: Absorption Spectra of Agp1 and Agp2 mixture with the different types of illumination: *A and B show the absorption spectra of the illumination after mixing Agp1 and Agp2.A) represent the dark-adapted state of the mixture D (dark), followed R(red) = (D-R) and finally followed by FR (far-red) (D-R-FR). B) shows the illumination of the mixture first in its dark-adapted state, then followed by the illumination of FR (D-FR) and finally followed by R (D-FR-R). C) shows the absorption spectra of the mixture, where Agp1 and Agp2 were illuminated separately and then mixed (§ 4.5). These spectra show that the photoconversion does occur even after Agp1 and Agp2 form a complex after their interaction*

9 Table of figures

References

Assafa TE, Anders K, Linne U, Essen L-O, Bordignon E (2018) Light-Driven Domain Mechanics of a Minimal Phytochrome Photosensory Module Studied by EPR. Structure (London, England : 1993):1534-1545.e4

Bai Y, Rottwinkel G, Feng J, Liu Y, Lamparter T (2016) Bacteriophytochromes control conjugation in Agrobacterium fabrum. Journal of photochemistry and photobiology. B, Biology 161:192–199

Bajar BT, Wang ES, Zhang S, Lin MZ, Chu J (2016) A Guide to Fluorescent Protein FRET Pairs. Sensors (Basel, Switzerland) 16

Bellanger X, Payot S, Leblond-Bourget N, Guédon G (2014) Conjugative and mobilizable genomic islands in bacteria: evolution and diversity. FEMS microbiology reviews 38:720–760

Bhate MP, Molnar KS, Goulian M, DeGrado WF (2015) Signal transduction in histidine kinases: insights from new structures. Structure (London, England : 1993) 23:981–994

Björling A, Berntsson O, Lehtivuori H, Takala H, Hughes AJ, Panman M, Hoernke M, Niebling S, Henry L, Henning R, Kosheleva I, Chukharev V, Tkachenko NV, Menzel A, Newby G, Khakhulin D, Wulff M, Ihalainen JA, Westenhoff S (2016) Structural photoactivation of a full-length bacterial phytochrome. Science advances:e1600920

Borucki B, Lamparter T (2009) A polarity probe for monitoring light-induced structural changes at the entrance of the chromophore pocket in a bacterial phytochrome. The Journal of biological chemistry 284:26005–26016

Bucci E, Steiner RF (1988) Anisotropy decay of fluorescence as an experimental approach to protein dynamics. Biophysical Chemistry 30:199–224

Burgie ES, Vierstra RD (2014) Phytochromes: an atomic perspective on photoactivation and signaling. The Plant cell 26:4568–4583

Burgie ES, Zhang J, Vierstra RD (2016) Crystal Structure of Deinococcus Phytochrome in the Photoactivated State Reveals a Cascade of Structural Rearrangements during Photoconversion. Structure (London, England : 1993):448–457

Butler WL, Norris KH, Siegelman HW, Hendricks SB (1959) DETECTION, ASSAY, AND PRELIMINARY PURIFICATION OF THE PIGMENT CONTROLLING PHOTORESPONSIVE DEVELOPMENT OF PLANTS. Proceedings of the National Academy of Sciences of the United States of America 45:1703–1708

Cabezón E, Ripoll-Rozada J, Peña A, La Cruz F de, Arechaga I (2015) Towards an integrated model of bacterial conjugation. FEMS microbiology reviews 39:81–95

Cai Y, Su M, Ahmad A, Hu X, Sang J, Kong L, Chen X, Wang C, Shuai J, Han A (2017) Conformational dynamics of the essential sensor histidine kinase WalK. Acta crystallographica. Section D, Structural biology 73:793–803

Casino P, Fernández-Alvarez A, Alfonso C, Rivas G, Marina A (2007) Identification of a novel two component system in Thermotoga maritima. Complex stoichiometry and crystallization. Biochimica et biophysica acta 1774:603–609

Cho H, Winans SC (2007) TraA, TraC and TraD autorepress two divergent quorum-regulated promoters near the transfer origin of the Ti plasmid of Agrobacterium tumefaciens. Molecular Microbiology 63:1769–1782

Christie PJ (2004) Type IV secretion: the Agrobacterium VirB/D4 and related conjugation systems. Biochimica et biophysica acta 1694:219–234

Ciruela F (2008) Fluorescence-based methods in the study of protein-protein interactions in living cells. Current opinion in biotechnology 19:338–343

Dago AE, Schug A, Procaccini A, Hoch JA, Weigt M, Szurmant H (2012) Structural basis of histidine kinase autophosphorylation deduced by integrating genomics, molecular dynamics, and mutagenesis. Proceedings of the National Academy of Sciences of the United States of America:E1733-42

Delaforge E, Milles S, Huang J-R, Bouvier D, Jensen MR, Sattler M, Hart DJ, Blackledge M (2016) Investigating the Role of Large-Scale Domain Dynamics in Protein-Protein Interactions. Frontiers in molecular biosciences:54

Dikiy I, Edupuganti UR, Abzalimov RR, Borbat PP, Srivastava M, Freed JH, Gardner KH (2019) Insights into histidine kinase activation mechanisms from the monomeric blue light sensor EL346. Proceedings of the National Academy of Sciences of the United States of America 116:4963–4972

Dilucca M, Cimini G, Giansanti A (2019) Bacterial protein interaction networks: connectivity is ruled by gene conservation, essentiality and function

El Kurdi A (2016) Function of phytochromes' histidine kinase during the conjugation in Agrobacterium tumefaciens. Master thesis, Karlsruhe, Germany

Elich TD, Chory J (1997) Phytochrome: If It Looks and Smells Like a Histidine Kinase, Is It a Histidine Kinase? Cell 91:713–716

Essen L-O, Jo M, Jon Hughes† (2008) The structure of a complete phytochrome sensory module in the Pr ground state. PNAS 105:14709–14714

Fankhauser C (2000) Phytochromes as light-modulated protein kinases. Seminars in Cell & Developmental Biology 11:467–473. http://www.sciencedirect.com/science/article/pii/S1084952100902015

Förster T (1948) Zwischenmolekulare Energiewanderung und Fluoreszenz. Ann. Phys. 437:55–75

Gayrard C, Borghi N (2016) FRET-based Molecular Tension Microscopy. Methods (San Diego, Calif.) 94:33–42

Gillespie JJ, Brayton KA, Williams KP, Diaz MAQ, Brown WC, Azad AF, Sobral BW (2010) Phylogenomics reveals a diverse Rickettsiales type IV secretion system. Infection and immunity 78:1809–1823

Giusti MdlÁ, Pistorio M, Lozano MJ, Tejerizo GAT, Salas ME, Martini MC, López JL, Draghi WO, Del Papa MF, Pérez-Mendoza D, Sanjuán J, Lagares A (2012) Genetic and functional characterization of a yet-unclassified rhizobial Dtr (DNA-transfer-and-replication) region from a ubiquitous plasmid conjugal system present in Sinorhizobium meliloti, in Sinorhizobium medicae, and in other nonrhizobial Gram-negative bacteria. Plasmid 67:199–210

Goodner B, Hinkle G, Gattung S, Miller N, Blanchard M, Qurollo B, Goldman BS, Cao Y, Askenazi M, Halling C, Mullin L, Houmiel K, Gordon J, Vaudin M, Iartchouk O, Epp A, Liu F, Wollam C, Allinger M, Doughty D, Scott C, Lappas C, Markelz B, Flanagan C, Crowell C, Gurson J, Lomo C, Sear C, Strub G, Cielo C, Slater S (2001) Genome sequence of the plant pathogen and biotechnology agent Agrobacterium tumefaciens C58. Science (New York, N.Y.) 294:2323–2328

Grant BJ, Gorfe AA, McCammon JA (2010) Large conformational changes in proteins: signaling and other functions. Current opinion in structural biology:142–147

HORIBA Scientific (2020a) Time -resolved fluorescence lifetime meausurements. Technical Note TRFT-1. https://www.horiba.com/de/scientific/products/fluorescence-spectroscopy/application-notes/

HORIBA Scientific (2020b) Time-resolved fluorecence anisotropy. Technical Note TRFT-2. https://www.horiba.com/de/scientific/products/fluorescence-spectroscopy/application-notes/

Hsing W, Russo FD, Bernd KK, Silhavy TJ (1998) Mutations that alter the kinase and phosphatase activities of the two-component sensor EnvZ. J. Bacteriol. 180:4538–4546

Ibrahim Njimona (2011) Molecular studies on light-induced protein conformational changes on Agrobacterium tumefaciens phytochrome, Agp1, Karlsruhe, Germany

Jeffry BS, Ann MS, James MM (1990) signal transduction in Bacteria. Nature reviews. Microbiology 334:395–400

Jiang Y, Wen X, Benda A, Sheng R, Ho-Baillie AW, Huang S, Huang F, Cheng Y-B, Green MA (2016) Time-resolved fluorescence anisotropy study of organic lead halide perovskite. Solar Energy Materials and Solar Cells 151:102–112

Kacprzak S, Njimona I, Renz A, Feng J, Reijerse E, Lubitz W, Krauss N, Scheerer P, Nagano S, Lamparter T, Weber S (2017) Intersubunit distances in full-length, dimeric, bacterial phytochrome Agp1, as measured by pulsed electron-electron double resonance (PELDOR) between different spin label positions, remain unchanged upon photoconversion. The Journal of biological chemistry 292:7598–7606

Kapusta P, Erdmann R, Ortmann, Uwe and Wahl, Michael (2003) Time-resolved fluorescence anisotropy measurements made Ssmple. Journal of Fluorescence 13

Karniol B, Vierstra RD (2004) The HWE histidine kinases, a new family of bacterial two-component sensor kinases with potentially diverse roles in environmental signaling. Journal of bacteriology 186:445–453. https://jb.asm.org/content/186/2/445

Kim T-Y, Schlieter T, Haase S, Alexiev U (2012) Activation and molecular recognition of the GPCR rhodopsin--insights from time-resolved fluorescence depolarisation and single molecule experiments. European journal of cell biology 91:300–310

Kim Y, Ho SO, Gassman NR, Korlann Y, Landorf EV, Collart FR, Weiss S (2008) Efficient site-specific labeling of proteins via cysteines. Bioconjugate chemistry 19:786–791

Kopec J, Bergmann A, Fritz G, Grohmann, Elisabeth and Keller, Walter (2005) TraA and its N-terminal relaxase domain of the Gram-positive plasmid pIP501 show specific oriT binding and behave as dimers in solution. Biochemical Journal 387:401–409

Krall L, Reed JW (2000) The histidine kinase-related domain participates in phytochrome B function but is dispensable. Proceedings of the National Academy of Sciences of the United States of America 97:8169–8174

Kurenbach B, Grothe D, Farías ME, Szewzyk U, Grohmann E (2002) The tra region of the conjugative plasmid pIP501 is organized in an operon with the first gene encoding the relaxase. Journal of bacteriology 184:1801–1805

La Riva G de, González-Cabrera J, Vásquez-Padrón R, Ayra-Pardo C (1998) Agrobacterium tumefaciens: a natural tool for plant transformation. EJB Electronic Journal if Biotechnology Vol.1 No.3

Lacroix B, Citovsky V (2019) Pathways of DNA Transfer to Plants from Agrobacterium tumefaciens and Related Bacterial Species. Annual review of phytopathology 57:231–251

Lakowicz JR (2006a) Principle of Fluorescence Spectroscopy. Chapter 1, 3rd edn. Springer

Lakowicz JR (2006b) Principles of fluorescence spectroscopy, 3rd edn. Springer, New York

Lamparter T, Carrascal M, Michael N, Martinez E, Rottwinkel G, Abian J (2004) The biliverdin chromophore binds covalently to a conserved cysteine residue in the N-terminus of Agrobacterium phytochrome Agp1. Biochemistry 43:3659–3669

Lamparter T, Krauß N, Scheerer P (2017) Phytochromes from Agrobacterium fabrum. Photochemistry and photobiology 93:642–655

Lamparter T, Michael N, Mittmann F, Esteban B (2002) Phytochrome from Agrobacterium tumefaciens has unusual spectral properties and reveals an N-terminal chromophore attachment site. Proceedings of the National Academy of Sciences of the United States of America 99:11628–11633

Lang J, Faure D (2014) Functions and regulation of quorum-sensing in Agrobacterium tumefaciens. Frontiers in Plant Science 5:14

Li J, Li G, Wang H, Wang Deng X (2011) Phytochrome signaling mechanisms. The arabidopsis book 9:e0148

Llosa M, Gomis-Rüth FX, Coll M, La Cruz F de (2002) Bacterial conjugation: a two-step mechanism for DNA transport. Molecular Microbiology:1–8

McCullen CA, Binns AN (2006) Agrobacterium tumefaciens and plant cell interactions and activities required for interkingdom macromolecular transfer. Annual review of cell and developmental biology 22:101–127

Mitchell JG, Kogure K (2006) Bacterial motility: links to the environment and a driving force for microbial physics. FEMS microbiology ecology 55:3–16

Modesti M (2011) Fluorescent labeling of proteins. Methods in molecular biology (Clifton, N.J.) 783:101–120

Möglich A (2019) Signal transduction in photoreceptor histidine kinases. Protein science : a publication of the Protein Society:1923–1946

Möglich A, Yang X, Ayers RA, Moffat K (2010) Structure and function of plant photoreceptors. Annual review of plant biology 61:21–47

Multamäki E, Nanekar R, Morozov D, Lievonen T, Golonka D, Yuan Wahlgren W, Stucki-Buchli B, Rossi J, Hytönen VP, Westenhoff S, Ihalainen JA, Möglich A, Takala H (2020) Illuminating a Phytochrome Paradigm – a Light-Activated Phosphatase in Two-Component Signaling Uncovered

Nagano S (2016) From photon to signal in phytochromes: similarities and differences between prokaryotic and plant phytochromes. Journal of plant research 129:123–135

Nagano S, Scheerer P, Zubow K, Michael N, Inomata K, Lamparter T, Krauß N (2016) The Crystal Structures of the N-terminal Photosensory Core Module of Agrobacterium Phytochrome Agp1 as Parallel and Anti-parallel Dimers. The Journal of biological chemistry 291:20674–20691

Nester EW (2014) Agrobacterium: nature's genetic engineer. Frontiers in Plant Science 5:730

Njimona I, Lamparter T (2011) Temperature effects on Agrobacterium phytochrome Agp1. PLoS ONE 6:e25977

Njimona I, Yang R, Lamparter T (2014) Temperature effects on bacterial phytochrome. PLoS ONE 9:e109794

Noack S, Lamparter T (2007) Light Modulation of Histidine-Kinase Activity in Bacterial Phytochromes Monitored by Size Exclusion Chromatography, Crosslinking, and Limited Proteolysis. Methods in enzymology 423:203–221

Păcurar DI, Thordal-Christensen H, Păcurar ML, Pamfil D, Botez C, Bellini C (2011) Agrobacterium tumefaciens: From crown gall tumors to genetic transformation. Physiological and Molecular Plant Pathology 76:76–81

Pengguang W, Ludwig B (1994) Resonance Energy Transfer: Methods and Applications. Academic Press, Inc.

Peter Kapusta (2002) Time-resolved fluorescence anisotropy measurements made simple

Peter Kapusta (2010) Absolute Diffusion Coefficients: Compilation of Reference Data for FCS Calibration

Piston DW, Kremers G-J (2007) Fluorescent protein FRET: the good, the bad and the ugly. Trends in Biochemical Sciences 32:407–414

Purcell EB, Crosson S (2008) Photoregulation in prokaryotes. Current opinion in microbiology 11:168–178

Rockwell NC, Su Y-S, Lagarias JC (2006) Phytochrome structure and signaling mechanisms. Annual review of plant biology 57:837–858

Rottwinkel G (2011) Studien zu Verbreitung, Charakteristika und Funktionen der Bakteriophytochrome in Rhizobiales. mbv, Mensch-und-Buch-Verl., Berlin

Rottwinkel G, Oberpichler I, Lamparter T (2010) Bathy phytochromes in rhizobial soil bacteria 192:5124–5133

Sahoo H (2012) Fluorescent labeling techniques in biomolecules: a flashback. RSC Adv. 2:7017

Schröder GF, Alexiev U, Grubmüller H (2005) Simulation of fluorescence anisotropy experiments: probing protein dynamics. Biophysical journal 89:3757–3770

Schuler B (2013) Single-molecule FRET of protein structure and dynamics - a primer. Journal of nanobiotechnology 11 Suppl 1:S2

Schwille P, Haustein E Fluorescence Correlation Spectroscopy : An Introduction to its Concepts and Applications

Sherman E, Itkin A, Kuttner YY, Rhoades E, Amir D, Haas E, Haran G (2008) Using fluorescence correlation spectroscopy to study conformational changes in denatured proteins. Biophysical journal 94:4819–4827

Smillie C, Garcillán-Barcia MP, Francia MV, Rocha EPC, La Cruz F de (2010) Mobility of plasmids. Microbiology and molecular biology reviews : MMBR 74:434–452

Smith DA, McKenzie G, Jones AC, Smith TA (2017) Analysis of time-correlated single photon counting data: a comparative evaluation of deterministic and probabilistic approaches. Methods and applications in fluorescence 5:42001

Smith TA, Ghiggino KP (2015) A review of the analysis of complex time-resolved fluorescence anisotropy data. Methods and applications in fluorescence 3:22001

Söveges B, Imre T, Póti ÁL, Sok P, Kele Z, Alexa A, Kele P, Németh K (2018) Tracking down protein-protein interactions via a FRET-system using site-specific thiol-labeling. Organic & biomolecular chemistry 16:5756–5763

Takala H, Björling A, Berntsson O, Lehtivuori H, Niebling S, Hoernke M, Kosheleva I, Henning R, Menzel A, Ihalainen JA, Westenhoff S (2014) Signal amplification and transduction in phytochrome photosensors. Nature:245–248

Takala H, Lehtivuori HK, Berntsson O, Hughes A, Nanekar R, Niebling S, Panman M, Henry L, Menzel A, Westenhoff S, Ihalainen JA (2018) On the (un)coupling of the chromophore, tongue interactions, and overall conformation in a bacterial phytochrome. The Journal of biological chemistry 293:8161–8172

Toseland CP (2013) Fluorescent labeling and modification of proteins. Journal of chemical biology 6:85–95

van der Horst MA, Hellingwerf KJ (2004) Photoreceptor proteins, "star actors of modern times": a review of the functional dynamics in the structure of representative members of six different photoreceptor families. Accounts of chemical research 37:13–20

Wagner JR, Brunzelle JS, Forest KT, Vierstra RD (2005) A light-sensing knot revealed by the structure of the chromophore-binding domain of phytochrome. Nature 438:325–331

West AH, Stock AM (2001) Histidine kinases and response regulator proteins in two-component signaling systems. Trends in Biochemical Sciences 26:369–376

Wood DW, Setubal JC, Kaul R, Monks DE, Kitajima JP, Okura VK, Zhou Y, Chen L, Wood GE, Almeida NF, Woo L, Chen Y, Paulsen IT, Eisen JA, Karp PD, Bovee D, Chapman P, Clendenning J, Deatherage G, Gillet W, Grant C, Kutyavin T, Levy R, Li MJ, McClelland E, Palmieri A, Raymond C, Rouse G, Saenphimmachak C, Wu Z, Romero P, Gordon D, Zhang S, Yoo H, Tao Y, Biddle P, Jung M, Krespan W, Perry M, Gordon-Kamm B, Liao L, Kim S, Hendrick C, Zhao ZY, Dolan M, Chumley F, Tingey SV, Tomb JF, Gordon MP, Olson MV, Nester EW (2001) The genome of the natural genetic engineer Agrobacterium tumefaciens C58. Science (New York, N.Y.) 294:2317–2323

Xue P, El Kurdi A, Kohler A, Ma H, Kaeser G, Ali A, Fischer R, Krauß N, Lamparter T (2019) Evidence for weak interaction between phytochromes Agp1 and Agp2 from Agrobacterium fabrum. FEBS letters 593:926–941

Yang X, Jane k, Keithh M (2008) Crystal structure of Pseudomonas aeruginosa bacteriophytochrome: Photoconverson and signal transduction. PNAS 105:14715–14720

Young JM, Kuykendall LD, Martínez-Romero E, Kerr A, Sawada H (2001) A revision of Rhizobium Frank 1889, with an emended description of the genus, and the inclusion of all species of Agrobacterium Conn 1942 and Allorhizobium undicola de Lajudie et al. 1998 as new combinations: Rhizobium radiobacter, R. rhizogenes, R. rubi, R. undicola and R. vitis. International journal of systematic and evolutionary microbiology 51:89–103

Zienicke B (2011) Fluoreszenzeigenschaften und Photokonversion der Modell-Phytochrome Agp1 und Agp2 aus Agrobacterium tumefaciens. mbv, Mensch-und-Buch-Verl., Berlin

Zienicke B, Molina I, Glenz R, Singer P, Ehmer D, Escobar FV, Hildebrandt P, Diller R, Lamparter T (2013) Unusual spectral properties of bacteriophytochrome Agp2 result from a deprotonation of the chromophore in the red-absorbing form Pr. The Journal of biological chemistry 288:31738–31751

Declaration

Hiermit erkläre ich, dass ich die vorliegende Dissertation unter der Benutzung der angegebnen Hilfsmittel selbständig verfasst habe.

Alle Stellen, die gemäß Wortlaut oder Inhalt aus anderen Arbeiten entnommen sind, wurden durch Angabe der Quelle als Entlehnungen kenntlich gemacht.

Diese Dissertation liegt in gleicher oder ähnlicher Form keiner anderen Prüfungsbehorde vor.

Die Satzung des KIT zur Sicherung guter wissenschaftlicher Praxis in ihrer aktuellen Form wurde beachtet.

Karlsruhe, den 02. März 2021